National Library of Canada
Bibliothèque nationale du Canada

Canadian Theses Service
Service des thèses canadiennes

Ottawa, Canada
K1A 0N4

NOTICE

The quality of this microform is heavily dependent upon the quality of the original thesis submitted for microfilming. Every effort has been made to ensure the highest quality of reproduction possible.

If pages are missing, contact the university which granted the degree.

Some pages may have indistinct print especially if the original pages were typed with a poor typewriter ribbon or if the university sent us an inferior photocopy.

Reproduction in full or in part of this microform is governed by the Canadian Copyright Act, R.S.C. 1970, c. C-30, and subsequent amendments.

AVIS

La qualité de cette microforme dépend grandement de la qualité de la thèse soumise au microfilmage. Nous avons tout fait pour assurer une qualité supérieure de reproduction.

S'il manque des pages, veuillez communiquer avec l'université qui a conféré le grade.

La qualité d'impression de certaines pages peut laisser à désirer, surtout si les pages originales ont été dactylographiées à l'aide d'un ruban usé ou si l'université nous a fait parvenir une photocopie de qualité inférieure.

La reproduction, même partielle, de cette microforme est soumise à la Loi canadienne sur le droit d'auteur, SRC 1970, c. C-30, et ses amendements subséquents.

NL-339 (r. 88/04) c

Canada

THE UNIVERSITY OF ALBERTA

MASS MOVEMENT, SEISMICITY AND NEOTECTONICS IN THE NORTHERN ST. ELIAS MOUNTAINS, YUKON

by

Michael A. Power

A THESIS

SUBMITTED TO THE FACULTY OF GRADUATE STUDIES AND RESEARCH

IN PARTIAL FULFILLMENT OF THE REQUIREMENTS FOR THE DEGREE

OF MASTER OF SCIENCE

IN

GEOPHYSICS

DEPARTMENT OF PHYSICS

EDMONTON, ALBERTA

Fall 1988

Permission has been granted to the National Library of Canada to microfilm this thesis and to lend or sell copies of the film.

The author (copyright owner) has reserved other publication rights, and neither the thesis nor extensive extracts from it may be printed or otherwise reproduced without his/her written permission.

L'autorisation a été accordée à la Bibliothèque nationale du Canada de microfilmer cette thèse et de prêter ou de vendre des exemplaires du film.

L'auteur (titulaire du droit d'auteur) se réserve les autres droits de publication; ni la thèse ni de longs extraits de celle-ci ne doivent être imprimés ou autrement reproduits sans son autorisation écrite.

ISBN 0-315-52757-9

THE UNIVERSITY OF ALBERTA

RELEASE FORM

NAME OF AUTHOR Michael A. Power

TITLE OF THESIS MASS MOVEMENT, SEISMICITY AND NEOTECTONICS IN THE NORTHERN ST. ELIAS MOUNTAINS, YUKON.

DEGREE FOR WHICH THESIS WAS PRESENTED Master of Science

YEAR THIS DEGREE GRANTED Fall 1988

Permission is hereby granted to THE UNIVERSITY OF ALBERTA LIBRARY to reproduce single copies of this thesis and to lend or sell such copies for private, scholarly or scientific research purposes only. The author reserves other publication rights, and neither the thesis nor extensive extracts from it may be printed or otherwise reproduced without the author's written permission.

(SIGNED) M.Power

PERMANENT ADDRESS:
255 Touzin Ave
Dorval P.Q.
H9S 2N1

DATED Sept 26, 1988

THE UNIVERSITY OF ALBERTA

FACULTY OF GRADUATE STUDIES AND RESEARCH

The undersigned certify that they have read, and recommend to the Faculty of Graduate Studies and Research, for acceptance, a thesis entitled MASS MOVEMENT, SEISMICITY AND NEOTECTONICS IN THE NORTHERN ST. ELIAS MOUNTAINS, YUKON submitted by MICHAEL POWER in partial fulfillment of the requirements for the degree of MASTER OF SCIENCE in GEOPHYSICS.

.....

Supervisor

.....

.....

.....

Date Sept 22, 1988

This thesis is dedicated to my parents,

Bernard and Pauline Power

in gratitude.

Abstract

An unusual landslide, originally reported as an uplift feature, occurred during the winter of 1983 at Cement Creek in the northern St. Elias Mountains. This landslide was a bedding controlled block slide (estimated volume $4x10^6$ m^3) with 30-40 m of predominantly horizontal translation and minor clockwise rotation. Ground motion triggered subsidiary ground failure west of the landslide and was responsible for much of the shallow ground failure on the slide mass. Rapid Holocene uplift and fluvial dissection of favourably oriented strata predispose Neogene volcanic rocks in the area to fail along hydrothermally altered flow-top breccias. The landslide was probably triggered by microearthquake activity. Two seismograph arrays were operated in the area for 6 weeks during 1987 to monitor low magnitude seismicity. To accurately locate earthquakes outside of the arrays, a location algorithm using the difference in arrival times to formulate a residual and a modified conjugate gradient search to minimize the residual was developed. Moderate and microearthquake activity in the northern St. Elias Mountains together with geological structure define three zones of seismicity: (1) a zone of low level seismicity centred on thrusts and reverse faults beneath the Icefield ranges (2) an active zone, 15 km wide, beneath the Duke River Fault and structures north of it and (3) a moderately active zone of shallow seismicity beneath low-lying areas north of the Duke River Fault. Epicentral distributions, composite focal plane solutions and the projection of foci down structural trends suggests that a positive flower structure, centred just north of the Duke River Fault, exists in the subsurface.

Acknowledgements

This research was supported by a research contract and logistical support from the Exploration and Geological Services Division of the Department of Indian Affairs and Northern Development in Whitehorse, Y.T., by grants from the Boreal Institute for Northern Studies and by funds from Natural Sciences and Engineering Research Council grants to Dr. D.I. Gough and E. Nyland. The author was supported by scholarships from the Canadian Society of Exploration Geophysicists (1986-1987) and the Natural Sciences and Engineering Research Council (1987-1988).

I wish to thank Dr. D.I. Gough for his backing and encouragement of the Cement Creek research. S. Morison, G. Abbot and the staff of the Exploration and Geological Services Division are thanked for their generous help prior to and during field work. Drs. D. Cruden, A.E. Peterson, C.J. Dodds, R. Horner and T. Skulski provided valuable advice during the course of this work. Drs. R. Ellis and D. Bingham are thanked for generously loaning seismographs and ancillary equipment to the field party for the microearthquake survey. Dr. P. Erdmer provided help and advice both in the field (1986) and in interpreting the results of the earthquake survey (1987). The success of the fieldwork is largely due to the capable assistance rendered by P. Von Gaza (1986) and W. Kruggel (1987). L. Tober is thanked for his meticulous instrument preparation and technical instruction. C. McLoughan and B. McGavin shared their wealth of experience with the author and co-workers Q. Li, Y. Wang and G. Lorentz freely lent him their bug-free programs and assistance.

Lastly, I wish to thank Dr. Edo Nyland for the freedom of action, profitable discussions and unqualified backing I enjoyed under his supervision.

TABLE OF CONTENTS

CHAPTER — PAGE

INTRODUCTION 1

1. RECENT LANDSLIDING IN TERTIARY VOLCANIC ROCKS AT CEMENT CREEK, ST. ELIAS MOUNTAINS, YUKON 3

1.1 Introduction 3

1.2 Geology 3

1.3 Landslide morphology 11

1.4 Current deformation rates 15

1.5 Geophysical investigations 19

2. SEISMICITY AND.NEOTECTONICS OF THE DUKE RIVER FAULT, DENALI FAULT SYSTEM, SOUTHWEST YUKON 31

2.I Introduction 31

2.2 Field procedure 31

2.3 Data analysis 35

2.4 Results 40

2.5 The historical record 49

2.6 Possible evidence for Holocene tectonism 51

3. CONCLUSIONS 54

The Cement Creek landslide 54

Seismicity 57

Discussion..... 61

BIBLIOGRAPHY 63

APPENDIX A RESISTIVITY SOUNDING INVERSION PROGRAM..... 68

APPENDIX B FOCUS - AN EARTHQUAKE LOCATION PROGRAM
USING THE TIME DIFFERENCE RESIDUAL METHOD..... 74
Program listing 78

APPENDIX C. THE CEMENT CREEK FAULT STRAIN ARRAY..... 109

List of Figures

Figure		Page
1	Location of the 1983 Cement Creek landslide.	4
2	Geology and geomophology of the Cement Creek area.	5
3	Principle elements of the 1983 landslide.	7
4	Equal area projection of poles to bedding in the synclinal pericline	8
5	Aerial photography of the Cement Creek area.	9
6	Ground failure and measured horizontal displacements on the Cement Creek landslide.	13
7	Geophysical and deformation survey network on the Cement Creek landslide	16
8	Deformation survey results	17
9	Refraction from a single dipping layer and the definition of delay time.	20
10	Geophysical survey results.	22
11	Composite cross-section through the Cement Creek landslide.	30
12	Tectonic elements in the southwest Yukon and southeast Alaska.	32
13	Seismicity in the southwest Yukon.	33

14	Seismograph sites, microearthquake epicentres coded for focal depth and geological structure in the study area.	34
15	Time difference residuals surrounding a focus outside of a small seismograph array.	37
16	A cause of the ambiguity in the determination of radial distance and focal depth.	39
17	Test of the time-difference residual method using earthquakes in a half-space velocity model and a 10 km wide tripartite array.	41
18	Histograms of S-P separation and daily earthquake frequency	45
19	A sudivision of the study are based on microseismicity and geological structure.	47
20	Cross-sections showing projections of earthquake foci into the planes of section together with the structural geology along the line of section.	48
21	Epicentres of earthquakes with Local magnitudes greater than 4.0 from the Canadian Earthquake Catalogue.	50
22	Structural data for tectonically disturbed tills and fluvial deposits at Bull Creek.	52
23	A schematic diagram illustrating rotation of the slide mass in the core of the pericline.	55
24	A schematic model for neotectonics on the western segment of the Duke River Fault (DRF).	59
25	Cement Creek Fault strain array.	110

List of Tables

Table		Page
1.	Earthquakes within 160 km of the Cement Creek area between February 15, 1983 and March 15, 1983.	12
2.	Focal coordinates and time difference residuals for earthquakes located by the Boundary Creek and St. Clare Creek arrays.	43

Introduction

During the late winter of 1983, D Makkonen, a helicopter pilot with Trans North Turbo Air Ltd., reported that ground failure affecting an area of approximately 1.0 km^2 was occurring at Cement Creek in the St. Elias Mountains, 45 km west of Burwash Landing in the southwest Yukon Territory (Figure 1, Chapter 1). According to his report and those of subsequent observers, radial cracks were developing in a domal hill in the centre of the disturbed area and this suggested that active uplift might be occurring at this site. In most other areas of Canada this might be dismissed as fantastic but the recent geologic history of the St. Elias Mountains dictated that the report merited investigation.

The St. Elias Mountains are the physiographic expression of compressional and transform tectonic interactions between the Pacific and North American plates. In the Gulf of Alaska, the offshore Yakutat Block (Lahr and Plafker 1980) is being actively accreted to the North American plate and great earthquakes with moment magnitudes up to 9.2 (Kanamori 1977) have occurred on north- to northeast-dipping reverse faults and thrusts. Further inland, significant seismicity occurs on the Denali Fault System (St. Amand 1957, Horner 1983), a major right lateral transform fault composed of several segements, some of which predate the development of the transform (Stout and Chase 1980). The Benioff zone of the descending Pacific Plate has been traced to depths of approximately 80 km beneath southeastern Alaska and Quaternary volcanoes such as Mt. Wrangell are the result of subduction (Stephens *et al.* 1984). Cement Creek is located near the Duke River Fault, a seismically active segment of the Denali Fault System, in an area which has been affected by recent volcanism (Muller 1967). In this context, reports of active uplift deserve investigation both as potential geologic hazards and as phenonema of purely scientific interest.

This thesis consists of two parts, the first documenting an investigation of the reported uplift at Cement Creek and the second being an investigation of seismicity and neotectonics along the western Duke River Fault. The aims of this work were to (1) determine the sense, rate and cause of deformation at Cement Creek, (2) to determine the significance of the deformation at Cement Creek in the context of local tectonic processes and (3) to examine the relationship between the seismicity and geological structure of the Duke River Fault in order to understand neotectonic processes. The first chapter summarizes investigations of the Cement Creek landslide conducted during 1986 and the

second describes a microearthquake survey conducted in the same area in 1987. During the latter study, a tectonic strain array consisting of 6 reinforced concrete survey monuments was constructed near an apparently active fault in the area to measure long term crustal strains. Programs for the inversion of resistivity sounding data and the location of earthquakes together with initial measurements for the strain array are contained in Appendices A through C.

Chapter 1

Recent landsliding in Tertiary volcanic rocks at Cement Creek, Saint Elias Mountains, Yukon Territory[1].

1.1 Introduction

A landslide affecting an area of approximately 1 km^2 was reported on Cement Creek (Figure 1) in the St. Elias Mountains, Y.T. (139° 56' W 61° 23' N) during the winter of 1983. The slide was sighted by D. Makkonen, a pilot with Trans North Turbo Air Ltd. in Haines Junction, Y.T. and according to his best recollection and that of a passenger, occurred between February 15 and March 15, 1983. The two eyewitnesses cannot agree on even an approximate date for their sighting and the stated period includes both their estimates. According to Makkonen all the current principal features of the landslide were present during his initial sighting. At the time of the landslide, the area was thoroughly frozen and runoff in the adjacent creek was minimal. Some later observers suggested that active uplift may be occurring at Cement Creek and an investigation was initiated by the Exploration and Geological Services Division of the Department of Indian Affairs and Northern Development in Whitehorse, Y.T. We summarize here displacement, topographic and geophysical surveys and geologic and geomorphologic mapping conducted at this site during June-August 1986. No previous work has been done on this feature.

1.2 Geology

Cement Creek is 45 km west of Kluane Lake in the northern St. Elias Mountains. Regional mapping in this area (Muller 1967, Souther and Stanciu 1975, Campbell and Dodds' 1982, and Skulski and Francis 1986) delineated four rock units (Figure 2) beneath thin Holocene and Pleistocene surficial deposits. Landsliding is confined to rocks in the lower unit of the Neogene Wrangell Lavas; the other units have been described in the paper referenced in the footnote.

---

[1]A version of this chapter has been accepted for publication. Power, M. A. Landsliding at Cement Creek, Kluane area, Yukon. Yukon Geology (in press)

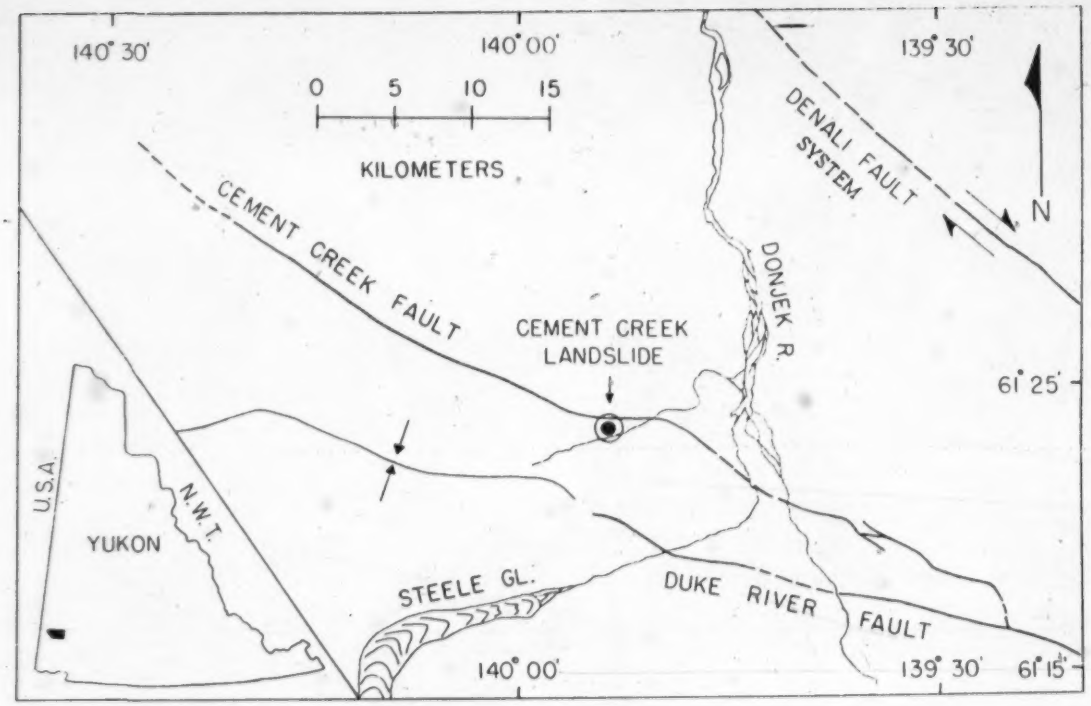

Figure 1. Location of 1983 Cement Creek landslide. Principal faults and associated structure after Campbell and Dodds (1982).

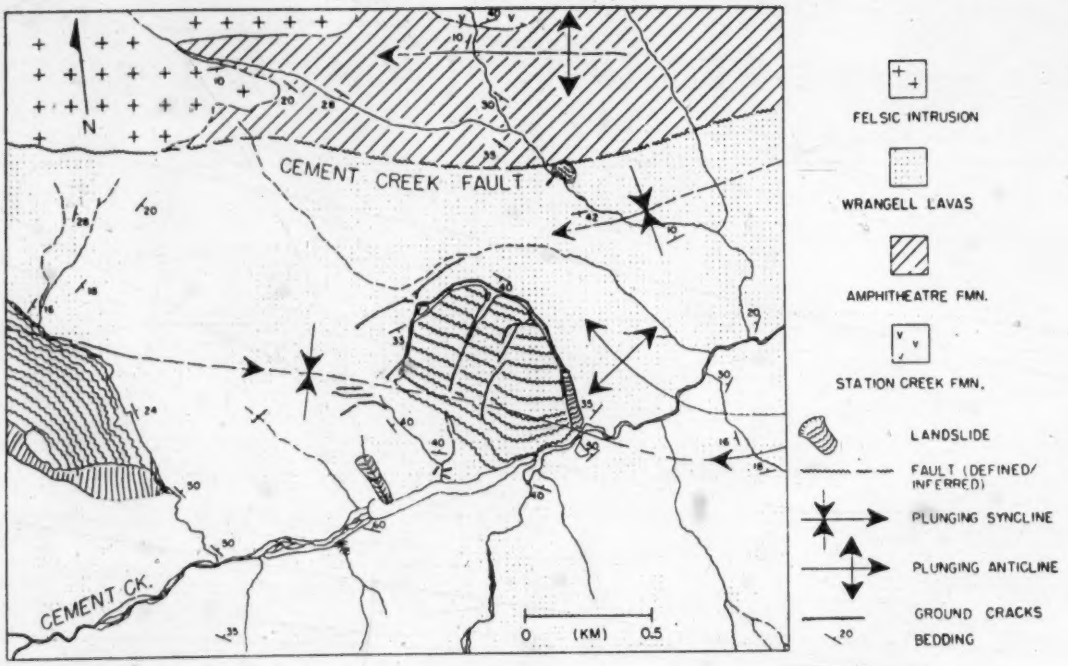

Figure 2. Geology and geomorphology of the region surrounding the 1983 landslide (center) based on mapping by the author, Campbell and Dodds (1982) and Muller (1967).

The stratigraphy, geochemistry and petrogenesis of the Wrangell Lavas has been documented by Souther and Stanciu (1975) and Skulski and Francis (1986). The succession exposed north of Cement Creek immediately east of the landslide consists of basaltic andesite flows, 5-15 m thick. Individual flows can be traced for more than a kilometer along the exposure and are blocky with a joint spacing of 0.5-1.0 m. Amphibole and plagioclase phenocrysts increase in abundance from base to top of flows. Vesicles are common, but amygdules of jasper, quartz, calcedony and green clay minerals predominate, especially at the top of individual flows.

Flows are capped by breccias composed of altered purple to red-brown clasts of underlying basaltic andesite, 5-30 cm long, in a matrix of alteration products. X-Ray diffraction analysis of matrix material indicates that it is composed of montmorillonite, kaolinite, muscovite, and chlorite in decreasing order of abundance. Hydrothermal alteration has also proceeded along joint sets perpendicular to both bedding and the axis of a major fold. This is particularly evident in wall rock exposed in the major medial crack which nearly bisects the landslide (Figure 3a).

A major vertical fault which outcrops 300 m north of the landslide and a synclinal pericline, the axis of which transects the slide, dominate the local geologic structure (Figure 2). The Cement Creek Fault (Skulski and Francis 1986) runs from the Wade Mountain Fault Zone (Read and Monger 1975) to St. Clare Creek (Souther and Stanciu 1975). Near the Cement Creek landslide the fault trace strikes east-west and is about 300 m north of the headscarp. In the eastern part of the area depicted in Figure 2, the fault crops out as a 20 m-wide steeply dipping zone of sheared and bleached rock. Rock in the fault zone and adjacent to it are locally folded about horizontal to shallow dipping axes, suggesting that the most recent displacement on the fault has been vertical.

Bedding in the area of the landslide has been infolded along an east-west trending axis and weakly cross-folded to form a synclinal pericline with its depression close to the point where the axial trace crosses Cement Creek. Equal area projections of poles to bedding in rocks east and west of the depression (Figure 4) were prepared using TRIPOD (Charlesworth *et al.* 1987). Limited exposure and large scale primary structures (> 10 m) in the Wrangell Lavas cause the poor distribution in these projections but the folding in each domain is nevertheless evident. Landsliding is almost completely confined to rocks in the north limb of the structure and west of the fold depression. A larger and older landslide is located immediately west of the plateau (Figure 5(a)) where a creek has incised

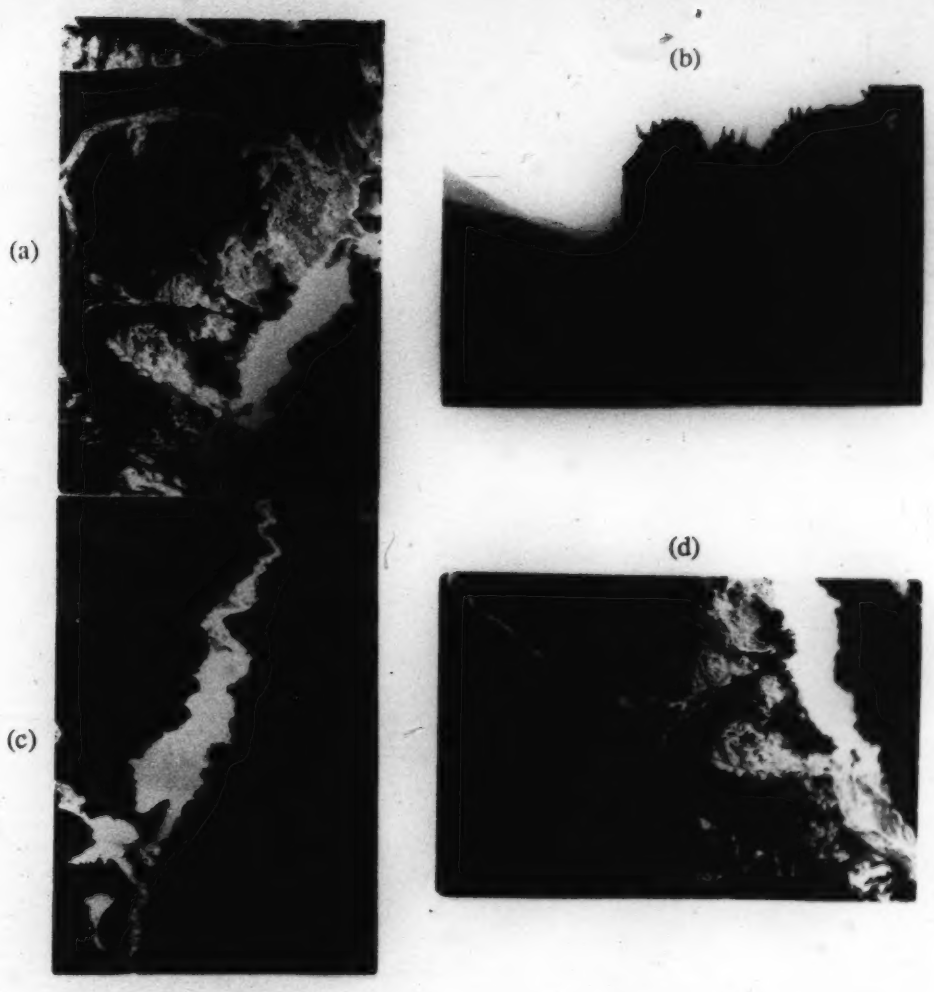

Figure 3. Principal elements of the 1983 landslide. (a) Aerial view of the landslide looking northeast from south of Cement Creek. (b) Detached blocks in the toe of the slide resting on a ledge formed by resistant flows (looking west from the eastern extremity of the landslide) (c) Aerial view of the impounded lake looking west; note the absence of runup on the south wall of the canyon. (d) Aerial view of separate subsidiary ground failure west of the main landslide looking east from the western end of the landslide .

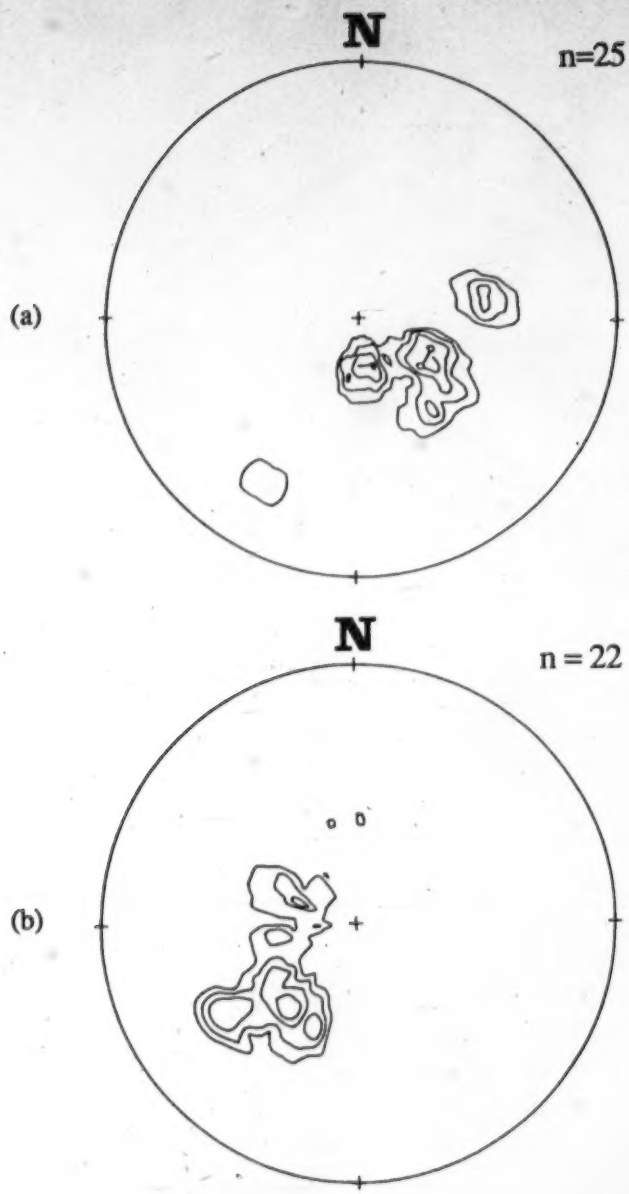

Figure 4. Equal area projection of poles to bedding in the synclinal pericline (a) east and (b) west of the fold depression. Contours represent percentages poles in a 1% area counting circle at intervals of 5, 10, 15, 20 and 30%.

Figure 5. Air photographs of the study area taken in 1981 (Canada A25288-13) (a) A view of the plateau and adjacent area. a- indicates the area affected by the 1983 landslide; b-is an older landslide mentioned in text. (b) Enlargement of area involved in the 1983 landslide. a- indicates the incipient trace of the medial crack. The headscarp, partially formed and overgrown, lies immediately to the north. b- is a tree covered ledge which formed the rupture surface during subsequent landsliding .

the western end of the pericline and a number of small mudslides occur along the southern perimeter of the plateau.

Cement Creek has incised the local bedrock as much as 100 m below the base level of the valley since the retreat of the St. Elias ice sheet at the end of the Wisconsin (Muller 1967) and this may be partly due to tectonic uplift. Holocene down-cutting increases significantly in the axial region of the pericline and a steep walled canyon borders the creek west of the 1983 landslide to the point where the Cement Creek Fault crosses the stream. Several hundred meters beyond this point, the canyon disappears and the stream turns sharply to the north as it enters the Donjek River valley. This incision is probably not an artifact of differential riverbed erosion by the St. Elias icesheet; hanging valley features are not present in adjacent streams on the west side of the Donjek River and it is unlikely that 6 km of Holocene back-cutting has occurred on the creek. This rapid dissection of the valley suggests rejuvenation of the local topography via uplift. Muller (1967) noted other instances of this phenomenon on St. Clare and Steele creeks but it seems most pronounced in the lower Cement Creek drainage basin.

The Cement Creek landslide is located in a zone of significant seismicity parallelling the Dalton, Shakwak and Duke River segments of the Denali Fault System. Seismically induced mass movements have been noted in this area (Clague 1979) and seismological investigations (Boucher and Fitch 1969, Horner 1983) indicate that seismicity along the Duke River segment of the Denali Fault System broadly straddles the exposed and covered trace of the Duke River Fault. The historical record (Horner 1983) documents events up to M_L=6.0 in an area where the detection threshold of the regional network is about M_L=2.0. Seismic events detected during the period in which the landslide probably occurred were quite small and are listed in Table 1 but the landslide may have occurred later (Doug Makkonen 1986, personal communication). A moderate earthquake of M_L=5.0 occurred approximately 20 km north of the landslide on March 30, 1983 causing ice avalanches at sites south of the Cement Creek area in the Icefield Ranges (G.Abbot 1987, personal communication) and in view of the discrepancies between the reports of the eyewitnesses and the uncertainty in their assignment of the exact date, the possibility that the landslide was triggered by this earthquake cannot be ruled out.

If the landslide did occur prior to this moderate earthquake, microseismicity may have contributed to landslide initiation. A reconnaissance seismicity survey along the Alaska Highway (Boucher and Fitch 1969) documented 2-3 events per day probably

originating within 50 km of the Cement Creek area. There are frequent bursts of microseismicity ($M_L < 2.0$) in the area. The study summarized in Chapter 2 detected up to 5 events with similar magnitudes originating in the same locality within the space a few minutes. This observation suggests that low intensity ground motion might be a contributing factor in landslide initiation in this area.

1.3 Landslide morphology

The landslide and related ground failure at Cement Creek is confined to the south margin of a triangular plateau in the center of Figure 5(a) and Figure 3 contains photographs of the landslide as it appeared in 1986. It is a block slide 850 m wide, centered on a hill that protrudes 110 m above the plateau. Displacement is directed towards a 90 m high open face which forms the south boundary of the plateau. Substantial breakup of the slide mass is visible only near the toe where blocks 60 m high and up to 0.15 ha in areal extent have separated from the main slide mass. Slide volume is about 4.0×10^6 m^3 and maximum horizontal displacement of the main portion of the slide is 30 to 40 m. No evidence of uplift was found in either ground or aerial surveys of the area; the radial crack pattern which led to the original suggestions of uplift probably resulted from rotation of the slide mass during displacement

The toe of the slide extends across the creek bed but debris was not projected up the south wall of the canyon (Figure 3(c)). The debris fan has impounded a lake 1 km long, but it has been partially breached and is permeable. During a period in June 1986 the entire discharge of the creek percolated through the barrier with no surface flow.

The headscarp is roughly circular in plan and reduces in width from 75 m in the east to about 10 cm at its western end. At its western end, the headscarp is deflected along jointing towards the axis of the synclinal pericline. The portion of the slip surface exposed in the headscarp dips at approximately 50^o towards the toe, cutting across bedding and exposing highly altered bedrock. At the toe of the slide, the rupture surface appears to follow the tops of resistant flows which jut out from the north wall of the canyon to form a curved ledge. This ledge displays the projection of the synclinal pericline in the open face and is evidently intact, for it supports the large blocks shown in Figures 3(a)-(b) and 11.

Several classes of major cracks may be distinguished on the basis of age and

Table 1. Reported Seismic Events within 160 km of Cement Creek Landslide between February 15, 1983 and March 15, 1983.

DATE/TIME (UTC)	MAGNITUDE (M_L)	DISTANCE (km)
7 MAR 83/16:18:25	2.7	90
8 MAR 83/12:12:42	3.8	150
9 MAR 83/12:28:58	3.1	75
11 MAR 83/22:43:26	2.7	110
13 MAR 83/02:45:49	2.3	110

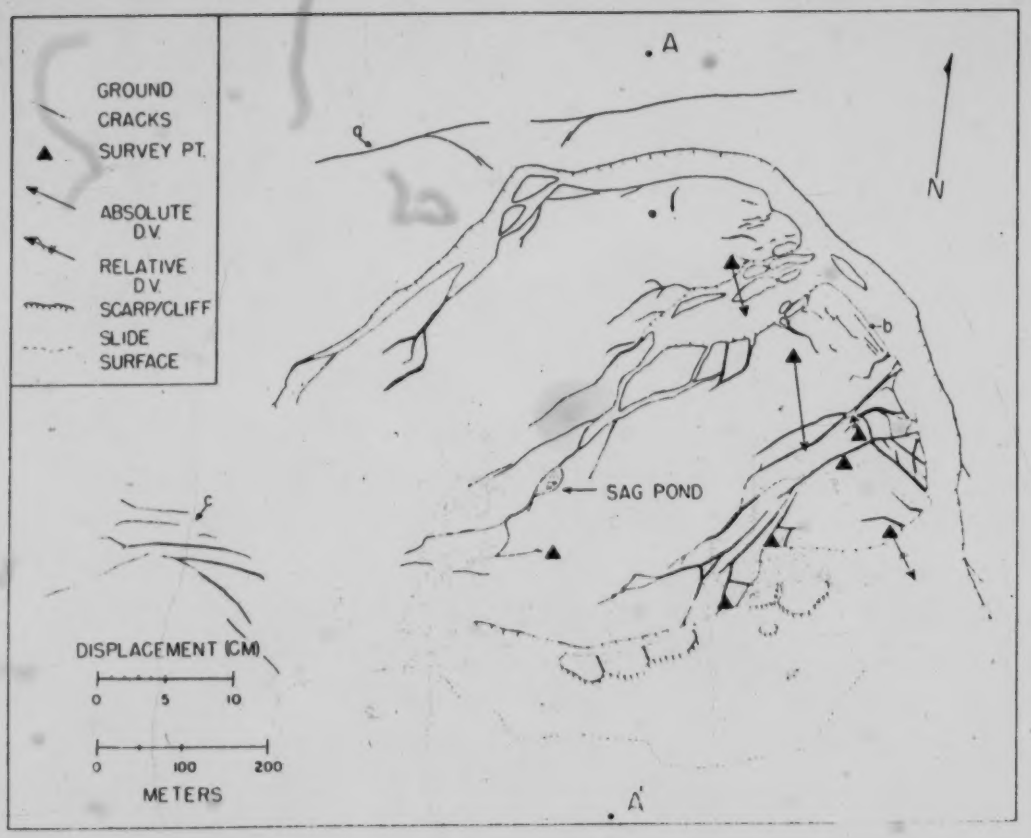

Figure 6. Ground failure and measured horizontal displacements on the Cement Creek Landslide.

morphology and these are shown in Figure 6. The oldest cracks present predate the 1983 landslide and lie north of the slide at the break in slope between the hill and the plateau ((a) in Figure 6). These are individually up to 100 m long and form a linear en-echelon system extending 570 m . They strike across the northwest side of the landslide, deviating only near the deflection of the headscarp along jointing. They do not wrap around the back of the slide as would be expected if they reflected upslope migration of the headscarp; instead they continue northeast and disappear in soft ground. They are up to 40 cm deep with weathered and partially overgrown sides.

Cracks formed during the 1983 landslide may be subdivided into two categories on the basis of their depth. Shallow ground cracks are most common near the toe of the landslide and adjacent to deeper major crack systems but are not confined to these localities. Some clearly result from breakup of the slide mass near openings or the open face in the toe but others in the centers of the larger blocks do not appear to have been generated by this mechanism. Seismic refraction surveys conducted on the slide mass using a single channel seismograph indicated that most of these ground cracks are rooted at depths of no greater than 15-20 m in a low velocity layer composed of weathered rock. Exposures in the headscarp and toe indicate that this layer is formed of highly altered bedrock and frozen glacial till. The second group consists of cracks up to 50 m wide and at least 40 m deep which probably extend down to the rupture surface and separate the slide mass into major blocks. Most prominent of these is a major medial crack which nearly bisects the landslide and narrows along strike from north to south (center of Figure 6). The overall pattern of both sets of cracks is slightly radial with the strike of individual cracks rotating in a clockwise sense from west to east.

A series of solifluction scars run across the north slope of the slide mass and were formed after 1983 ((b) in Figure 6). These are up to 40 cm deep, affect only sod and the uppermost soil horizon, and are not present on that portion of the hill below the headscarp. This suggests that the north face of the slide mass has been rotated through an angle sufficient to destabilize the overlying vegetation and implies that the upper portion of the rupture surface is semicircular in profile.

Ground failure dating from 1983 found immediately west of the landslide (Figure 3(d) and (c) in Figure 6) probably occurred at the same time as the main landslide. The cracks have similar appearance to shallow ground failure on the main landslide and formed prior to the initial sighting. They are up to 5 m deep and clustered on the edge of the

plateau. The headscarp ends about 100 m north of their location, has a different strike and does not link up with them. No evidence of bedrock displacement was observed in the adjacent open face where bedding dips into the exposed face.

The area affected by the 1983 landslide appears to have undergone mass movement prior to 1943 . Aerial photography of this area dating from 1943 shows the incipient trace of the headwall scarp and overgrown, apparently unconsolidated debris at its eastern end. The incipient trace of the medial crack and headscarp are faintly visible in enlargements of 1981 photography (Figure 5(b)). The ledge forming the outcrop of the slip surface in the open face is partially covered by black spruce, suggesting no significant activity for perhaps the past 100 years and the incipient headscarp is only approximately 10 m wide. The 1983 landslide is therefore the reactiviation of an older incipient landslide of minimal displacement.

1.4 Current deformation rates

A series of survey stations were installed (Figure 7) to measure displacement rates on the landslide. At each of these sites, the motion of one or two points fixed on the slide mass was measured with respect to two fixed points on the plateau. Relative displacements across apparently active cracks was measured using the method of trilateral signs (Ter Stepanian 1980).

Displacement relative to the plateau was detected by measuring the distances and vertical angles between the three or four sites at each survey station. Each site consisted of a survey tripod centered over a 40 cm long scribed spike anchored firmly in permafrost. The distances along the three sides of the triangle formed by the two sites off the slide and the third on it were measured using a Sokkisha Red 1A electronic distance measuring device (EDM). The vertical angles between each of sites 1, 2 and 3 and corresponding sites on the plateau and the slide were measured using a Kern DKM-II triangulation theodolite. The position of each site on the slide was then calculated relative to an orthogonal coordinate system with the positive x-axes being the horizontal projections of the vectors 1-1A, 2-2A and 3-3A and the positive y-axes being the horizontal projections of vectors orthogonal to the x-axes and pointing towards the landslide. The apparent motion of the four survey sites on the slide is shown in Figure 8.

In general, measurement error is less than error introduced by enviromental factors

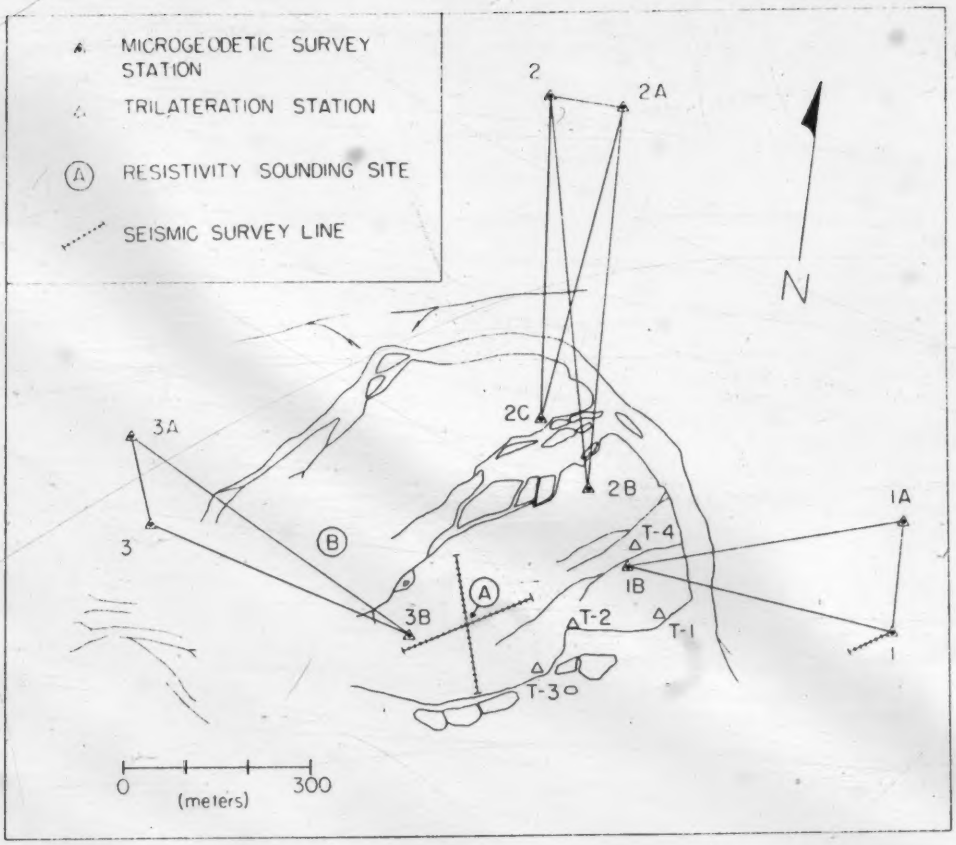

Figure 7. Geophysical and deformation survey network on the Cement Creek landslide.

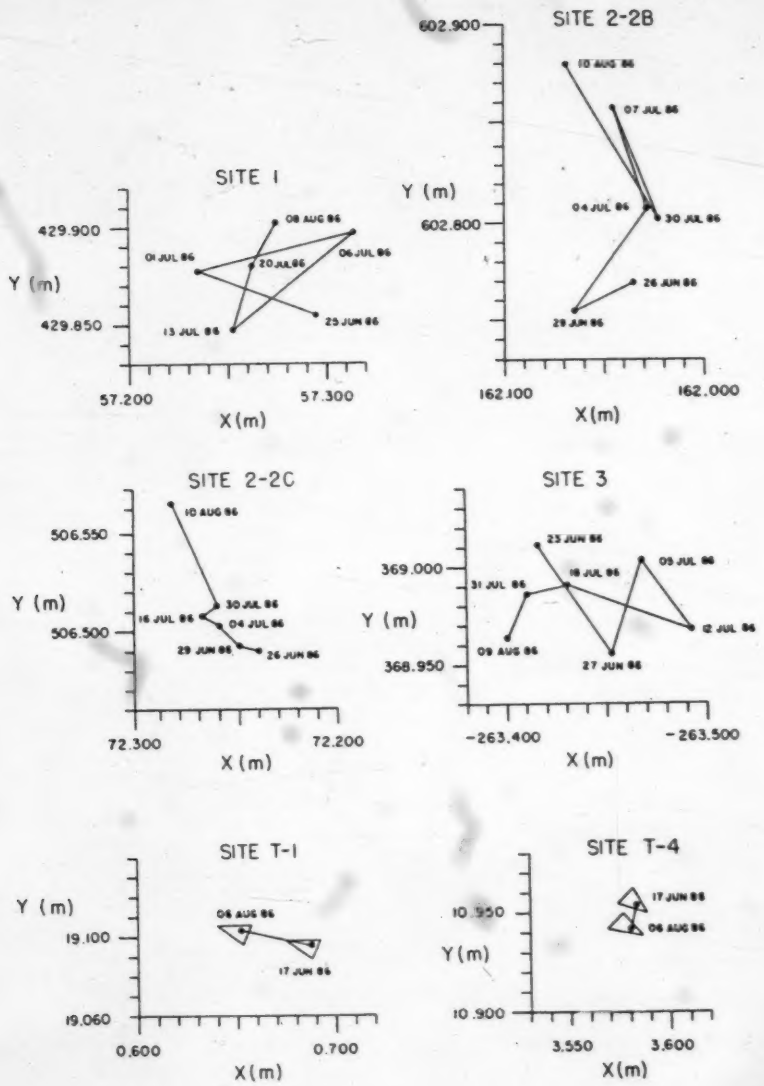

Figure 8. Deformation survey results.

such as refraction and frost heave. The standard error of the EDM is ≤6.5mm over the distances encountered in this survey. To nullify the effects of an incorrect atmospheric correction or any other systematic error, the reference distances measured during each survey were normalized by comparing them with the reference distances measured during the initial survey. The DKM-II may be read directly to 1.0 s of arc and measurements accurate to within 3.0 s were obtained using 5 repetitions. Refraction, heat shimmer and instrument levelling error caused by poor ground conditions introduced significant additional error. This rendered the detection of vertical motion impossible for small displacements but did not seriously affect measurements in the horizontal plane since vertical angles did not exceed 10°. Combined error was assessed to be 30.0" for any survey or a maximum of 2.1 cm of error in horizontal distances derived from the longest shot in the network. A maximum combined error of ±3.0 cm in the horizontal coordinates of any point is therefore reasonable. Thus significant displacement occurred if the initial and final survey points were separated by at least 6.0 cm and the overall trend of the displacement was smooth. Using these criteria, the apparent random motion of sites 1B and 3B is attributed to combined error and frost heave or some other site-specific effect not related to overall landslide displacement. Apparent motion of 10 ±6 cm and 12 ±6 cm was detected at stations 2B and 2C. No displacement was observed in the toe of the slide beyond the local displacement detected at trilateration station T-1 and the rates of absolute displacement are consistent with this. Current displacement probably results from seasonal creep of material in the upper portion of the landslide.

Extension across major, apparently active cracks was measured using the method of trilateral signs described by Ter Stepanian (1980). This consists of the installation of 3 scribed spikes in the base of trees on either side of the crack and the measurement of the sides of the triangle so-formed using a survey chain and puller. The displacement of one of the points with respect to the pair on the opposite side (the reference points) is calculated in the plane of the three points. To nullify the effects of temperature, measurements taken on the final survey were normalized against the reference distance measured on the first survey using the latter as a standard. The error in any single chained distance was ±3mm and regions of error were determined using extreme values. Relative displacements were detected at only two of the four trilateration sites and these are plotted in Figure 8. Displacement at T-1 is consistent with the overall motion suggested by the absolute displacement vectors and the pattern of cracks in the slide mass. This site is near a local

gully and the deflection of the displacement to the southeast is a consequence of this. The small negative extension detected at T-4 may represent the closure of a major deep crack or degradation of the margins of the crack.

1.5 Geophysical investigations

Seismic refraction and electrical resistivity surveys were conducted to delineate the rupture surface and to assess the geotechnical properties of material in the slide mass. In many landslides, the juxtaposition of fractured, low velocity slide material over intact bedrock presents a situation where the interface between them may be mapped using the seismic refraction technique (Muller 1977). In addition, impermeable gouge or strata-bound clay may be present along the rupture surface and should groundwater be perched at this level, it might be detected as a conductive layer via electrical resistivity soundings. At Cement Creek, geophysical surveys failed to detect the rupture surface but did yield valuable information on hydrogeological conditions at the rupture surface and the origin of shallow ground failure on the slide mass.

Seismic refraction surveys were conducted using a Bison 1570B single channel seismograph with both hammer and explosive energy sources. Three survey lines were shot (Figure 7); an unreversed test section to determine velocities off the slide and two reversed profiles oblique to the inferred dip of the rupture surface beneath site A.

The data was inverted using the delay-time method of Wyrobek (1956). The method is suitable for data from flat or shallow-dipping refractors and is outlined below. Figure 9 illustrates the simple case of a shallow dipping refractor. Following Telford *et al.* (1976), the delay time (δ) associated with the ray travelling from A to D is the difference between the travel time for the refracted ray ABCD and the travel time from A' to D' where A' and D' are the projections of A and D onto the refractor. Thus the relation in the figure may be rewritten as

$$\delta = \left\langle \frac{AB}{V_1} - \frac{A'B}{V_2} \right\rangle + \left\langle \frac{CD}{V_1} - \frac{C'D}{V_2} \right\rangle = \delta_s + \delta_g \qquad (1.1)$$

where δ_s and δ_g are defined as the delay times at the shot and geophone respectively. Now if the refractor is flat or nearly so ($\theta \leq 10^o$),

$$\delta \approx t - \frac{x}{V_2} \qquad (1.2)$$

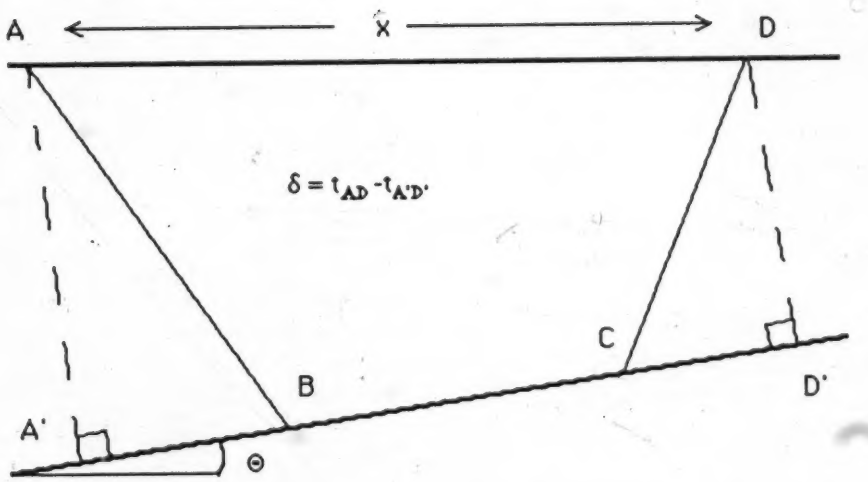

Figure 9. Refraction from a single dipping layer and the definition of delay time.

In other words, the delay time is equal to the intercept time under these circumstances. Furthermore, for a shallow-dipping refractor and a given shot spread, the curve of δ approximately parallels the half-intercept time curve. Thus the curve of δ can be used to extend the half-intercept curve and the extended curve can be inverted to obtain the depth to the refractor. Wyrobek's method uses this in a three-step process (Telford *et al.* 1976):

(a) Determine the delay time at each geophone and the intercept time at each shot.

(b) Plot δ–X and T_{int}-X diagrams. Adjust δ-X curve segments until they are aligned to form a "phantom horizon". If the velocity of the refracting layer is chosen incorrectly, the phantom horizon and half-intercept time curve will not intersect.

(c) The half-intercept time curve is converted into depth for each shot and phone using

$$z = \frac{V_1 t_{int}}{2 \cos\theta} \qquad (1.3)$$

Since reversed profiles were available, velocities of the upper and lower layers could be determined from the travel-time curves. Variations in the velocity of the upper layer were evident in the travel-time curves and a consistent solution was found by varying this parameter within the limits imposed by the travel-times curves. Travel time curves and interpretations are displayed in Figure 10 (a-d). Depths are probably accurate to within 10%. Significant changes in the velocity of the upper layer were detected in the NW-SE line while that of the NE-SW line was constant. The velocity of the lower layer remained essentially constant in all profiles. The average depth to the refractor, between 10 - 20 m, was too deep to be the base of surficial deposits as seismic explosions frequently exposed bedrock at depths of around 0.5 m. Rather, it seems to represent the base of a combined layer of weathered rock and frozen surficial cover. The anisotropic velocity profile of the upper layer along the NW-SE line most likely reflects the presence of ground cracks; this line is transverse to them while the NE-SW line parallels the ground failure and does not intersect any cracks. Cracks in the survey area were partially filled in and no deeper than about 6-8 m. The upper layer is thus probably composed of low velocity ($V_p \approx 1900$ m/s) weathered rock in which much of the ground failure is localized.

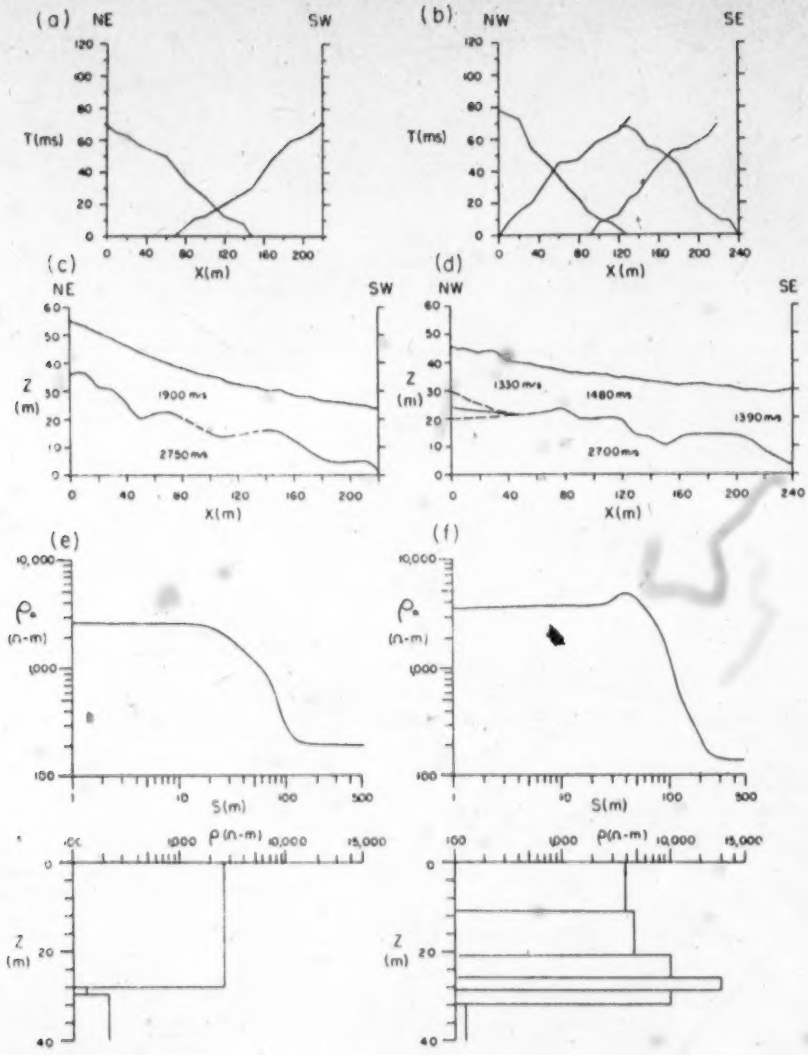

Figure 10. Geophysical survey results. (a)-(b) T-X curves for seismic refraction lines on the landslide. (c)-(d) models derived using Wyrobek's method (Wyrobek 1957). (d)-(e) Apparent resistivity profiles at sites A and B respectively. Best fit models obtained using the method described in the text are shown below each profile.

The seismic survey failed to locate the base of the rupture surface - a result which is probably due to the large dimensions of blocks comprising the slide mass. Neither of the profiles transected any of the major cracks in the slide mass and no evidence of a deep refractor appeared on any of the profiles. The absence of the refractor may be due to the short spread length since any reasonable projection of the rupture surface indicates that it lies approximately 60 m below the survey lines and the maximum spread length was 150 m. The absence of any velocity anisotropy in the lower layer, however, suggests that this unit is intact and thus the rupture surface may not be detectable using conventional refraction techniques.

Electrical resistivity soundings were conducted at two sites using an expanding Schlumberger array with current electrode spacings of between 20 and 240 m at 20 m intervals. Apparent resistivity profiles for the two sites are shown in Figure 11 (e)-(f). The data was inverted using a resistivity interpretation technique suggested by Koefoed (1979) since more than two layers were present in the profile at site B and since master curves for such cases are not readily available. The technique is not in common use but can be easily derived from first principles as shown below.

The potential distribution for any dipole array may be determined using superposition of the potentials for two isolated current sources. For the region free of current sources

$$\nabla \cdot \mathbf{E} = 0 \tag{1.3}$$

For very low frequency or direct current flow, magnetostatic conditions apply. Thus

$$\nabla \times \mathbf{E} = -\frac{\partial \mathbf{B}}{\partial t} = 0 \tag{1.5}$$

As a consequence, a scalar potential (φ) may be defined and Laplace's equation can be applied to the source-free region

$$\nabla^2 \varphi = 0 \tag{1.6}$$

Following Koefoed (1979), consider a current source at the origin of a cylindrical coordinate system with an associated current sink at infinity. In such a case, the potential is a function only of distance from the source or, equivalently, r and z

$$\frac{\partial^2 \varphi}{\partial r^2} + \frac{1}{r}\frac{\partial \varphi}{\partial r} + \frac{1}{r^2}\frac{\partial^2 \varphi}{\partial z^2} = 0 \tag{1.7}$$

The equation can be solved using separation of variables. Setting

$$\varphi(r,z) = R(r)Z(z) \tag{1.8}$$

the following characteristic equation in r and z results

$$\frac{1}{R}\frac{\partial^2 R}{\partial r^2} + \frac{1}{Rr}\frac{\partial R}{\partial r} + \frac{1}{Z}\frac{\partial^2 Z}{\partial z^2} = -\lambda^2 = \frac{1}{Z}\frac{\partial^2 Z}{\partial z^2} \tag{1.9}$$

where λ denotes eigenvalues for which the equations may be solved. Solutions to equations in r and z are

$$R(r) = C_3 J_o(\lambda r) \tag{1.10}$$

$$Z(z) = C_1 e^{\lambda z} + C_2 e^{-\lambda z} \tag{1.11}$$

The general solution is the product of these two summed over all possible eigenvalues or

$$\varphi(r,z) = \int_0^\infty \left\langle \Phi(\lambda) e^{-\lambda z} + \psi(\lambda) e^{\lambda z} \right\rangle J_o(\lambda r)\, d\lambda \tag{1.12}$$

where $\phi(\lambda)$ and $\psi(\lambda)$ are functions replacing the specific constants used above and $J_O(\lambda r)$ is the Bessel Function of order zero. Resistivity sounding techniques are used to delineate one-dimensional models of earth resistivity and the simplest of these are multi-layer models. It is useful to explicitly decouple the effects of the current source and model geometry from each other in the general solution. The potential due to an isolated current source at the surface of a homogeneous earth can be shown to be

$$\varphi(r,z) = \frac{I\rho}{2\pi}\frac{1}{\sqrt{r^2 + z^2}} \tag{1.13}$$

(Telford *et al.* 1976, p 635). Further simplification results if Lipschitz's Integral (Bowman 1943)

$$\int_0^\infty e^{-\lambda z} J_o(\lambda r)\, d\lambda = \frac{1}{\sqrt{r^2+z^2}} \tag{1.14}$$

is used. The functions $\Phi(\lambda)$ and $\psi(\lambda)$ will be different in each layer and the general

solution for a multi-layer model can be written as

$$\varphi(r,z) = \frac{\rho I}{2\pi}\int_0^\infty \left\langle \left\langle 1 + \Theta_i(\lambda) \right\rangle e^{-\lambda z} + X_i(\lambda) e^{\lambda z} \right\rangle J_o(\lambda r)\, d\lambda \tag{1.15}$$

In a multi-layer model, five boundary conditions may be imposed. The first of these is that φ be continuous across each layer interface. If integral expressions for potential at the boundary at depth h_i are equated, then

$$\Theta_i(\lambda)e^{-\lambda h_i} + X_i(\lambda)e^{\lambda h_i} = \Theta_{i+1}(\lambda)e^{-\lambda h_i} + X_{i+1}(\lambda)e^{\lambda h_i} \tag{1.16}$$

The second boundary condition is that the normal component current density (J) be continuous across the interface. Since the interfaces are horizontal, the necessary condition is

$$J_z = \sigma E_z = \frac{1}{\rho_i}\frac{\partial \varphi}{\partial z} = \frac{1}{\rho_{i+1}}\frac{\partial \varphi}{\partial z} \tag{1.17}$$

at depth h_i. Using equation 1.15, the necessary condition is

$$\frac{1}{\rho_i}\left[\left\langle 1 + \Theta_i(\lambda) \right\rangle e^{-\lambda h_i} - X_i(\lambda)e^{\lambda h_i}\right] = \frac{1}{\rho_{i+1}}\left[\left\langle 1 + \Theta_{i+1}(\lambda) \right\rangle e^{-\lambda h_i} - X_{i+1}e^{\lambda h_i}\right] \tag{1.18}$$

No current should flow through the earth's surface and this is the third boundary condition. In this case, at the earth's surface (z=0), equation 1.15 becomes

$$E_z(r,0) = \frac{\rho I}{2\pi}\int_0^\infty \left\langle -1 - \Theta_1(\lambda) + X_1(\lambda) \right\rangle \lambda J_o(\lambda r)\, d\lambda = 0 \tag{1.19}$$

Here the separation of source and layer effects on the potential becomes useful. The potential due to source effects automatically satisfies this boundary condition since the partial derivative of equation 1.13 with respect to z, evaluated at z=0, is zero. Thus the boundary condition is satisfied if

$$X_1(\lambda) = \Theta_1(\lambda) \tag{1.20}$$

Finally, in the bottom layer, the potential must go to zero as the depth goes to infinity. This requires that the coefficient of the exponential term in equation 1.15 be zero or

$$X_n(\lambda) = 0 \tag{1.21}$$

where n refers to the last layer.

These boundary conditions give rise to 2n equations in 2n unknowns and the potential for a given model may be evaluated from

$$\mathbf{R} = \mathbf{AT} \tag{1.22}$$

where

$$\mathbf{R} = \begin{bmatrix} 0 \\ (p_1-1)u_1 \\ 0 \\ (p_2-1)u_2 \\ \cdot \\ \cdot \\ 0 \\ (p_{n-1}-1)u_{n-1} \end{bmatrix} \tag{1.23}$$

$$\mathbf{A} = \begin{bmatrix} (u_1+v_1) & -u_1 & -v_1 & 0 & 0 & \cdot\cdot & \cdot\cdot & 0 \\ (u_1-v_1) & -p_1u_1 & p_1 & v_1 & 0 & \cdot\cdot & \cdot\cdot & 0 \\ 0 & u_2 & v_2 & -u_2 & -v_2 & 0 & \cdot\cdot & 0 \\ 0 & u_2 & -v_2 & -p_2u_2 & p_2v_2 & 0 & \cdot\cdot & 0 \\ \cdot\cdot & & \cdot\cdot & & \cdot\cdot & & \cdot\cdot & \\ \cdot\cdot & & \cdot\cdot & & \cdot\cdot & & \cdot\cdot & \\ \cdot\cdot & \cdot\cdot & \cdot\cdot & 0 & u_{n-1} & v_{n-1} & -u_{n-1} & 0 \\ \cdot\cdot & \cdot\cdot & \cdot\cdot & 0 & u_{n-1} & -v_{n-1} & -p_{n-1}u_{n-1} & 0 \end{bmatrix} \tag{1.24}$$

$$\mathbf{T} = \begin{bmatrix} \Theta_1 \\ \Theta_2 \\ X_2 \\ \cdot \\ \cdot \\ \Theta_{n-1} \\ \Theta_n \end{bmatrix} \tag{1.25}$$

and

$$u_i = e^{-\lambda h_i}$$

$$v_i = e^{\lambda h_i}$$

$$p_i = \frac{\rho_i}{\rho_{i+1}} \qquad (1.26)$$

When modelling resistivity sounding data, only $\Theta_1(\lambda)$ is required since potential measurements are usually conducted at the earth's surface. The quantity $K(\lambda)=1+\Theta_1(\lambda)$ is referred to as Slichter's Kernel Function and can be evaluated using Cramer's Rule and matrices defined in equations 1.23 through 1.25. Inserting it into the relation for the potential at any boundary gives the potential at the earth's surface

$$\varphi_1(r) = \int_0^\infty K(\lambda)\, J_o(\lambda r)\, d\lambda \qquad (1.27)$$

Pekeris (1940) showed how $K(\lambda)$ can be derived from model parameters starting from the bottom layer and working back up to the earth's surface. Koefoed (1979) has simplified the derivation by extracting the necessary relations directly from the boundary conditions. If $e^{-\lambda h_i}$ is added to both sides of the boundary condition governing the continuity of current density (eq. 1.18) and then this relation is divided by the boundary condition on the continuity of potential, the following results

$$\rho_i \frac{1 + \Theta_i(\lambda) + X_i(\lambda)e^{2\lambda h_i}}{1 + \Theta_i(\lambda) - X_i(\lambda)e^{2\lambda h_i}} = \rho_{i+1} \frac{1 + \Theta_{i+1}(\lambda) + X_{i+1}(\lambda)e^{2\lambda h_i}}{1 + \Theta_{i+1}(\lambda) - X_{i+1}(\lambda)e^{2\lambda h_i}} \qquad (1.28)$$

Slichter's Kernel Function may now be generalized for subsurface layers to define

$$K_i(\lambda) = \frac{1 + \Theta_i(\lambda) + X_{i+1}(\lambda)e^{-2\lambda h_{i-1}}}{1 + \Theta_i(\lambda) - X_{i+1}(\lambda)e^{-2\lambda h_{i-1}}} \qquad (1.29)$$

and the reader will note that the boundary condition governing the potential in the bottom layer requires that $K_n(\lambda)=1$. If a recurrence relation between $K_{i+1}(\lambda)$ and $K_i(\lambda)$ could be extracted from the above two equations, it would be possible to work from the bottom up and calculate the potential at the surface resulting from a layered earth structure. With a little algebra, it can be shown that

$$K_i = \frac{K_{i+1} + p_i \tanh(\lambda t_i)}{p_i + K_{i+1} \tanh(\lambda t_i)} \qquad (1.31)$$

where $t_i = h_i - h_{i-1}$ and this constitutes the Pekeris Recurrence Relation. Koefoed (1970) introduced the Resistivity Transform, defined as

$$T_i = \rho_i K_i \qquad (1.32)$$

and rewrote the Pekeris Recurrence Relation as

$$T_i = \frac{T_{i+1} - \rho_i \tanh(\lambda t_i)}{1 + \frac{T_{i+1}}{\rho_i} \tanh(\lambda t_i)} \qquad (1.33)$$

A Schlumberger array consists of a current electrode and potential electrode pair with current electrode separation s and potential electrode separation l where s>>l. When conducting resistivity sounding measurements using such an array symmetric about its midpoint, the apparent resistivity (ρ_a) is

$$\rho_a = \frac{\pi s^2}{2l}\left[\frac{\Delta V}{I}\right] \qquad (1.34)$$

where ΔV is the measured potential and I is the applied current (Telford *et al.* 1976). O'Neill (1975) developed a discrete filter for the conversion of Schlumberger apparent resistivity measurements into values of the Resistivity Transform. Apparent resistivity is sampled at an interval of six s-spacings per natural logarithmic decade using values either measured directly or interpolated from the apparent resistivity curves with 8 predictive samples (samples at s-spacings less than the s-spacing at which the Resisitivity Transform is being evaluated) and 16 following samples being used in the filtering operation.

To invert the resistivity sounding data, values of the apparent resistivity at an interval of six per natural logarithmic decade were interpolated from the field curves and filtered to obtain values of the Resistivity Transform at eigenvalues of 1.1396/s. The dimensions of λ are the reciprocal of distance and it is at the reciprocal of the current electrode spacing that the Resistivity Transform is to be evaluated for both the model and field data. The digital filter converts the apparent resistivity at the given eigenvalue into a value of the Resistivity Transform value at a slightly offset eigenvalue. A multi-layer model consisting of up to 20 layers thicknesses and resistivities was then specified and

values of its Resistivity Transform, evaluated at the offset eigenvalue, were calculated and compared with the Resistivity Transform of the field data. Model parameters were adjusted until the Resistivity Transform of both the model and the field data agreed within 2% at all sample points. The program used in this procedure is listed in Appendix A. It was tested against analytical expressions for apparent resistivity soundings over 2 and 3 layer resistivity models in Telford *et al.* (1976) and provided satisfactory depth resolution (ie. error in depth determinations of ±10%).

Best fit models for the resistivity profiles are shown in Figure 11 (e)-(f). They seem to delineate the base of permafrost in the slide mass; the abrupt change in resistivity at around 30 m lies below the base of the weathered rock layer and above any reasonable projection of the rupture surface beneath the survey sites.

The contrast in frozen layer resistivity might be a consequence of hydrothermal alteration. McNeill (1980) states that bound water in clay minerals allows current paths to remain open in frozen rock and lowers electrical resistivity. Hydrothermal alteration of rock exposed in the headscarp was most intense near the medial crack and decreased to the west. This condition, if persistent in the subsurface, could explain the discrepancy in upper layer resistivities between the two sites.

A composite cross section displaying the results of topographic and geophysical surveys and a possible configuration of the rupture surface is shown in Figure 11. The location of the rupture surface in the headscarp and toe were fixed during a topographic survey of the slide and the base of the fractured weathered rock layer was fixed by the seismic profile on the NW to SE line.

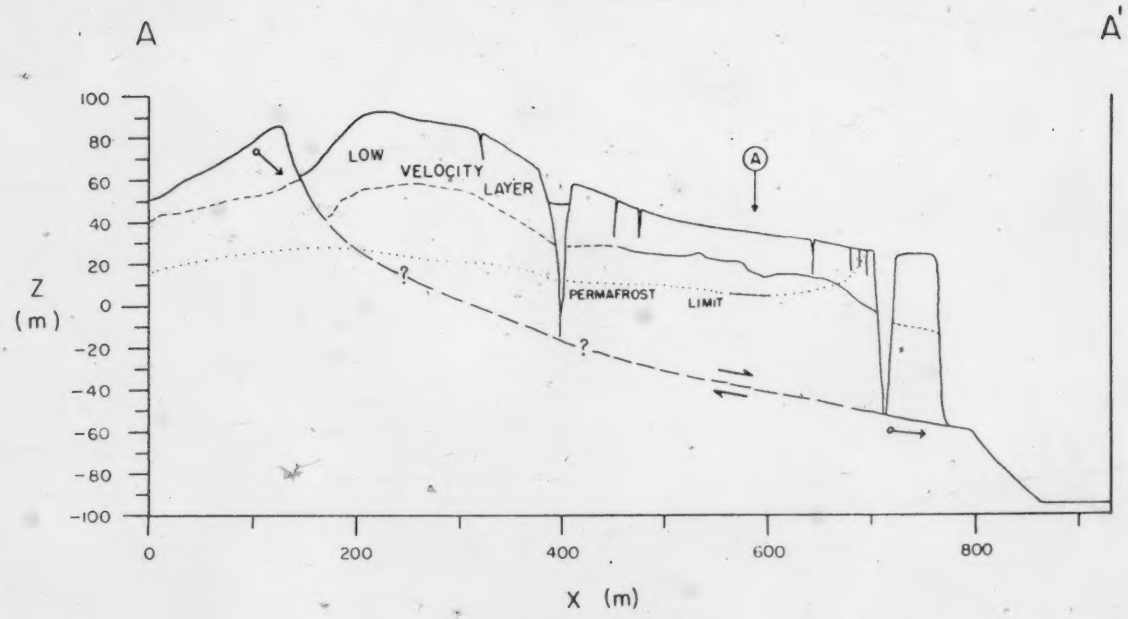

Figure 11. Composite cross-section through the Cement Creek landslide along the line A-A' in figure 6 incorporating the results of topographic, electrical resistivity and refraction seismic surveys. Boundaries are dashed where inferred. "A" indicates the resistivity sounding site and the arrows indictate the local projection of bedding into the plane of section.

Chapter 2.
Seismicity and neotectonics of the Duke River Fault, Denali Fault System, southwest Yukon[1]

2.1 Introduction

Seismicity in the southwest Yukon Territory is generally restricted to two zones; one along the Pacific/North American plate boundary and the other straddling the Denali Fault System (Figure 12, Figure 13) (Horner 1983). At the plate boundary, the Yakutat Block is being actively accreted to the North American Plate along the Fairweather, Chugach-St. Elias and Border Ranges faults and earthquakes up to magnitude 8.6 have occurred here. A lower level of seismicity with recent earthquakes up to magnitude 6.5 occurs along the Dalton, Shakwak and Duke River segments of the Denali Fault System. Historically, the greatest number of small to moderate earthquakes has occurred on the section of the Duke River Fault extending from its westward bend near the Duke River Depression to the Yukon/Alaska boundary. Displacement on the Denali Fault System is dominantly right-lateral (Campbell and Dodds 1978) but the western portion of the Duke River Fault has been mapped as a transpressional bend across which crustal shortening is occurring (Plafker *et al.* 1978). This chapter describes a survey of earthquake activity along this portion of the Duke River Fault during May - August 1987. Previous surveys of microseismicity along the Denali Fault System in the Yukon Territory have been conducted by Boucher and Fitch (1969) and Horner (1983); neither were conducted in the area described in this chapter.

2.2 Field procedure

An array of seven seismographs was installed and operated for 5 to 6 weeks at two

[1] A version of this chapter has been accepted for publication: Power, M.A. Microearthquake activity on the Duke River Fault, Denali Fault System, Yukon . Yukon Geology (in press)

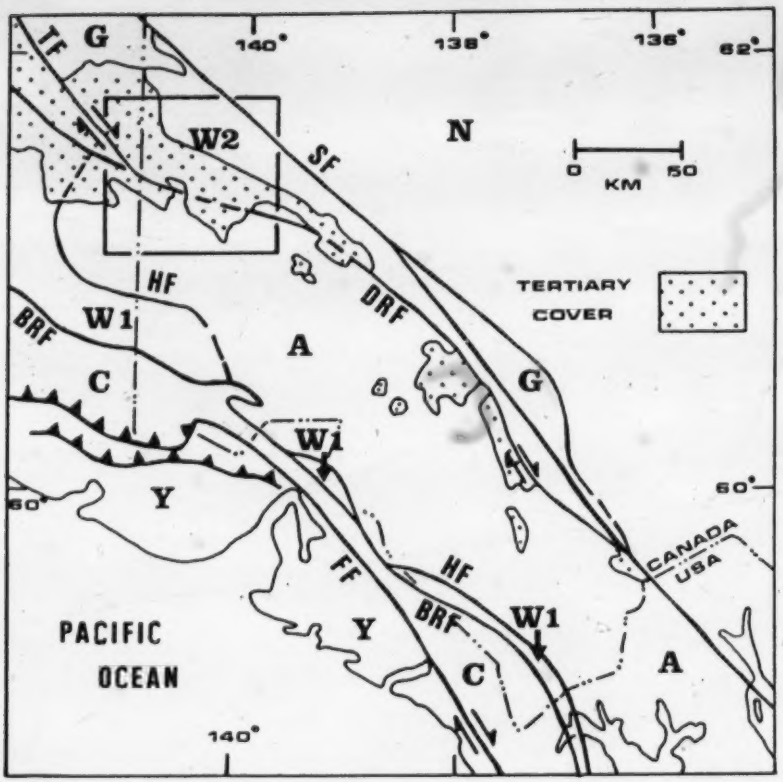

Figure 12. Tectonic elements of the southwest Yukon Territory and southeastern Alaska after Campbell and Dodds (1987). The study area is the rectangular region enclosed in the top left corner of the map. Symbols for elements of the Wrangellia Terrane;W1 and W2, Alexander Terrane; A, Chugach Terrane; C, Gravina-Nutzotin Terrane; G, Yakutat Block;Y, in-board elements of the North American plate;N, Border Ranges Fault; BRF, Hubbard Fault; HF, Fairweather Fault; FF, Totschunda Fault; TF, Duke River Fault; DRF, Shakwak Fault; SF

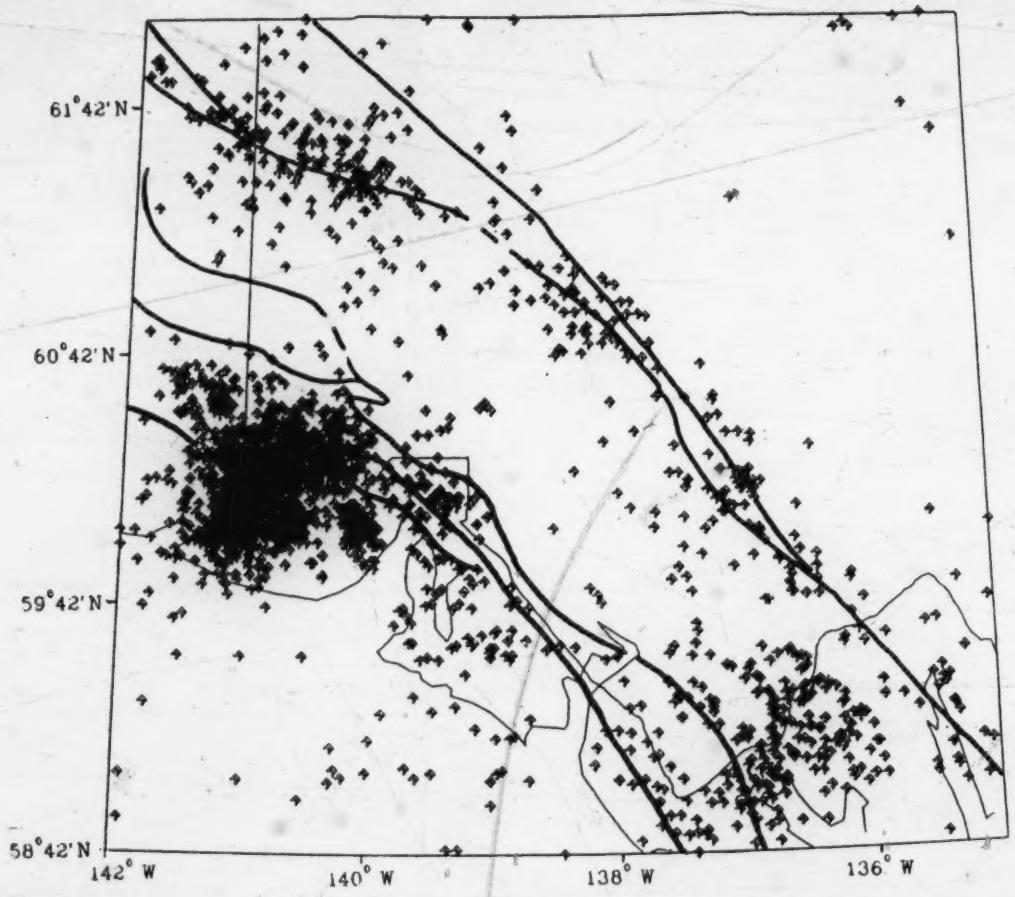

Figure 13. Seismicity in the southwest Yukon . Epicentres from the Canadian Earthquake Catalogue are shown together with fault traces.

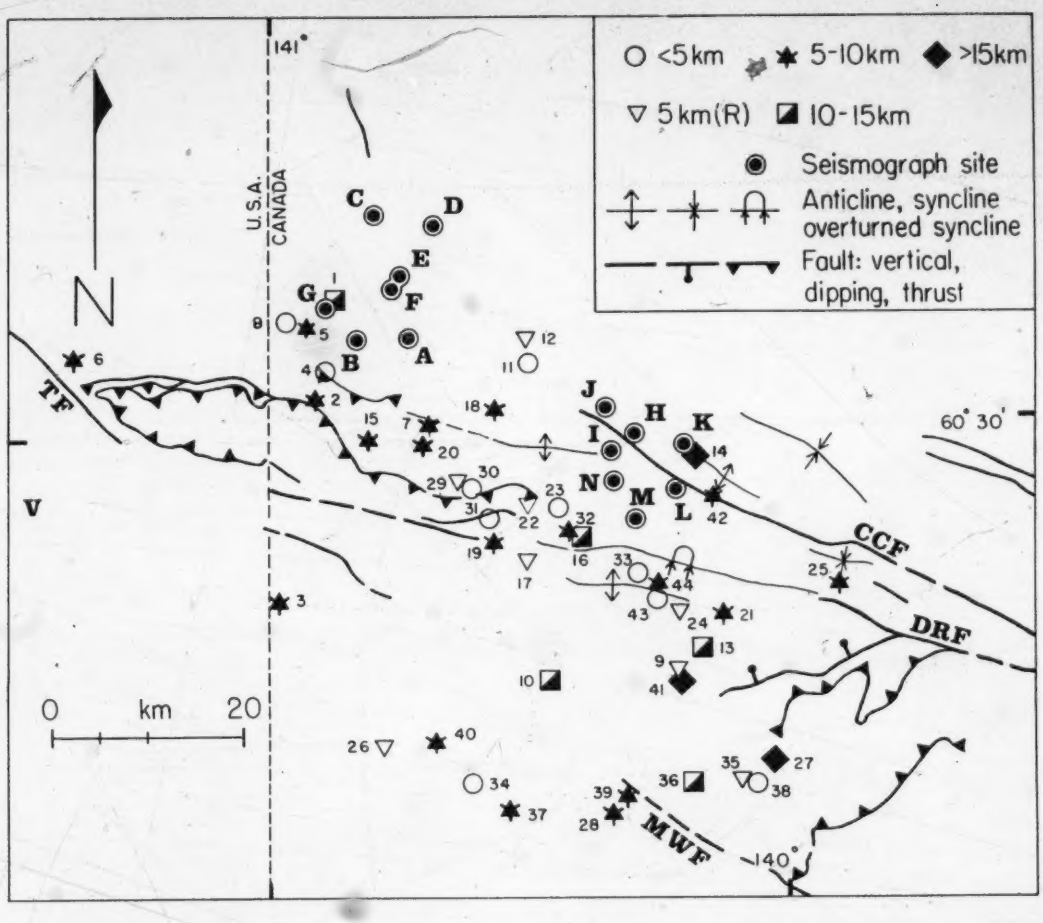

Figure 14. Seismograph sites, microearthquake epicentres coded for focal depth and geological structure in the study area. Event numbers correspond to those in Table 1.. Symbols include: TF-Totschunda Fault, DRF- Duke River Fault, CCF- Cement Creek Fault, MWF-Mount Wood Fault. V indicates the recent volcano (1400 B.P.) which is the source of the White River Ash. Geology after Campbell and Dodds (1982) and MacKevett (1978).

locations shown in Figure 14. Sites A-G were located near Big Boundary Creek and operated from May 22, 1987 to July 2, 1987 and sites H-N were centered south of the confluence of St.Clare and Bull Creeks and operated from July 5, 1987 to August 13, 1987. The array consisted of 2 Sprengnether DR-100 and 2 Teledyne MCR digital event recorders and 3 Sprengnether MEQ-800 smoked paper drum seismographs; one MCR was configured with one vertical and two horizontal seismometers whereas the rest were equipped solely with vertical component seismometers. Digital event recorders are triggered by ground motion exceeding backround noise by a preset amplitude and record the 1.5 seconds of signal preceeding the trigger together with subsequent high amplitude ground motion whereas the drum seismographs provide a continuous record of ground motion. The array bandwidth was 29.75 Hz with a low cut at 0.25 Hz; individual instruments had wider response characteristics. Instrument gain varied between 66-78 dB depending upon site conditions and the level of microseisms. Seismograph sites were serviced every 1-4 days and this schedule together with terrain conditions limited the size of the networks. To ensure accurate timing, 2 Benest Portable Precision Clocks were synchronized daily with WWV and used to drift-correct seismograph clocks.

The smoked paper seismographs provided continuous coverage and produced the most useful records for the purpose of this study. Cool wet weather had a deleterious effect upon the performance of the digital event recorders causing rapid battery deterioration and often large clock drifts. Limited tape and pre-event buffer capacity also restrict the usefulness of such instruments in reconnaissance studies because site noise or teleseismic earthquakes can fill tapes rapidly and emergent P-wave onsets from local earthquakes are often not recorded if the S-P separation exceeds the buffer capacity. Earthquakes located in this study were usually detected by three of the smoked paper instruments and by up to two of the digital event recorders.

2.3 Data analysis

A total of 146 earthquakes were detected at one or more sites during the course of this study. Impulsive, high amplitude P and S-wave arrivals were timed to within ±0.05 s and ±0.2 s respectively; arrivals of lesser quality had larger errors and were weighted accordingly. All arrivals were corrected for clock drift using double interpolation to correct for portable clock drift with respect to WWV and seismograph clock drift with

respect to the portable clock. DR-100 and MEQ-800 seismograph clock drifts rarely exceeded 20 ms per day but MCR clock drift occasionally exceeded 100 ms per day and appeared to be disconcertingly non-linear. Arrivals detected at MCR sites were only used in solutions when their drift corrected arrival times were consistent with those recorded at surrounding stations.

Most earthquakes occurred outside of the detecting array and this created difficulty in determining focal coordinates. Least-squares methods often fail to converge to an acceptable solution when an event is outside of an array or when no site is closer to the epicenter than the focal depth (Lee and Stewart 1981). The time difference residual method eliminates origin time from the problem as an explicit variable and uses the geometry of the incoming body waves to locate the focus. Convergence to a solution using a combined geometric and gradient search is possible under conditions where least squares solutions may fail.

Consider an array of n stations at which P and S arrivals t_{p_k} and t_{s_k} { k=0,1,2...n} are recorded. For a trial focus and origin time theoretical arrival times $t^*_{p_k}$ and $t^*_{s_k}$ may be calculated. The difference in arrival times between stations i and j denoted as $t_{ij}=t_i-t_j$, and the S-P separation at each station $t_{sp_i}=t_{s_i}-t_{p_i}$ may be calculated for both the actual data and the trial focus. These quantities together with weighting factors for each recorded arrival (w_{p_i},w_{s_i}) may be used to define a time difference residual

$$\tau = \sqrt{\frac{1}{2}\sum_{i=1}^{n}\sum_{j=1}^{n}\left\{ w_{p_i}w_p\left(t_{p_{ij}} - t^*_{p_{ij}}\right)^2 + w_{s_i}w_s\left(t_{s_{ij}} - t^*_{s_{ij}}\right)^2\right\} + \sum_{i=1}^{n}\left\{ w_{s_i}w_s\left(t_{sp_i} - t^*_{sp_i}\right)^2\right\}}$$

(2.1)

This form of residual depends only on the geometry of the incoming body wave with terms in the summation affected to various degrees by the azimuth, radial distance and depth of the focus.

The distribution of the residuals in space gives some insight into ambiguities in the earthquake location problem and suggests a method for locating a global minimum. Figure 15 displays contoured time difference residuals in the XY, YZ and XZ planes containing the focus of an earthquake located 20 km from a 10 km wide 4 station array. In this initial test, S-P times were not incorporated into the residual calculation. The solution space

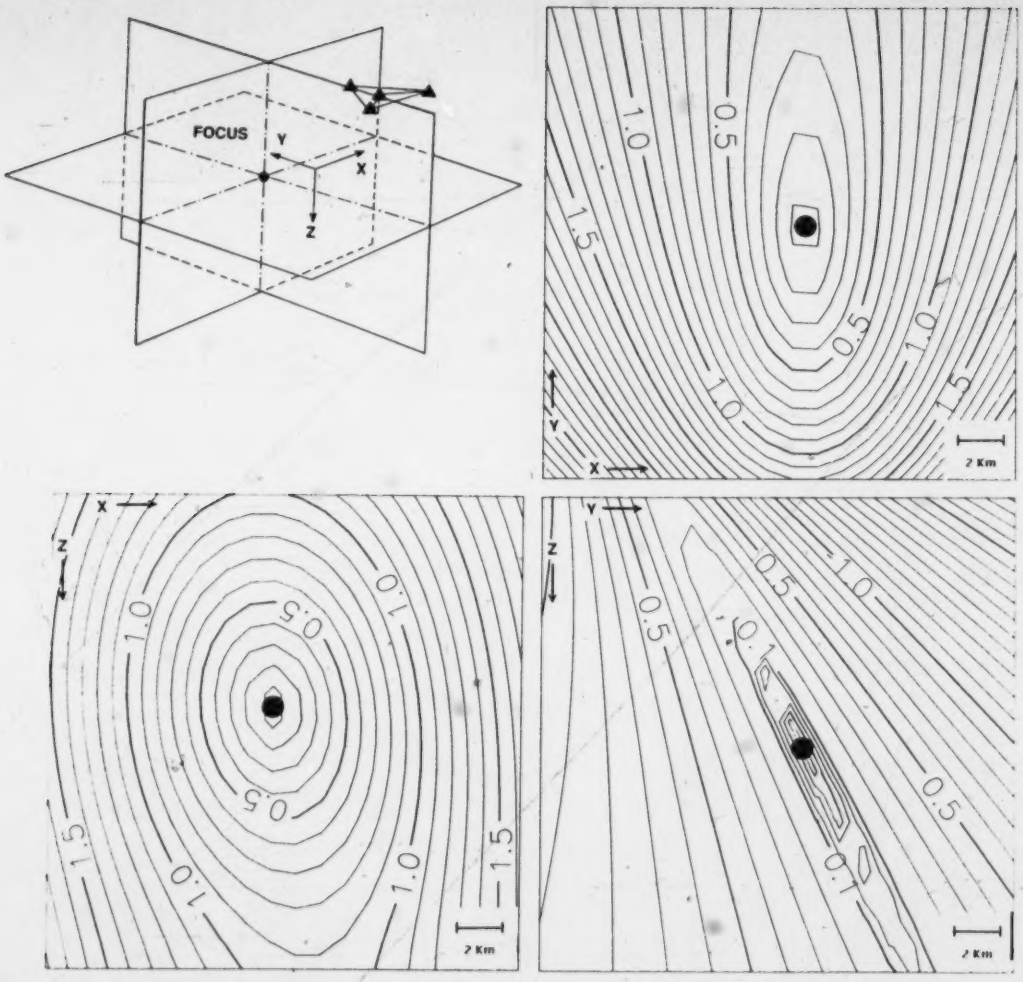

Figure 15. Time difference residuals surrounding a focus outside of a small seismograph array. Array width is 10 km and the focus is at an epicentral distance of 20 km and depth of 15 km. Residuals are contoured in the XY, YZ and XZ planes at a contour interval of 0.1 s. To clarify the shape of the solution space and the local gradient in the YZ plane, the contour interval below the 0.1 s level is 0.02 s.

consists of an elongate envelope axisymmetric with respect to a radial vector connecting the center of the array with the focus. There is a strong gradient with respect to radial vector azimuth, an intermediate gradient with respect to focal depth and a weak gradient with respect to radial distance. This pattern is largely independent of the station configuration and is slightly modified in more complex velocity models. For example, the axisymmetric region surrounding foci near a boundary may be "refracted" along the interface if the velocity contrast is high. The trade off between radial distance and depth has been documented by Uhrhammer (1980). For a similar tripartite array he found a high correlation between X and Z where the XZ plane parallels the radial vector. The case of a spherical wave incident on a square array provides an explanation for this effect in the TDR distribution by segregating the influence of radial distance and focal depth from that of azimuth (Figure 16). The time differences t_{AC} and t_{BD} could be caused by either the curvature of the incident wave or the inclination of the radial vector from the horizontal. The ambiguity between focal depth and radial distance can be mitigated by increasing the contrast in station elevation. The strong azimuthal gradient arises from the fact that changes in the azimuth of the radial vector affect all time differences in the array whereas variations in radial distance and focal depth affect only t_{AC} and t_{BD}. In the general case the arrival time difference between any two stations will be influenced by all of these factors to various extents but azimuthal variation will outweigh the other two factors in the overall time difference residual. In test with real data it was found that perturbations in the order of arrival times caused by either timing errors or deviations of the earth's velocity structure from that assumed in the models caused the location program to search for a best fit plane wave solution (ie. a focus at infinity) and for this reason S-P times were subsequently incorporated into the residual calculation. This modification changes the shape of the solution space somewhat but does not invalidate the above remarks.

Since time difference residuals are solely a function of spatial coordinates, geometric search techniques may be applied to the earthquake location problem. We found that the combination of a geometric search to locate the general area of the global minimum and a modified conjugate gradient search to pinpoint it worked satisfactorily. The geometric search consisted of evaluating the residual at the corners and center of a cubic search volume, selecting the minimum and reconstructing a reduced search volume about this point. The process was repeated until the search volume had contracted to a cube of $0.001 km^3$. This generally locates a search point near or in the axial region of the global

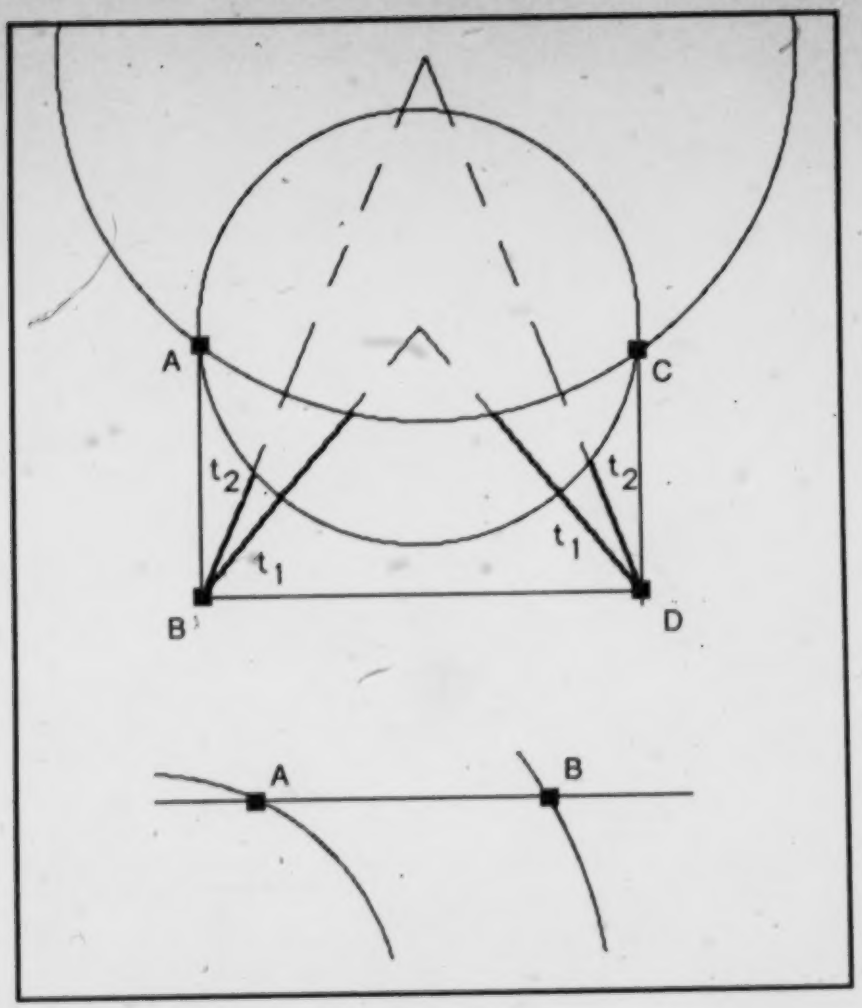

Figure 16. A cause of the ambiguity in the determination of radial distance and focal depth. Variation in azimuth of the incoming wave will cause variations in all time differences in the array. Variation in radial distance and focal depth affect only affect the time differences t_{BD} and t_{AC} and variations in these time differences can be produced by variation in the radius of curvature of the wave front (ie. varying radial distance) and/or inclination of the incoming wave as a consequence focal depth. The ambiguity is reduced if stations are at different elevations.

minimum. The contrast in axial and transverse gradients prevents the application of a steepest descent search: Such a procedure causes the search point to oscillate transverse to the axis and make very slow progress along it. In 3-D space, a parallel tangent (PARTAN) search restarted after every third leg behaves like a conjugate gradient search (Luenberger 1973) and exhibits better convergence behavior. A suitable cutoff value for the search is

$$\tau_{cut} = \sqrt{\frac{1}{2}\sum_{i=1}^{n}\sum_{j=1}^{n}\left\{w_{p_i}w_{p_j}\left(\Delta t_{p_i} + \Delta t_{p_j}\right)^2 + w_{s_i}w_{s_j}\left(\Delta t_{s_i} + \Delta t_{s_j}\right)^2\right\} + \sum_{i=1}^{n}\left\{w_{s_i}w_{s_j}\left(\Delta t_{s_i} + \Delta\, t_{p_i}\right)^2\right\}}$$

(2.2)

where Δt_{p_i} and Δt_{s_i} are standard errors in P and S arrivals. Once a suitable solution has been found, origin time is back calculated using the average of the recorded arrival times less the travel times from focus to array stations.

This algorithm has been tested using synthetic data (Figure 17). A tripartite array with station spacing of approximately 10 km and maximum elevation contrast of 1 km was tested with synthetic P and S arrivals rounded to ±0.01 s for foci at distances of 20 and 40 km from the center of the array. Focal depths were varied between 0 and 30 km using a non-linear function of the focal X and Y coordinates in a velocity model consisting of a half-space (V_p=6.0 km/s, V_s=3.5 km/s). Histograms of error in focal coordinates and Euclidean distance from calculated to true focus illustrate that the method breaks down somewhat at distances between 2 and 4 array widths. In practice this occurs most readily for foci near planes of symmetry. In general, small timing errors and errors in weighting translate into large errors in focal coordinates.

The earthquakes detected in this study were located using the velocity model determined by Stephens *et al.* (1984). This minimized residuals in a limited test data set and is probably the best regional velocity model available. Focal coordinates of earthquakes more than 2 array widths from the center of the detecting array are considered accurate to ±5 km while focal coordinates of events nearer the arrays are probably accurate to ±3 km. A number of events had focal depths restrained to 5.0 km but this did not significantly alter their epicentral coordinates.

2.4 Results

Focal coordinates and time-difference residuals of earthquakes detected in this study

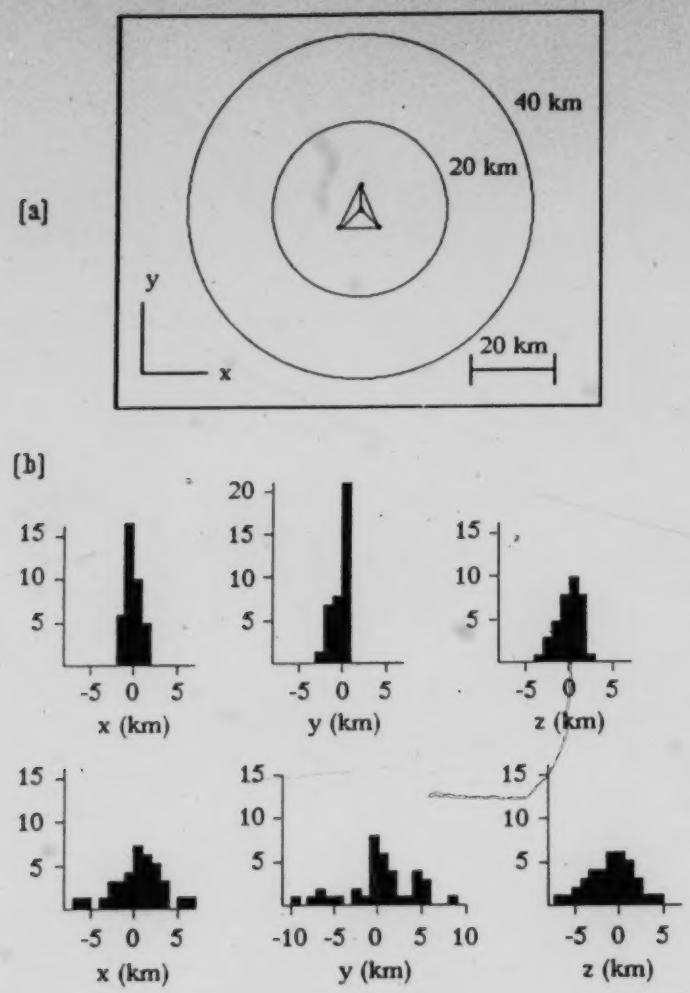

Figure 17. Test of the time difference residual method using earthquakes in a half-space velocity model and a 10 km wide tripartite array. (a) Array configuration showing coordinate axes (positive z is down). Test earthquakes with epicentres 20 km and 40 km from the centre of the array are located at 10° intervals on the circles. (b) Histograms of error in focal coordinates. Error in focal coordinates for the set of earthquakes 20 km from the centre of the array are shown on the top row and for the set 40 km from the centre of the array on the bottom row.

are tabulated in Table 2 and displayed together with geological structures in Figure 14. Most events are located near the Duke River Fault and structures associated with it. Very little activity was detected near the Totschunda Fault but this may be a consequence of the distance of the arrays from this feature. The central portion of the map area is underlain by a deformed succession of calc-alkalic volcanic rocks (Neogene Wrangell Lavas) and by basement rocks of the Wrangellia and Alexander Terranes juxtaposed along the Duke River Fault. The Tertiary rocks are most intensely deformed in a wide zone astride the exposed and buried trace of the Duke River Fault and most of the detected seismicity occurs here.

A number of events are located in the Icefield Ranges, a rugged region south of the Duke River Fault where extensive glaciers limit geological mapping. Ten events on July 31 and August 6, 1987 define an arcuate band of seismicity which originates near mapped faults south of the Duke River Fault and extends to the west for 40 km, cutting across the inferred trace of the Mt. Wood Fault (Campbell and Dodds 1987). North of the Duke River Fault and its associated structures, a small number of earthquakes were located beneath the Wolverine Plateau and the valley of the White River, a low-lying region covered by undisturbed Quaternary surficial deposits.

All but three of the located earthquakes had focal depths less than 15 km. Event 41 was an isolated earthquake detected nearly simultaneously at sites H, J, K and N which yielded a focal depth of 36 km. No deep focus events have been detected in this area by the regional network (R. Horner 1987, personal communication) but deep earthquakes have been detected beneath Quaternary volcanoes 100 km west of this site (Stephens *et al.* 1984). A recent (1400 yr B.P.) volcano, located at the western edge of the map in Figure 14, is responsible for the deposition of the White River Ash throughout much of the Yukon and southeastern Alaska. Muller (1967) noted that intrusive activity in this area is localized along the Duke River Fault and attributed the White River Ash volcano to alkalic magmatism during the waning stages of arc volcanism. The three deep events may arise from this cause since they are below the seismogenic zone (~15 km) and above any reasonable eastward projection of the Alaska Benioff Zone.

The paucity of earthquakes north of the Duke River Fault is partially the result of technical problems encountered during the operation of the Boundary Creek array. Figure 18(a) is a histogram of S-P separations for unlocated events detected at both arrays. The

Table 1. Focal coordinates and time difference residuals for events detected at the Boundary Creek and St. Clare Creek arrays.

Event	Date	Time (UTC)	UTM	X (km)	Y (km)	Z (km)	Residual	n-m
1	June 7,1987	10:19:56.7	EU	6.86	31.56	12.69	0.00	0
2	June 12, 1987	13:04:27.9	EU	4.95	21.62	6.21	1.56	2
3.	June 12, 1987	18:04:58.9	EU	1.16	0.60	7.91	1.18	1
4	June 25, 1987	00:38:40.5	EU	5.70	24.00	4.33	0.55	1
5	June 25, 1987	16:35:08.7	EU	4.09	29.4	5.24	1.10	1
6	June 29, 1987	09:08:37.9	DU	79.61	25.85	8.06	0.63	0
7	June 30, 1987	09:01:26.3	EU	16.86	18.93	8.32	0.04	0
8	June 31, 1987	18:11:39.7	EU	1.98	29.69	4.81	0.59	3
9	July 17, 1987	01:58:52.6	ET	42.87	93.25	5.00(R)	1.62	2
10	July 21, 1987	05:06:45.0	ET	29.53	92.25	13.15	1.82	2
11	July 22, 1987	12:00:08.8	EU	27.35	25.36	4.10	0.75	2
12	July 22, 1987	12:01:49.5	EU	27.06	28.10	5.00(R)	0.74	2
13	July 27, 1987	08:06:44.7	ET	45.40	95.84	10.43	0.82	2
14	July 27, 1987	08:11:15.8	EU	44.62	15.76	20.72	0.57	1
15	July 27, 1987	10:22:06.5	EU	10.59	17.47	6.55	1.44	1
16	July 27, 1987	23:31:36.8	EU	31.95	7.71	10.73	0.50	1
17	July 28, 1987	14:48:10.2	EU	27.17	4.89	5.00(R)	0.59	1
18	July 29, 1987	12:04:02.0	EU	23.82	20.63	8.89	0.74	1
19	July 29, 1987	17:40:45.6	EU	23.72	6.80	6.69	0.25	2
20	July 29, 1987	23:19:35.8	EU	16.25	16.88	6.25	0.30	0
21	July 30, 1987	18:14:49.3	ET	47.58	99.45	6.58	1.89	3
22	July 30, 1987	18:15:25.2	EU	27.28	10.65	5.00(R)	0.86	1
23	July 30, 1987	23:38:29.4	EU	30.41	10.37	-0.31	1.10	1
24	July 31, 1987	08:34:57.0	ET	43.01	99.71	5.00(R)	0.38	1
25	July 31, 1987	09:10:33.8	EU	59.58	2.60	7.50	3.20	3
26	July 31, 1987	09:11:35.7	ET	12.20	85.6	5.00(R)	1.10	1
27	July 31, 1987	09:12:21.9	ET	52.88	84.09	17.31	0.51	1
28	July 31, 1987	09:16:09.9	ET	36.06	78.62	7.75	1.15	2
29	July 31, 1987	13:09:50.5	EU	19.92	13.17	5.00(R)	1.11	2
30	August 1, 1987	15:53:57.7	EU	21.44	12.29	3.21	0.67	1
31	August 1, 1987	15:24:39.8	EU	23.38	9.08	4.00	1.14	1
32	August 1, 1987	18:58:39.5	EU	31.56	7.94	7.56	0.24	0
33	August 2, 1987	03:13:08.2	EU	38.72	3.50	3.45	0.59	1
34	August 6, 1987	14:14:39.4	ET	21.51	81.64	4.47	0.59	2
35	August 6, 1987	14:15:01.5	ET	49.49	81.90	5.00(R)	0.24	1
36	August 6, 1987	14:15:40.7	ET	44.44	81.64	13.14	1.30	1
37	August 6, 1987	14:16:05.8	ET	25.34	79.02	7.42	0.85	2
38	August 6, 1987	14:16:34.9	ET	51.09	81.64	2.23	0.88	1
39	August 6, 1987	14:17:58.7	ET	37.51	80.4	5.07	0.96	2
40	August 6, 1987	14:29:41.1	ET	17.59	85.99	6.40	2.80	2
41	August 7, 1987	09:39:20.3	ET	43.17	92.34	36.64	0.96	2
42	August 7, 1987	21:07:16.8	EU	46.49	11.77	6.73	1.51	2
43	August 11, 1987	05:23:36.1	EU	40.73	0.81	4.26	0.86	1
44	August 12, 1987	05:47:12.2	EU	40.8	2.61	6.89	0.51	1

Notes: (1) Datum plane is sea level. (R) indicates depth restrained solution.

(2) n-m denotes the degree of freedom; the number of recorded arrivals less the number of arrivals required for an exact solution.

(3)UTM Grid denotes the Universal Transverse Mercator grid zone designation used by the National Topographic Service, Energy Mines and Resources Canada. X,Y and Z coordinates denote distances from the UTM grid origin

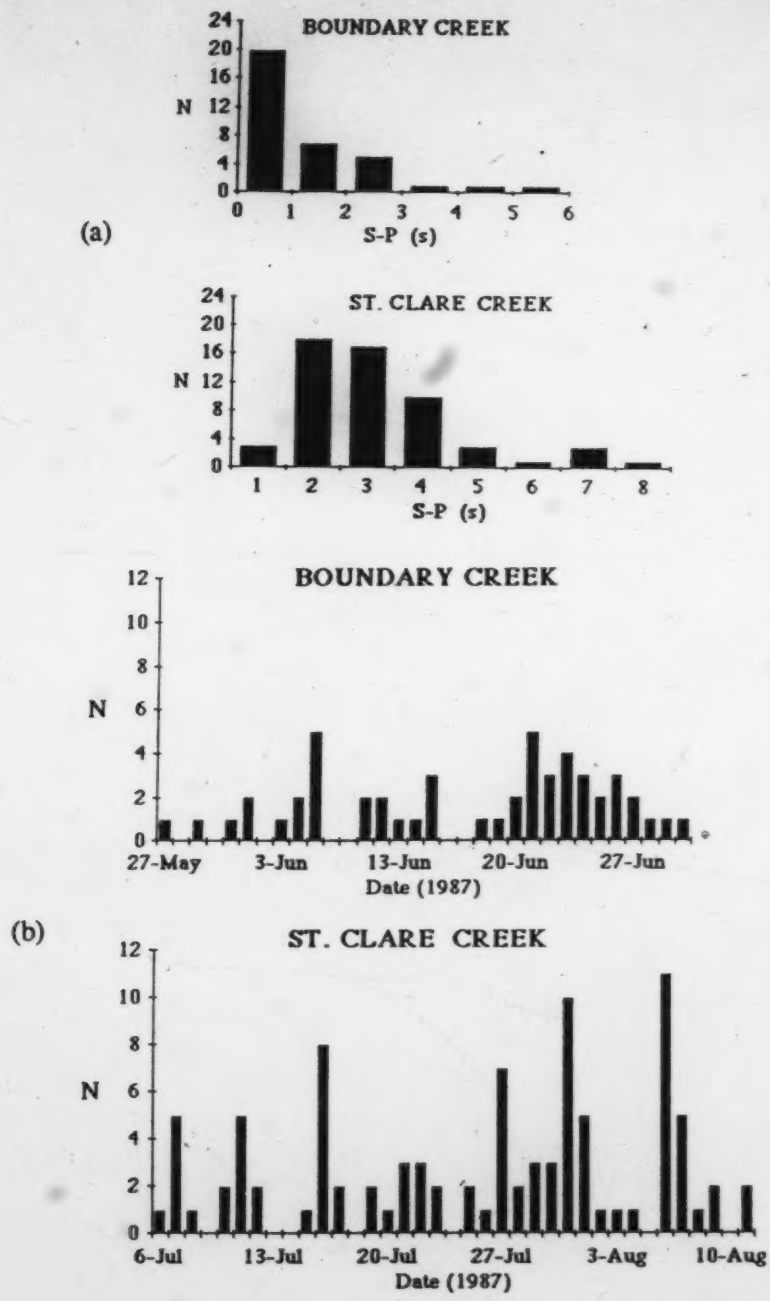

Figure 18. Histograms of S-P separation and daily earthquake frequency. (a) Histograms of S-P separations for unlocated earthquakes at both arrays. N is the number of events. (b) Daily frequency of earthquakes at both arrays. All events are included.

large number of events with S-P separations of 0-1 s recorded at Boundary Creek indicate that significant shallow earthquake activity occurs beneath the Valley of the White River. The pattern of S-P separations recorded at the St. Clare Creek array is consistent with the distribution of earthquakes recorded there; most are 10-30 km from the array along the length of the Duke River Fault .

The temporal pattern of earthquakes is characterized by bursts of seismicity. (Figure 18(b)). The sequences recorded on July 31 and August 6, 1987 define the 40 km long trend of seismicity beneath the Icefield Ranges and occurred between 09:11 and 09:16 hrs (UTC) on July 31 and between 14:14 and 14:29 hrs on August 6, 1987. During July and August episodes of increased activity recurred every 4-6 days.

The epicentral distributions and geological structure suggest that the study area can be subdivided into 3 domains (Figure 19): (1) A northern domain, centered the valley of the White River and, by extension, the Wolverine Plateau, characterized by relatively shallow seismicity, (2) a central domain straddling the Duke River Fault and associated structures north of it, and (3) a southern domain, centered on the Icefield Ranges.

Axial traces of major faults and folds are essentially parallel in the central domain and this suggests that the relationship between earthquake foci and geological structures may be clarified by projecting hypocentres up or down a vector parallel to the structural trend. This procedure was performed using TRIPOD (Charlesworth *et al.* 1987) for foci in all 3 domains using horizontal projection vectors parallel to the mountain front separating the north and central domains in the north domain, the mean structural trend in the central domain, and the mean trend of the July 31 / August 6, 1987 earthquake sequences in the south domain. Lines of section and projection vectors are indicated in Figure 19 and the sections are shown in Figure 20. The trend of the projection vector in the central domain could vary by $\pm 5^{o}$ but this will not seriously alter the distribution of foci as most are near the projection plane.

No conclusive results can be inferred from projections in the north and south domains; the association between earthquake foci and the Mt. Wood Fault is coincidental. In the central domain, seismicity is concentrated beneath the Duke River Fault and structures north of it in a zone approximately 15 km wide. Earthquakes in this domain are well located and the distribution of foci suggests that a complex zone of disruption rather than a single fault or set of discrete faults exists in the subsurface.

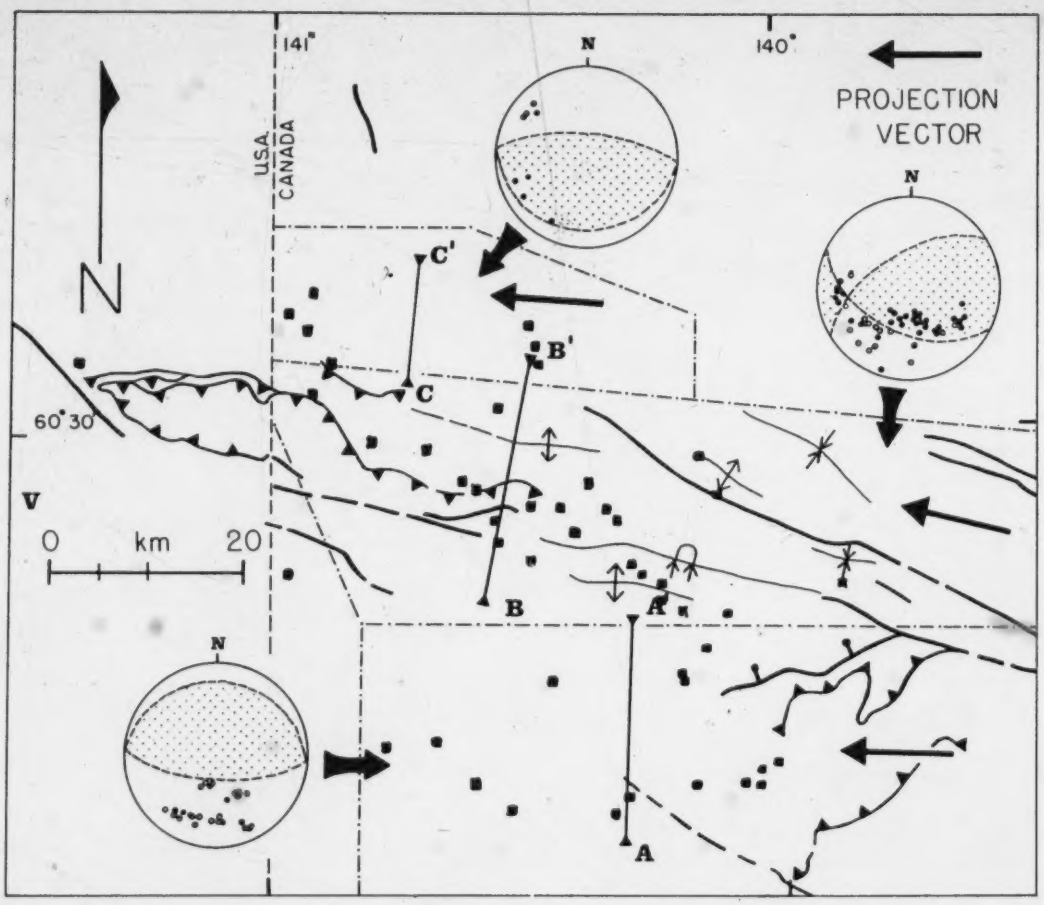

Figure 19. A subdivision of the study area based on microseismicity and geological structure. A-A', B-B' and C-C' are the traces of vertical projection planes in the south, central and north microseismicity zones. Focii are projected into the projection planes along the horizontal vectors shown in each domain. Equal area projections of first motions prepared using events with focal depths less than 15 km show compressions as filled circles and compressional quadrants with stippling.

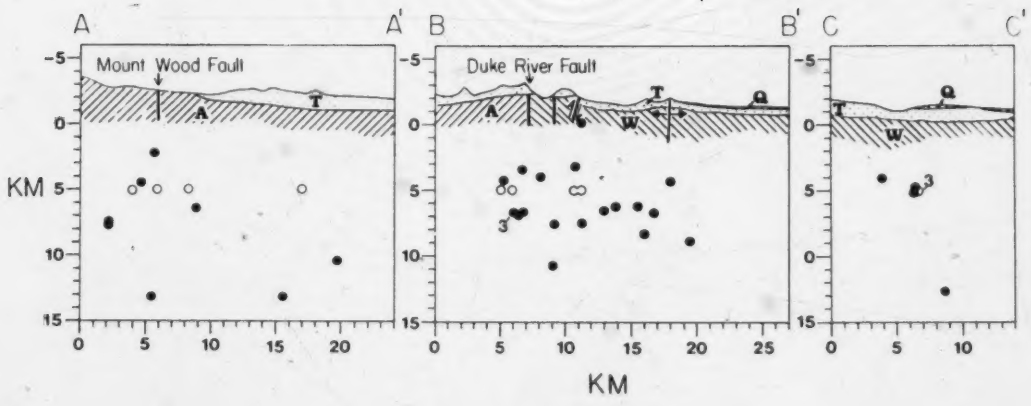

Figure 20. Cross-sections showing projections of earthquake focii into the planes of section together with the structural geology along the line of section. A-Alexander Terrane W-Wrangellia Terrane, T-Tertiary cover rocks (Wrangell Lavas), Q - Quarternary surficial deposits. Lines of section correspond to those in figure 19.

Equal-area projections of first motions and preferred composite focal plane solutions for the three domains are shown in Figure 19. Solutions involving pure strike or dip slip may be constructed for data in the north domain; the solution shown was constructed by contraining the strike of nodal planes using the trend of the mountain front separating the north and central domains. First motions from 21 earthquakes in the central domain constrain a unique solution with oblique thrusting along either 147° 30° (hanging wall up) or 25° 40° (hanging wall up). Eight of the 50 first motions are inconsistent with this solution but 6 of these are close to the focal planes and thus subject to reading errors. The southwest-dipping nodal plane contains the first of the two displacement vectors, strikes parallel to the trace of Cement Creek Fault (Skulski and Francis 1986) and the axial traces of a number of minor folds associated with it and seems to be the most probable slip plane. Antithetic faulting is not common in the map area although a splay from the Duke River Fault 10 km west of site M seems appropriately oriented. Thus slip on the other nodal plane cannot be ruled out. In the south domain, the first motion pattern is more complex with 7 compressions evenly distributed amongst 23 dilitations. The dominant first motion is dilatational and the preferred solution was constructed by setting the strike of the nodal planes parallel to the trend of the July 31, 1987 and August 6, 1987 earthquake sequences. This solution is non-unique but other solutions involving substantial components of strike slip will produce nodal planes which are oblique both to the traces of mapped faults and to the trend of the earthquake sequences. This suggests that oblique thrusting or reverse faulting probably is occurring here. Campbell and Dodds (1982) have mapped a fault of unspecified displacement dipping steeply to the north and a thrust fault cutting a small pocket of Wrangell Lavas in the northeast corner of this domain. The orientation and vergence of these two faults suggests that any current displacement will be to the south.

2.5 The historical record

Figure 21 shows the distribution of earthquakes with Local (Richter) magnitudes greater than 4.0 in the Canadian Earthquake Catalogue superimposed on the geological structure in the study area. Horner (1983) states that earthquakes occurring prior to 1965 are probably located to ±50 km whereas more recent events are considered accurate to ±25

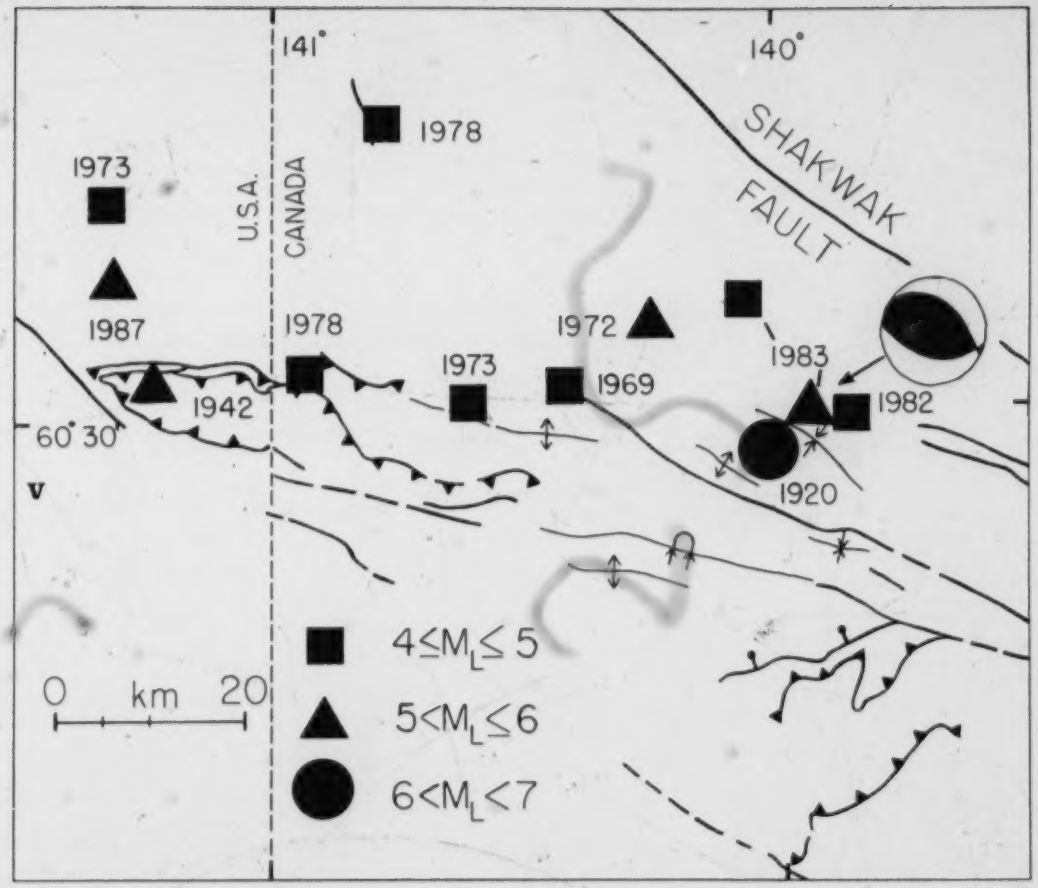

Figure 21. Epicentres of earthquakes with Local magnitudes greater than 4.0 from the Canadian Earthquake Catalogue. A focal plane solution for the March 30, 1983 M_L=5.0 earthquake prepared by the Geophysics Institute of the University of Alaska (1980) is shown.

km. Complete coverage down to magnitude 5.0 and 4.0 dates from the 1950's and 1971. Despite limitations in the historical record, the prevalence of moderate earthquakes north of the Duke River Fault and the absence of seismicity on the Shakwak Fault north of its divergence from the Duke River Fault are apparent. Even if the 1920 earthquake occurred on the Shakwak Fault, the complete record indicates relative quiescence on this feature (see Figure 13). The pattern of moderate earthquake seismicity on the Duke River Fault resembles the pattern of microseismicity; most activity is confined to the area immediately north of the Duke River Fault with some earthquakes of moderate magnitude occurring beneath the Wolverine Plateau and the valley of the White River. A catalogue of focal plane solutions for these earthquakes would be useful. The solution shown in Figure 21 for the 1983 M_L=5.0 earthquake beneath the Wolverine Plateau indicates thrust faulting along a southwest dipping nodal plane (Alaska Geophysical Institute 1984) but the constraints on this solution were not indicated. Given the absence of any vertical faults in the north domain, the prevalence of compressional features in the central zone and the transpressional nature of tectonics in the study area, oblique thrusting is the most probable prevalent focal mechanism.

2.6 Possible evidence for Holocene tectonism

No geomorphological evidence of Holocene displacement on the Duke River Fault or any of its subsidiary faults is evident in airphotography (Clague 1979) while up to 146 m of dominantly right-lateral Holocene displacement has occurred on the Totschunda Fault (Plafker *et al.* 1977). Eisbacher (1977) describes a Holocene fault scarp northeast of the Duke River Fault, south of the westward bend in the Duke River Fault. The scarp is 6 km long, has a vertical offset of about 1.5 m and follows the contact between the Oligocene Amphitheatre Formation and underlying Permian volcanic rocks. Till and fluvial deposits of indeterminate age adjacent to the Cement Creek fault (near site H - Figure 14) show evidence of tectonic disturbance (C. Dodds 1987, personal communication, Souther and Stanciu 1976). Where exposed at Bull Creek, the succession is uniformly tilted 20° to the southwest (Figure 22). Tilting does not seem to have resulted from glacial tectonism; the sediments at Bull Creek shows no evidence of internal disruption and tilting is uniform throughout the exposure. A section of approximately 400 m running from Bull Creek to

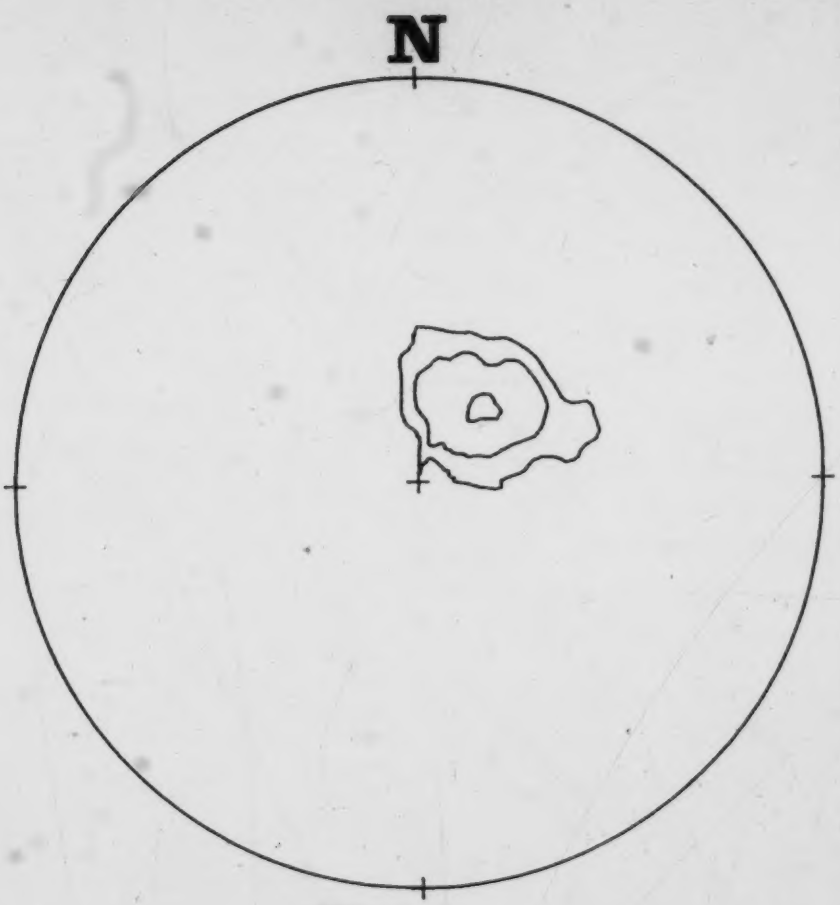

Figure 22. Structural data for tectonically distrurbed tills and fluvial deposits at Bull Creek . An equal area projection of poles to bedding measured from the base to the top of the exposed section is shown with contours denoting 5% 20% and 50% of 28 poles in a 1% counting circle. The mean pole to bedding (first eigenvalue of the distribution of orientations) is 38.7° 70.1°.

the top of the adjacent west ridge approximately 200 m north of site H (Figure 14) consists of predominant till with minor interbedded fluvial deposits and, at the base, lacustrine sediments. West of St. Clare Creek, the surficial deposits are capped by volcanic breccias and tuff (Muller 1967); this led Eisbacher (1977) to group them with Miocene-Pliocene tills intercalated with the Wrangell Lavas further west in Alaska. The stratigraphy at Bull Creek differs markedly from that described by Muller in that (1) tills rather than conglomerates predominate, (2) boulders of granite and gabbro in addition to Wrangell volcanic rocks are found in the section, (3) volcanic breccias are not present in the section and only one possible tuff bed is found and (4) the section is not capped by flow breccia and/or tuffs. Campbell and Dodds (1983) assigned an age of "Pliocene-Pleistocene(?)" to a unit comprising surficial deposits west of St. Clare Creek and at Bull Creek. Differences in stratigraphy suggest that two different deposits might be present in the area. On the basis of a brief examination of their stratigraphy, sedimentology and appearance, S Morison (1987, personal communication) has concluded that the deposits at Bull Creek are probably Late Wisconsin and thus essentially part of a blanket of Quaternary surficial deposits covering most of the low lying area north of the Duke River Fault.

Chapter 3. Conclusions

The aims, scope and methods used in the investigations described in Chapters 1 and 2 differ considerably and conclusions for each study are discussed separately.

3.1 The Cement Creek landslide

The 1983 landslide at Cement Creek underscores the well documented hazards of Tertiary volcanic rocks throughout the Cordillera. (Evans 1984, Cruden 1985 for example). Bedding appears to have exerted strong control on the location of the rupture surface and on slide kinematics. The rupture surface is at the top of a series of resistant lava flows which form a prominent ledge in the toe of the slide. This ledge, visible in airphotographs taken prior to 1983, remains intact and consequently the landslide could not have been triggered by removal of material in the toe. The upper portion of the rupture surface departs from bedding beneath the slide and appears to be concave since sod on the north slope of the hill comprising the slide mass has been destabilized by rotation. Preferential hydrothermal alteration of flow top breccias to clay creates planes of weakness between the flow units, and the rupture surface probably follows the alteration zone capping the resistant flows in the ledge. Landsliding appears to have initiated along bedding dipping at approximately 10^{o} in the toe of the slide.

The orientation of displacement vectors and the pattern of ground failure suggest that slide mass translation was accompanied by a small component of rotation. Variation in the strike of individual cracks from west to east, the narrowing of major cracks such as the medial crack, from north to south, and the narrowing of the headwall scarp crack from east to west indicate clockwise rotation of the slide mass away from the headwall scarp. This could result from the influence of non-cylindrical folding. Figure 23 displays a schematic diagram of bedding in the core of the pericline and its outcrop in the open face bordering Cement Creek. As blocks are transported down the rupture surface, the gradient in the direction of the hinge line is reduced approaching the depression of the pericline. The component of motion directed along the axis would decrease while that perpendicular to it would be relatively unaffected. A net clockwise rotation of displacement vectors would result. This effect is suggested in the displacements measured at survey sites 2B and 2C. This unusual rotation created the pattern of ground failure which led the

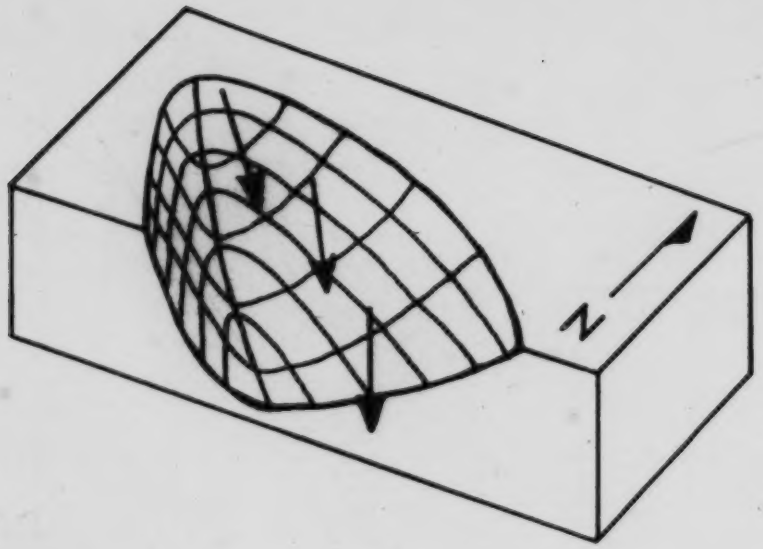

Figure 23. Schematic diagram illustrating rotation of the slide mass in the core of pericline. Vectors indicate local maximum gradient which changes as the depression is approached, resulting in clockwise rotation of descending blocks. The effect has been exaggerated.

initial observers to suggest that uplift was involved.

The plateau is underlain by continuous permafrost and experiences considerable runoff during the early summer. Unconsolidated deposits exposed in the walls of ground cracks are frozen and the depth of tree root systems suggest that annual thawing does not extend below 0.5-1.0 m. The two resistivity soundings delineated the base of permafrost at around 30m. Since much of the rupture surface lies below this depth, the influence of groundwater cannot be discounted as a factor predisposing the rocks to fail.

Ground motion during the 1983 landslide must have been locally quite intense. The ground failure west of the main slide occurred in a locality where bedrock dips into the open face and thus is not favourably oriented to landslide. In view of the fact that these cracks are structurally separate from the main landslide and seem to have originated simultaneously with it, they were probably triggered by ground motion arising from the motion of the adjacent slide. Surface investigations of the ground failure on the landslide and the results of seismic refraction work have established that the landslide is composed of large, essentially intact blocks and thus the observed shallow ground failure must result from ground motion on individual blocks rather than from breakup of the slide mass itself. Both of these phenomena indicate that locally intense ground motion occurred during the main landslide.

The uncertainty surrounding the time of landslide initiation and the lack of any direct evidence makes it difficult to determine a triggering mechanism. A combination of factors including seismicity and the influence of groundwater, rather than any single agent, seems probable given the characteristics of the local area. Although this particular landslide cannot be conclusively categorized as seismically induced, seismicity in the area must have been a contributing factor; this landslide occurred at a time of year when the area is thoroughly frozen and stream runoff minimal. A possible scenario might include ground preparation by groundwater entrapment and the consequent lowering of the effective stress at the base of the slide followed by initiation of the landslide during a burst of low magnitude seismicity.

The root cause of all landsliding in the Cement Creek area is the rapid incision of bedrock by the various drainages coupled with favourable orientation of strata bordering the creek. The topography is being rejuvenated and tectonic uplift seems to be the most probable cause. Holocene tectonic uplift has been documented on a larger scale in the immediate area by Templeman-Kluit (1980). While similar drainage rejuvination occurs in

nearby drainages (Muller 1967), it is locally most pronounced in the Cement Creek area and thus uplift in the Cement Creek area may not be due solely to a regional tectonic effect. The clustering of two major landslides and a larger number of smaller mudslides in the lower section of the valley and the coincident rejuvenation of this section of the creek suggest that rocks in the synclinal pericline are being preferentially destabilized by slow tilting.

3.2 Seismicity and neotectonics of the western Duke River Fault

Microearthquake activity, the pattern of moderate earthquake epicentres and the structural geology define 3 zones of seismicity on the western Duke River Fault. Most seismicity occurs in a central zone straddling the fault and structures north of it. The complex pattern of focii observed in projections parallel to the trend of the local structure suggests that a wide zone of faulting exists beneath structures in the deformed Tertiary cover. Shallow seismicity occurs beneath low lying areas north of the Duke River and Cement Creek faults and a number of moderate earthquakes have been been reliably located in this zone. A southern zone, centred on the Icefield Ranges, is characterized by a low level of microseismicity, by crustal shortening along high angle reverse faults or thrust faults and by an absence of moderate earthquake activity. The July 31 and August 6, 1987 earthquake sequences appear to have resulted from failure along a single discrete structure; the two bursts of seismicity (3 events in 5 minutes on July 31 and 7 events in 15 minutes on August 6, 1987) define an arcuate trend originating near the traces of known faults. First motions and the trend of the structure in relation to the local stress field strongly suggest that it is either a thrust fault or high angle reverse fault. Both possibilities are consistent with faults observed on the eastern end of the trend.

Microearthquake activity in the central zone constrains a focal plane solution consistent with local structure and the regional tectonic setting. Displacement on the Totschunda Fault is dominantly horizontal and its mean trend (~140°) differs by approximately 7° from that of the displacement vector in the central zone (147°). The trend of the central zone displacement vector and the mean trend of the Duke River Fault (~285°) differ by approximately 42° suggesting that nearly equal components of dextral displacement and crustal shortening characterize the local tectonic regime. Horner (1983) calculated an estimated slip rate of $d \leq 1.0$ mm/yr based on the rate of seismic moment

release but given the higher level of seismicity on the western portion of the Duke River Fault, the estimate may be a lower limit . The overall pattern of earthquake activity suggests that the deformation front has migrated north from the Duke River Fault and although surficial deposits at Bull Creek may provide evidence of Holocene tectonism, this hinges on definitive dating. Holocene compression and the concomitent folding or thrust faulting of strata north of the Duke River Fault are consistent with the observed pattern of microseismicity and moderate earthquake activity in this area.

Recent models for Holocene tectonics in the Gulf of Alaska infer a connecting transform fault between the Totschunda and Fairweather faults through the St. Elias Mountains (eg. Lahr and Plafker 1980, Richter and Matson 1971). The data summarized in this report suggest that no such connection exists; faulting in the southern zone cuts across the inferred trend of this transform at a high angle, no microearthquake activity was observed at the southeastern end of the Totschunda Fault and no firm evidence of such a connecting fault exists in the regional record of epicentres (figure 14). The discrepancy between displacements on the Duke River and Totschunda segments of the Denali Fault System may be resolved if large, predominantly dextral strike-slip displacements on the Totschunda Fault and small oblique displacements along faults in a wide zone parallel to the Duke River Fault are equivalent.

The findings of this study and the existing maps can constrain a model which reconciles the disparity in apparent displacements. Its principle features are illustrated in figure 24. The Duke River Fault is assumed to be an essentially intact, vertical break in the subsurface from which subordinate faults bifurcate. These splays are assumed to be arcuate in plan, oblique northwest- or southwest-verging thrusts or reverse faults which collectively form a positive flower structure (Woodcock and Fischer 1985) centred just north of the Duke River Fault. Some of the splays outcrop and others are blind, ending in folds of overlying cover rocks; this phenomenon occurs in the study area (figure 15) where thrusts in the western part of the map change into folds in cover rocks near the St. Clare Creek array. Lobate thrust or reverse faults in basement rocks can account for the observed heterogeneity of structures along strike (Skulski and Francis 1986) and match the trend of active faulting detected in microearthquake sequences south of the Duke River Fault. Deformation would migrate progressively northward and deeper, deforming overlying strata and structures in the process; this could account for the homoclinal tilting of surficial deposits north of the Cement Creek Fault. Partitioning of the total horizontal displacement

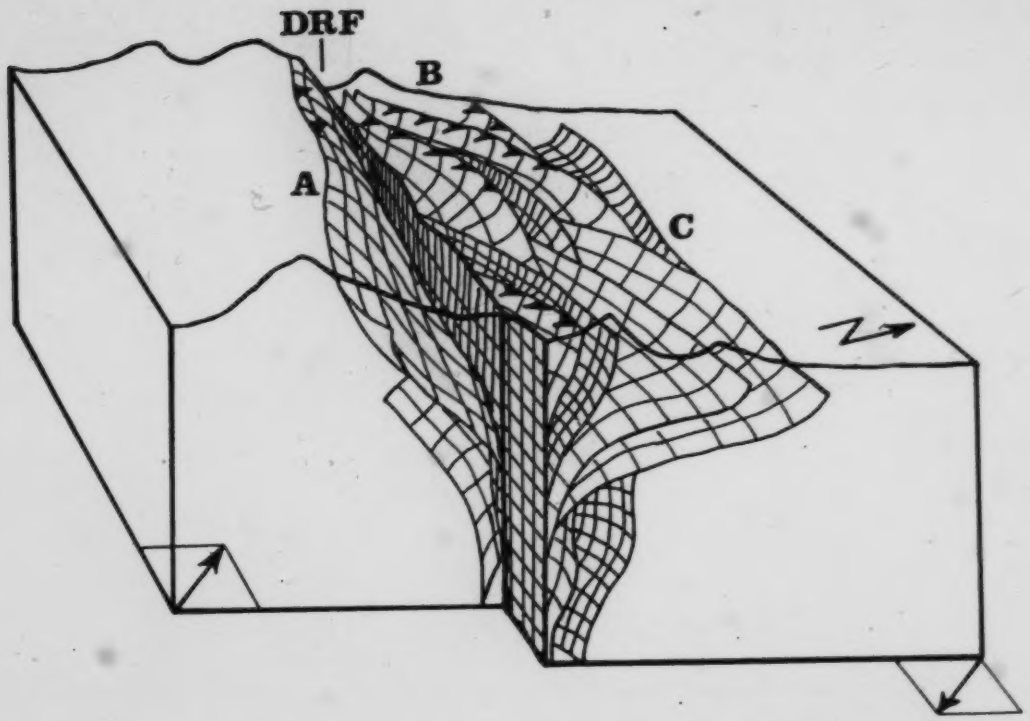

Figure 24. A schematic model for neotectonics on the western segment of the Duke River Fault (DRF). Approximately equal components of compressional and transcurrent stress along the fault create an asymmetric positive flower structure. Strain is taken up by oblique displacement on thrust and reverse faults which verge predominantly to the northeast. Faults may outcrop or merely fold the overlying rocks. Folds oblique to the trace of the faults (not shown) take up most of the transcurrent strain. A,B and C are the south, central and north zones of seismicity discussed in the text.

among a number of separate compressional faults will create oblique folds rather than wrench faults in overlying cover rocks because the areal horizontal strain density will be reduced: This phenomenon is described by Lowell (1972) and occurs near the Cement Creek Fault where folds trending approximately 20° from its strike are present (Campbell and Dodds 1983). Displacements on individual faults will be small and striking horizontal separations such as those observed on the Totschunda Fault will be absent. No significant Holocene displacement is observed on the Duke River Fault southeast of the area discussed in this study, and in all probablility displacement dies out eastwards along strike between the Totschunda Fault and the southeastern segment of the Duke River Fault.

The pattern of seismicity predicted by this model matches that observed in the historical record. The largest earthquakes would occur on the least disupted and youngest faults north of the Duke River Fault. Compressional earthquakes on southwest-dipping fault planes would predominate and the distribution of epicentres would be diffuse. Recurrence relations for the Denali Fault System predict average recurrence intervals of 11 and 43 years for earthquakes of magnitude 5 and 6 respectively (Horner 1983). The only portion of the fault zone which has not experienced a moderate earthquake in the recent past is the segment near the Klutlan Glacier and seismic gap theory suggests this might be the site of the next significant rupture. A major earthquake south of the Duke River Fault cannot be ruled out, particularly since a large active fault exists beneath the Icefield Ranges. In the long term, however, the most hazardous areas may be at the east and west end of the bend in the Duke River Fault. Gelfand *et al.* (1976) applied pattern recognition techniques to the historical seismicity record in California and in the area of the Transverse Ranges identified dangerous (D) zones at the east and west ends of the big bend in the San Andreas Fault. In these zones, the epicentres of major earthquakes (M>6.5) are likely to recur; the technique does not predict the direction of rupture or rupture dimensions. In the case of the transverse ranges they infer that the rupture propagates from along a fairly smooth contiguous section of the fault. The D zones seem to occur most commonly at the intersection of faults or at inflections of a major fault where subsidiary splays develop. The results of the present study suggest that the point of initiation for major earthquakes on this segment of the Denali Fault System might be at either end of the western Duke River Fault (ie. the Burwash Uplands or the western Klutlan Glacier) and that such earthquakes will rupture the Totschunda or southeastern Duke River Faults rather than the bend itself.

Most detected seismicity occurred at depths consistent with the hypothesis of crustal

shortening and strike slip faulting (≤ 15 km) but three somewhat deeper events may be caused by magmatic sources in the lower crust. Stephens *et al.* (1984, figure 3) documented earthquakes at focal depths of 10 to 30 km beneath Quaternary volcanoes 80 km west of the Yukon/Alaska boundary and a recent (1400 yrs BP.) volcano is located in the western part of the study area. The deep events are tentatively ascribed to this cause and the low level of deep seismicity suggests that any recurrence of volcanic activity is unlikely.

3.3 Discussion

The St. Elias Mountains in the southwest Yukon are the product of regional tectonic compression at the plate boundary and local compression along segments of the Denali Fault System. Eisbacher and Hopkins (1977) and Templeman Kluit (1980) have described the effects of uplift on the stratigraphy and structure of the area and summarize evidence for on-going uplift but the details of how this is occurring remain to be clarified. The results of this work may shed some light on the process.

Crustal shortening along thrust and reverse faults, typified by the 1979 St. Elias earthquake, can account for most of the uplift occurring near the Gulf of Alaska. On the northeastern flank of the St. Elias Mountains, the morphology of the Shakwak, Dalton and southeastern Duke River faults and a composite fault plane solution for microearthquakes near Kluane Lake (Horner 1983) indicate that predominantly right-lateral displacement is occurring. Northeast facing scarps and mounds in the Donjek River basin documented by Clague (1979) and a northeast facing Holocene fault scarp near the Burwash uplands described by Eisbacher and Hopkins (1977) indicate that a subsidiary component of compression exists as well. Plafker *et al.* (1977) documented similar dominantly right-lateral displacement on the Totschunda fault but also noted evidence for subordinate compression. While Muller (1967) maintains that the dominant sense of displacement on the adjacent Shakwak Fault has been vertical and Templeman-Kluit (1980) describes the Shakwak trench as a graben, these findings contradict geological evidence for substantial right-lateral displacement of the Dezadeash flysch in the Yukon (Eisbacher 1976) and similar evidence for horizontal transport summarized by Lanphere (1978). It seems more likely that compression on the southeastern Duke River fault rather than normal faulting in the Shakwak trench is responsible for the relative uplift of the Kluane ranges with respect

to the Shakwak valley floor documented by Templeman-Kluit (1980). On the northern boundary, the results of this work corroborate earlier suggestions (eg. Muller 1967, Eisbacher and Hopkins 1977, Lahr and Plafker 1980) that crustal shortening is occurring on the Duke River Fault and faults north of it in a broad zone of seismicity. Simplistically, the region resembles a pop-up structure with compressional shortening of various degrees occurring on the three boundaries in Canadian territory and presumably also to the west in Alaska.

The physiography of the region correlates well with this interpretation. The highest peaks in the St. Elias Mountains overlie large thrust and reverse faults near the Pacific Plate boundary. (eg. Mt. St. Elias overlies the Mt. St. Elias Fault and Mt. Logan overlies the Hubbard and Columbus faults - Campbell and Dodds 1982a, 1982b.) Another range of high mountains (the Icefield Ranges) occurs immediately south of the Duke River Fault and thrust or reverse faulting is occurring beneath them as well. The rest of the region, including the ranges bordering the Denali Fault system to the east and the vast icefields in the interior of the St. Elias Mountains is comparatively low-lying. The high mountains are thus physiographic indicators of on-going tectonic compresssion.

The restraining bend in the Duke River Fault and ongoing crustal shortening are the probable cause of uplift and drainage rejuvination in the Cement Creek, Steele Creek and St. Clare Creek watersheds. Rapid fluvial down-cutting and the favourable orientation of folded strata are the principle causes of recent landsliding in the area but extensive hydrothermal alteration in the predominantly volcanic Tertiary cover rocks and a high level of local seismicity also contribute to the landslide hazard. If the age of tilted surficial deposits at Bull Creek is confirmed as Wisconsin, the possibility that local tectonic flexion is contributing to the problem must be considered.

Bibliography

Boucher G. and T.J. Fitch (1969) Microearthquake seismicity of the Denali Fault. Journal of Geophysical Research Vol. 74 pp6638-6648.

Bowman F. (1938) Introduction to Bessel Functions. Toronto: Longmans, Green and Company.

Buland R. (1976) The mechanics of locating earthquakes . Bulletin of the Seismological Society of America Vol 66 pp 173-187.

Campbell R. B. and C.J. Dodds (1987). Structural elements, terrane distributions and cover rock sequences, Saint Elias Mountains (unpublished)

Campbell R. B. and C.J. Dodds (1982a). S.W. Kluane Lake Map Area (115G and F(E half)) Geological Survey of Canada Open File 829.

Campbell R. B. and C.J. Dodds (1982b). Mt. St. Elias Map Area (115 B and C (E 1/2)) Geological Survey of Canada Open File 830.

Campbell R. B. and C.J. Dodds (1978). Operation Saint Elias, Yukon Territory. Geological Survey of Canada Paper 78-1A pp35-41.

Charlesworth H.A.K., Gold C., Wynne D. and Guidos J. (1987) TRIPOD 2.1, A microcomputer-based system for collecting, storing, retrieving and processing structural, stratigraphic and positional data from outcrops and drillholes. Edmonton: Department of Geology. 70pp.

Clague J.J. (1979) The Denali Fault System in southwest Yukon Territory - A geologic hazard? in: Current Research Part A. Geological Survey of Canada Paper 79-1A p50-56.

Cruden D.M. (1985) Rock slope movements in the Canadian Cordillera. Canadian Geotechnical Journal Vol. 222 pp528-540.

Drysdale J.A., Horner R.B. and Wetmiller R.J. (1984) Candian Earthquakes National Summary - January - March 1983. Seismological Service of Canada, Earth Physics Branch.

Eisbacher G.H. (1976) Sedimentology of the Dezadeash flysch and its implications for strike-slip faulting along the Denali Fault, Yukon Territory and Alaska. Canadian Journal of Earth Sciences, Vol. 13 pp 1495-1513.

Eisbacher, G.H. and S.L. Hopkins (1977) Mid-Cenozoic paleogeomorphology and tectonic setting of the St. Elias Mountains, Yukon Territory. in: Geological Survey of Canada Paper 77-1b pp319-335.

Evans S.G. (1984) Landslides in Tertiary Basaltic Successions. Proceedings 4th International Symposium on Landslides Toronto Ont. Vol. 1 pp503-510.

Fitch T. J. (1972) Plate convergence, transcurrent faults and internal deformation adjacent to Southeast Asia and the Western Pacific. Journal of Geophysical Research Vol. 77 pp4432-4461.

Gelfand I.M., Sh. A. Guberman, V.I. Keillis-Borok, L. Knopoff, F. Press, E. Ya. Ranzman, I.M. Rotwain and A.M. Sadovsky. (1976) Pattern recognition applied to earthquake epicenters in California. Physics of the Earth and Planetary Interiors Vol. 11 pp227-283.

Geophysical Institute of the University of Alaska (1984) Alaska Geophysical Institute Annual Report 1982-1983. Anchorage:University of Alaska.

Horner R. (1983) Seismicity in the St. Elias region of northwestern Canada and southeastern Alaska. Bulletin of the Seismological Society of America Vol 73 No. 4 pp1117-1137.

Kanamori, H. The Energy Release in Great Earthquakes. Journal of Geophysical Research Vol. 82 pp2981-2987.

Koefoed, O. (1979) Geosounding Principles, 1 . New York: Elsevier

Koefoed, O. (1970) A fast method for determining the layer distribution from the raised kernel function in geoelectrical soundings. Geophysical Prospecting Vol. 18 pp564-570.

Lahr J.C. and G. Plafker (1980) Holocene Pacific-North American plate interactions in southern Alaska: implications for the Yakataga Seismic Gap. Geology Vol. 8 pp483-486.

Lanphere M.A. (1978) Displacement history of the Denali fault system, Alaska and Canada. Canadian Journal of Earth Sciences Vol. 15 pp187-822.

Lee W.K.H. and Stewart S.W. (1981) Principles and applications of microearthquake networks. Advances in Geophysics Supplement 2, Academic Press.

Lowell J.D. (1972) Spitzbergen Tertiery orogenic belt and the Spitzbergen Fracture Zone. Bulletin of the Geological Society of America Vol. 83 pp3091-3102.

Luenberger D.G. (1973) Introduction to linear amd nonlinear programming. Boston: Addison-Wesley Publishers Ltd.

MacKevett E.M. Jr. (1978) Geologic Map of the McCarthy quadrangle. United States Geological Survey Miscellaneous Inventory Series Map I-1032.

Muller J.E. (1967) Kluane Lake map area, Yukon Territory. Geological Survey of Canada, Memoir 340 137p.

O'Neill D.J. (1975) Improved linear filter coefficients for application in apparent resistivity computations. Bulletin of the Australian Society of Exploration Geophysicists Vol. 6 pp104-109

Pekeris, C.L. (1940) Direct method of interpretation in resistivity prospecting. Geophysics, Vol. 5. pp31-46.

Plafker G., T. Hudson and T. Bruns (1978) Late Quaternary offsets along the Fairweather Fault and crustal plate interactions in southern Alaska. Canadian Journal of Earth Sciences Vol. 15 pp805-816.

Plafker G., T. Hudson and D.H. Richter (1977) Preliminary observations on late Cenozoic displacements along the Totschunda and Denali Fault Systems. United States Geological Survey Circular 733 pp67-69.

Read P.B. and Monger J.W.H. (1975) Operation St. Elias, Yukon Territory: The Mush Lake Group and Permo-Triassic Rocks in the Kluane Ranges. in: Report of Activities,. Geological Survey of Canada, Paper 75-1 Part A p55-59.

Richter D.H. and N.A. Matson Jr. (1971) Quaternary faulting in the Eastern Alaska Range. Geological Society of America Bulletin Vol 82 pp1529-1540.

Skulski T. and Francis D. (1986) On the geology of the Tertiary Wrangell Lavas in the St. Clare Province, St. Elias Mountains, Yukon Territory. Yukon Geology 1984 Volume I. pp161-170.

Souther J.G. and Stanciu C. (1975) Operation St. Elias, Yukon Territory: Tertiary Volcanic Rocks in: Report of Activities, Geological Survey of Canada Paper 75-1 Part A, p63-70.

St. Amand P. (1957) Geological and geophysical synthesis of the the tectonics of portions of British Columbia, the Yukon Territory, and Alaska. Geological

Society of America Bulletin Vol. 68.pp1343-1370.

Stephens C.D., K.A. Fogleman, J.C. Lahr and R.A. Page (1984) Wrangell Benioff zone, southern Alaska. Geology Vol. 12 No. 6 pp373-376.

Stout J.H. and C.G. Chase (1980) Plate kinematics of the Denali fault system. Canadian Journal of Earth Sciences Vol. 17 pp1527-1537.

Telford W.M., L.P. Geldart, R.E. Sheriff and D.A. Keys (1976) Applied Geophysics. New York: Cambridge University Press.

Templeman-Kluit D. (1980) Evolution of physiography and drainage in southern Yukon. Canadian Journal of Earth Sciences Vol. 17, pp1189-1203.

Ter Stepanian G. (1980) Measuring displacements of wooded landslides with trilateral signs. Proceedings of the International Symposium on Landslides Vol. 1. New Delhi: Sraita Prakashan.

Uhrhammer R.A. (1980) Analysis of small seismographic station networks. Bulletin of the Seismological Society of America Vol 70. pp 1369-1379.

Woodcock N.F. and M. Fischer (1985?) Strike-slip duplexes. Journal of Structural Geology Vol. 8 No. 7. pp725-735.

Wyrobek S.M. (1956) Application of delay and intercept times in the interpretation of multilayer refraction time distance curves. Geophysical Prospecting Vol. 4 pp112-130.

Appendix A. Resistivity sounding inversion program

```
**********************************************************************
*
*                          Resistivity Inverter
*
*       This program inverts geoelectric sounding data using operator assisted
* modelling in  the Resistivity Transform domain.  The method consists of the
* following steps:
*
*         1. The interpolated apparent resistivities are converted into values of the
*            Resistivity Transform using the filter of O'Neill (1975) at intervals of six
*            per decade.  The eigenvalues are retained.
*
*         2. The operator is asked to input the parameters of the model which is to be
*            compared with the field data.  Resistivities and layer thicknesses of n layers
*            are required.
*
*         3. Values of the Resistivity Transform are calculated
*            using the Pekeris Recurrence Relation.
*
*         4. The theoretical and field values of the Resistivity Transform are
*            compared and the maximum error and root mean square error are calculated
*            and printed.  In addition, the field and model values of the Resistivity
*            Transform are printed.
*
*         5. The operator is asked whether a new model is to tried and, if so, steps
*            2-4 are repeated.
*
*   Input data consists of :
*
*         1. Apparent reistivity at s-spacings of 1/6 decade (natural logarithm)
*            interpolated from the field data.  The first resistivity value should be
*            for the current electrode spacing s=14.67m.
*
*            2. Model parameters:
*            (a) Number of layers (maximum of 20)
*            (b) Resistivity of each layer in ohm-metres.
*            (c) Thickness of each layer in metres.
*
*
```

```
      REAL*8 XA,ARHO(90),TEMP,T(90),TM(90),R(50),RHO(20)
      REAL*8 X(90),L(90),THIK(20),TH,DIF,RMS,PHI,TMM
      INTEGER NUMSPL,LAYER,MODEL,BED,LOC,PAR
      CHARACTER*1 ANS, ANS2
      CHARACTER*20 TITLE

      COMMON / AREA1 / ARHO,T
      OPEN(UNIT=7,FILE=LPT1,STATUS='OLD')

*  Prompt the user for the field data.

      WRITE(*,1) '    ** RESISTIVITY INVERTER **'
      WRITE(*,2)' WHAT IS THE SECTION TITLE?'
      READ(*,3) TITLE
      WRITE(*,2) 'INPUT SAMPLES START AT S=14.67M'
      WRITE(*,2) 'EACH ADDITIONAL SAMPLE IS 1.468 X LARGER THAN
     +  THE LAST'
      WRITE(*,2) 'HOW MANY SAMPLES ARE TO BE ANALYSED?'
      READ(*,*) NUMSPL

*  The first apparent resistivity (closest spacing) is taken as the apparent resistivity of
*  16 samples preceding it.  16 samples preceding the sample point and 8 following it
*  are required.

      NUMTFM=NUMSPL-8

   50 CONTINUE
      WRITE(*,4) 'TYPE IN ',NUMSPL, 'RESISTIVITIES (INCREASING S)'
      READ(*,*) TEMP

      DO 54  I=1,17
         ARHO(I)=TEMP
   54 CONTINUE

      DO 55 I=18,NUMSPL+16
         READ(*,*) ARHO(I)
   55 CONTINUE

      WRITE(*,2) 'ARE THOSE CORRECT?'
      READ(*,3) ANS
      IF(ANS .EQ. 'Y')THEN
         CONTINUE
      ELSE
```

```
            GO TO 50
        ENDIF

        CALL TRNSFM(NUMSPL)

*   The eigenvalues of the Resistivity Transform (RT) are 1/s. The first value of the
*   RT is calculted for s=10.51 m.Each subsequent RT coordinate X(I) is 1.468*
*   (X(I-1)). There is an offset between the s-spacing of the calculated RT and the
*   field s-spacing: X(transform domain) = X(field)/1.1396.

        X(1)=14.68
        L(I)=1.13963/14.68

        DO 100 I=1,NUMTFM-1
            X(I+1)=X(I)*1.468
            L(I+1)=1.0/X(I+1)
  100   CONTINUE

* Begin modelling the resistivity.

        WRITE(*,1) '  **MODEL CONSTRUCTION AND TESTING **'
        MODEL=1
        PAR=6

  101   CONTINUE

        WRITE(*,2) 'HOW MANY LAYERS ARE IN THE MODEL?:'
        READ(*,*) LAYERS

        WRITE(*,2) ' WORK FROM THE TOP DOWN'

        DO 105 I=1,LAYERS-1
            WRITE(*,5) 'WHAT ARE THE RESISTIVITY AND THICKNESS OF
       +  LAYER',I
            READ(*,*) ARHO(I),THIK(I)
  105   CONTINUE

        WRITE(*,5) 'WHAT IS THE RESISTIVITY OF LAYER',LAYERS
        READ(*,*) RHO(LAYERS)

*   Values of the model transform are calculated from the sample eigenvalues working
* from the bottom up using the Pekeris Recurrence Relation.

        DO 110 I=1,NUMTFM
            TM(I)=RHO(LAYERS)
```

```
110  CONTINUE

     DO 150 BED=LAYERS, 2, -1
        DO 130 I=1,NUMTFM
          TH=DTANH(L(I)*THIK(BED-1))
          TMM=TM(I)
          TM(I)=(TMM+RHO(BED-1)*TH)/(1+((TMM*TH)/RHO(BED-1)))
130     CONTINUE
150  CONTINUE

     LOC=0.0
     PHI=0.0
     RMS=0.0
     DIF=0.0

     DO 160 I=1,NUMTFM
        DIF=DABS(T(I)-TM(I))
        IF(DIF .GT. PHI) THEN
          PHI=DIF
          LOC=I
        ENDIF
        RMS=RMS+(DIF*DIF)
160  CONTINUE

     RMS=RMS/NUMTFM
     RMS=RMS**0.5

     WRITE(*,2) 'DO YOU WANT A HARD COPY?'
     READ(*,3) ANS2
     IF(ANS2 .EQ. 'Y')THEN
        PAR=7
     ELSE
        PAR=6
     ENDIF

     WRITE(PAR,6) '**  RESISTIVITY MODEL ',MODEL,' **'
     WRITE(PAR,15) TITLE
     WRITE(PAR, 7) ' MODEL PARAMETERS'
     WRITE(PAR,8) 'LAYER','RESISTIVITY','THICKNESS'
     WRITE(PAR,9) '(OHM-METRES)','(METRES)'

     DO 200 I=1,LAYERS-1
        WRITE(PAR,10) I,RHO(I),THIK(I)
200  CONTINUE
     WRITE(PAR,10) I,RHO(LAYERS)
```

```
      WRITE(PAR,7) 'TRANSFORM DOMAIN RESULTS'
      WRITE(PAR,11) 'SPACING','FIELD DATA','MODEL','% RELATIVE
     +  ERROR'

      DO 210 I=1,NUMTFM
         ERROR=100.0*(DABS(T(I)-TM(I))/T(I))
         WRITE(PAR,12) X(I),T(I),TM(I),ERROR
  210 CONTINUE

      WRITE(PAR,13) 'ROOT MEAN SQUARE ERROR WAS :',RMS
      WRITE(PAR,14) 'MAXIMUM ERROR WAS:',PHI,'  AT  X=',X(LOC)
      WRITE(PAR,7) '**********************************'

      WRITE(*,2) 'DO YOU WANT TO TEST ANOTHER MODEL?'
      READ(*,3) ANS

      IF(ANS .EQ. 'Y')THEN
         MODEL=MODEL+1
         GO TO 101
      ELSE
         CONTINUE
      ENDIF

    1 FORMAT(T30,A,//)
    2 FORMAT(T10,A)
    3 FORMAT(A)
    4 FORMAT(T10,A,I3,A,/)
    5 FORMAT(T10,A,I3,/)
    6 FORMAT(T25,A,I3,A,///)
    7 FORMAT(//,T28,A,//)
    8 FORMAT(T19,A,T35,A,T56,A)
    9 FORMAT(T34,A,T56,A,/)
   10 FORMAT(T19,I3,T36,F8.2,T57,F6.1)
   11 FORMAT(//,T7,A,T25,A,T48,A,T63,A,/)
   12 FORMAT(T7,F7.2,T26,F8.2,T46,F8.2,T68,F4.1)
   13 FORMAT(//,T10,A,F7.2,//)
   14 FORMAT(T10,A,F8.2,A,F7.2)
   15 FORMAT(T30,A,//)

      STOP
      END
*************************************************************************
*
*                          TRNSFM
```

```
*
*   This subroutine converts apparent resistivity data to Resistivity Transform values
* data by the application of a digital filter developed by O'Neill (1975). The value of
* the Resistivity Transform is calculated by multiplying the 8 preceding and 16
* following resistivities by the appropriate filter constants.
*************************************************************************

      SUBROUTINE TRNSFM(NUMSPL)
      REAL*8 ARHO(90),T(90),A
      INTEGER NUMSPL
      COMMON/AREA1/ARHO,T

      DO 505 I=17,NUMSPL+8
        A=0.001481*ARHO(I-16)+6.846E-4*ARHO(I-15)+1.022E-3*
     +  ARHO(I-14)+1.483E-3*ARHO(I-13)+2.194E-3*ARHO(I-12)+3.203E-3
     + *ARHO(I-11)+4.718E-3*ARHO(I-10)+6.907E-3*ARHO(I-9)+0.01015*
     +  ARHO(I-8)+0.01488*ARHO(I-7)+0.02184*ARHO(I-6)+0.03198
     + *ARHO(I-5)+0.04677*ARHO(I-4)+0.06802*ARHO(I-3)+0.09804*
     + ARHO(I-2)+0.1379*ARHO(I-1)+0.1853*ARHO(I)+0.2206*
     + ARHO(I+1)+0.1961*ARHO(I+2)+0.03287*ARHO(I+3)-0.1235*
     +  ARHO(I+4)+0.04501*ARHO(I+5)-0.008794*ARHO(I+6)+
     +  1.418E-3*ARHO(I+7)-2.766E-4*ARHO(I+8)
        T(I-16)=A
  505 CONTINUE
      RETURN
      END
```

Appendix B. FOCUS - an earthquake location program using the time difference residual method

Input data required by FOCUS includes arrival times, weighting factors, first motions, coordinates and elevations of seismograph sites, a velocity model and up to 3 different rectangular search volumes. Each type of input data is place in a different file: arrival times and first motions in TIMES, seismograph coordinates in SITES, the velocity model in VMODEL, weighting factors in SIGMA, and and search volumes in VOLUME1-3. With the exception of arrival times, all data is entered in free format.

Seismograph locations are specified with respect to a Cartesian coordinate system with X directed to the east, Y pointing north and Z measuring positive depth with distances along each axis are measured in kilometers. Depths may be computed relative to any desired datum; sea level is suggested. FOCUS can handle up to 7 recording sites for any given earthquake. The x, y and z coordinates with the positive z-direction being down are entered one set per line in free format as shown below:

line

1 45.6 34.6 -0.98
2 46.8 35.6 -1.2
3 23.7 44.5 -1.5

A velocity model consisting of up to 4 layers over a half space is specified in free format. The first entry specifies the number of layers in the model; 0 is entered for a half-space. Compressional and shear wave velocities in km/s and the depth to the lower boundary are then specified for each of the layers, one set per line in order of increasing depth. The last line contains only a P and S wave velocity and specifies the profile in the half space.

line

1 2
2 5.5 3.5 2.0
3 6.5 4.5 20.0
4 8.0 6.0

Arrival time, weighting factors and first motions are coded in the format shown below in file TIMES. The first line in the file specifies in free format an event number - the Julian day followed by a decimal followed by a two place identifying number is suggested. The arrival time is entered as an F11.3 REAL number in the form HHMMSS.sss where HH the hour , MM the minute and SS.sss the second specified to the nearest millisecond. The weighting factors assigned to each time measurement are arbitrary. A scheme used on data collected during the Duke River Fault Project is shown below

MEASUREMENT ERROR (s)	WEIGHTING FACTOR
<0.05	1.0
$0.05 < \Delta t \leq 0.25$	0.8
$0.25 < \Delta t \leq 0.50$	0.6
$0.50 < \Delta t \leq 0.75$	0.4
$0.75 < \Delta t \leq 1.00$	0.2

FOCUS computes two types of error statistics; the TDR and a chi-squared residual (Buland 1976). The latter requires timing error variance and consequently the operator is required to specify the standard errors in timing corresponding to the weighting factors in file SIGMA in free format as shown below

line	weighting factor	standard error
1	1.0	0.05
2	0.8	0.25

"Garbage in - garbage out" is an especially applicable dictum in the distant earthquake location problem and no combination of weighting factors can compensate for poor input data.

First motions are specified as either '+' (compressional) or '-' (dilatational). The input must be formated as shown below. Arrival times are entered in pairs, P followed by S in order of increasing site number. If arrivals are not detected at a station, the corresponding weighting factor should be set to zero. The arrival times are screened to ensure that arrivals occur within the same 1 hour period: If this condition is violated a warning will be sent to the screen and the program will terminate. An example of an event

entry in file TIMES together with explanatory comments is shown below :

LINE	COLUMN			
	1	12	17	
	|	|	|	
1	125.01			(first event on day 125)
2	161023.560	1.0	+	(P arrival - station1 @ 16:10:23.56)
3	161030.640	0.6	-	S arrival - station1 @ 16:10:30.64)
4	161045.340	1.0	+	(P arrival - station2 @ 16:10:45.34)
5	161105.210	0.6	+	(S arrival - station2 @16:11:05.21)
6	160000.000	0.0	?	(no P arrival at site 3)
7	160000.000	0.0	?	(no S arrival at site 3)

The initial geometric search is conducted in a volume specified in one of 3 files (VOLUME1-3) attached to units 9-11. The flexibility afforded by 3 search volumes is useful if the operator wishes to search for a solution in a given layer or set of layers within a velocity model. The geometric search is always constrained within the specified search volume; the subsequent PARTAN search is unconstrained. The coordinates of the corners are entered one set to a line in free format with the corners being specified as follows: The corners are numbered 1 to 8 starting at the northeast corner and proceeding counterclockwise and proceeding from the top surface down. Thus the northeast corner on the bottom surface would be number 5. A sample volume specification is shown below:

LINE	
1	100,100,0
2	100,0 ,0
3	0,0,0
4	0,100,0
5	100,100,30
6	0,100,30
7	0,0,30
8	0,100,30

Once the data have been entered into their respective files, the program is started. The user will be prompted for a cutoff value of the time difference residual and the

number of times the geometric search is to be repeated. Experiments with synthetic data suggest that the cutoff may be set at a slightly lower value than that indicated by equation 2.2 without seriously inhibiting convergence. Variance between true and model earth velocity structures and/or undetected systematic timing error will produce anomalously high values of the TDR; generally TDR's at the end of the geometric search should be about one order of magnitude larger than the cutoff residual.

Travel times are computed using analytic solutions summarized by Lee and Stewart (1981). Slight modifications to their nomenclature have been made and these are indicated in the program listing. Travel times for direct and refracted rays from the trial focus to each station are computed and the minimum selected as the travel time of the first arrival.

Once the geometric search is complete, the coordinates and value of the least residual found are echoed to the screen and PARTAN search commences. If the search fails to better the least residual on one of the 6 successive legs, the search is deemed to be diverging and the operator prompted for a new search point. The search distance along each gradient or parallel tangent vector may be reset up or down from its default value of 2.0 km at this juncture. If the search fails to reach a value below the cutoff after 15 legs, the operator is asked whether the search is to be continued and if so what is the new search point.

If the search diverges or fails to converge after 15 legs, the following observations may be of help in selecting a new search point. The user should be cautioned that these remarks apply to a half space velocity model and slight variation may be expected for other situations. A diverging search is often easily remedied by pulling the search point back about 5 km towards the center of the array along the radial vector connecting the initial PARTAN search point and the center of the array. New search points should not be placed inside the axial region where gradients are small. The change in current and global residuals will indicate whether this has occurred. Placing a new search point at a greater depth causes the search to progress outward from the array and if the new point is below the axisymmetric region surrounding the solution, it will tend to rise. The converse occurs if a point is placed at a shallower depth and if above the minimum region. A good general tactic is to pull the search down or raise it above this region; it will always return to it and make considerable progress towards a value below the cutoff residual in the process. The coordinates echoed during non-diverging searches progress towards the location of the global minimum and it is fairly easy to position a new search point from which a suitable solution may be reached within a few steps. The incorporation of S-P times into the

residual calculation dramatically stabilizes the search process and where possible, both S and P arrivals from a given station should be used. Depth discrimination deteriorates in multi-layered models for events distant from the array and the influence of a single erroneous reading, even in an amply overdetermined case, can switch the location of the global minimum by many kilometres.

Once a solution below the cutoff value has been reached, the search is suspended, the origin time is back calculated, arrival time residuals are calculated and the arrival times, take-off angles, first motions, chi-squared and time difference residuals, focal coordinates and origin time are printed in the file FOCUS.RESULTS.

Program listing

```
************************************************************************
*
*                                FOCUS
*
*  This program determines earthquake kinematic parameters using
* time difference residuals.
*
*
*  Input data includes:
*
*          1. Station coordinates(UTM) and elevation
*
*          2. The arrival times of P and S at each station, sense of first,
*             motion and a weighting factor to be used in a weighted least
*             squares calculation.
*
*          3. A velocity model consisting of up to 4 layers over a half space
*             with Vp Vs and Z specified.
*
*  The search for a solution may be performed automatically or with
* operator assistance.  The search is a two phase procedure with a geometric)
* search conducted to determine a starting point for a subsequent gradient
* search.
*
*  Output data includes:
*
*          1. The coordinates (x,y,z) and origin time of the event.
*
*          2. The combined P and S residual.
*
*  Variables:
*
*       SITES(Number=1-7, Coordinates(x,y,z)=1-3) - Contains the coordinates
*          of the recording sites.
```

```
*     NLAYER- The number of layers in the velocity model.
*     VP(I),VS(I) - P and S velocities in km/s.
*     WP(I),WS(I) - Weighting factors between 0.0 and 1.0 for arrival
*       times of P and S.
*     TP(I),TS(I) - Arrival times of P and S coded as:
*         HHMMSS.sss where HH is the hour (24 hr. clock)
*         MM is the minute and SS.sss is the second.
*     QUAKE - A number designating the earthquake: DDD.nn
*       where DDD is the Julian Day and nn is the event number.
*     CUBE(Number=1-8,Coordinates=1-3) - The coordinates of the 8 corners
*       of the rectangular volume specified in files VOLUME1-3.
*     CUTOFF - The value of the time difference residual below which the
*       search is to be terminated.
*     BOTTOM,TOP - The depth of the top and bottom of the search volume:
*         Searches are to be constrained between these depths.
*     YMAX,YMIN,XMAX,XMIN - X and Y coordinates within which the search
*       is to be constrained.
*     Z(I) - Depth of the LOWER boundary of the Ith layer. This differs
*         from the nomenclature used in Lee and Stewart (1981).
*     PTT(I=1-7, J=1,7) - Time differences between stations I and J.
*     STT(I=1-7, J=1-7)   for P and S.
*     PHI(I=1-7,J=1,2) - Plunge of take off angle vectors for P (J=1)
*         and S (J=2). Positive is down.
*     THETA(I) - Trend of take off angle vectors measured from North.
*     TTP,TTS - Theoretical travel times for P and S waves from a focus
*       to each of stations I=1,7
*     TQP(I),TQS(I) - Calculated time of an earthquake back-calculated
*         to each of stations I=1,7.
*     STEP - The number of times a simplex search is to be repeated
*         before switching to a PARTAN search.
*     RR(I=1,9) - Time difference residuals at the corners and centers
*         of the search volume.
*     XLEAST,YLEAST,ZLEAST - The coordinates of the point where the
*         least time difference residual was found.
*     MODE - Either manual or automatic: allows the operator to direct
*         the SIMPLEX search - in automatic  the corner with the least
*         value of the time difference residual is selected as the
*         point about which contraction is to occur.
*     X,Y,ZZ - The final coordinates of the focus
*     FILE - The unit number of the file containing the coordinates
*         of the initial search volume.
*     NEXT - The number of the corner about which the cube is to be
*       contracted during the geometric search.
*       The numbering  convention is that the corner #1 is at the top NE corner
*       and corners 2-4 are the SE,SW and NW corners of the top
*       of the volume.  Corners #5-8 aredirectly beneath corners
*       #1-4.
*       T,HOUR,MINIT,SEC - The raw time of the earthquake in seconds.
*       This is an internal variable which is transformed into
*       the absolute HOUR,minute(MINIT) and SECond of the
*       earthquake.
*       WTOT - The fotal of the weighting factors used to normalize
*       them prior to a weighted average calculation of the
*       origin time.
```

```
*       ERRLOC - The smallest length of the cubic volume at the
*       end of any geometric search.
*       ITER - A DO loop counter indicating the number of contractions
*         which have been performed during a single geometric
*         geometric search.          The loop is exited when the size
*         of any side of the search volume (INCR) becomes less
*         than ERRLOC.
*       T - The origin time of the earthquake calculated from the
*       weighted average of TQP.
*       ECHO - A variable denoting whether the time difference
*         residuals calculated during a geometric search are
*         to be echoed to the screen at each step.
*
*************************************************************************

      INTEGER FINAL,STEP,NSTEP
       INTEGER ITER,J,I,NLAYER,NEXT,CORNER,NUM,FILE,HR,NDA
      REAL PI,PTT(7,7),STT(7,7),SPT(7),PHI(7,2),TTP(7),TTS(7),FSD
      REAL ERRLOC,VP(5),VS(5),Z(5),CUBE(9,3),X,Y,ZZ,THETA(7)
      REAL INITZ,WS(7),WP(7),MIN,TQP(7),TQS(7)
      REAL NSD,DIFB,DIFT,BOTTOM,TOP,RLEAST,XLEAST,YLEAST,ZLEAST
      REAL YMAX,XMAX,XMIN,YMIN,CUTOFF,RMIN,RPASS,SP(7)
      REAL WTOT,T,VAR,SDP,SDS,SIGMA(2,10)
      REAL INCR,RR(9),T ,TP(7),TS(7),SITE(7,3),PT(7,7),ST(7,7),V(5)
      CHARACTER*1 MODE,ECHO,FMP(7),FMS(7)

      COMMON/BLOCK1/V,Z
      COMMON/BLOCK2/NLAYER,VP,VS
      COMMON/BLOCK3/TTP,TTS,SPT,PTT,STT,PHI
      COMMON/BLOCK4/SITE
      COMMON/BLOCK5/WP,WS,RR,PT,ST
      COMMON/BLOCK7/BOTTOM,TOP
      COMMON/BLOCK8/SP

      OPEN(UNIT=2,FILE='sites',STATUS='OLD')
      OPEN(UNIT=3,FILE='times',STATUS='OLD')
      OPEN(UNIT=4,FILE='vmodel',STATUS='OLD')
      OPEN(UNIT=7,FILE='focus.results',STATUS='OLD')
      OPEN(UNIT=8,FILE='volume1',STATUS='OLD')
      OPEN(UNIT=9,FILE='volume2',STATUS='OLD')
      OPEN(UNIT=10, FILE='volume3',STATUS='OLD')
      OPEN(UNIT=11, FILE='fpsdata',STATUS='OLD')
      OPEN(UNIT=12, FILE='sigma',STATUS='OLD')


* Initialize variables.

       RPASS=1.0
       RLEAST=9999999.0
       FINAL=0
       FSD=0.0
      DO 17 I=1,8
        DO 16 J=1,3
          CUBE(I,J)=0.0
```

```
16      CONTINUE
        RR(I)=0.0
17    CONTINUE

      DO 18 I=1,7
        TTP(I)=0.0
        TTS(I)=0.0
        TQS(I)=0.0
        TQP(I)=0.0
        TP(I)=0.0
        TS(I)=0.0
18    CONTINUE

      NUM=0
      RR(9)=0.0
       INCR=0.0
       INITZ=0.0
       PI=4*ATAN(1.0)
       NUM=0


* Prompt the user for mode of operation and final block dimensions.

      WRITE(6,*) ' *** FOCUS ***'
      WRITE(6,*) 'Do you want residuals echoed?'
      READ(5,'(A)') ECHO
      WRITE(6,*) 'Specify the residual cutoff for the PARTAN search.'
      READ(5,*) CUTOFF


* The recorded arrival times and weighting factors are read from file
* 3=TIMES.  The site coordinates and elevation are read in from file 2=
* SITES and converted to meters.

       READ(3,*) QUAKE
      DAY=INT(QUAKE)
       DO 15 I=1,7
         READ(3,9) TP(I),WP(I),FMP(I)
         READ(3,9) TS(I),WS(I),FMS(I)
         READ(2,*) (SITE(I,J),J=1,3)
15    CONTINUE
 9 FORMAT(F11.3,F5.1,A)

* Read in standard errors in arrival times with corresponding weighting
* factors. Weighting factor then sigma is read in that order.

      DO 19 I=1,5
        READ(12,*) SIGMA(1,I),SIGMA(2,I)
        SIGMA(2,I)=SIGMA(2,I)*SIGMA(2,I)*1000000.0
19    CONTINUE

* Read in the parameters of the velocity model from file 4=VMODEL.

      READ(4,*)NLAYER
```

```
      DO 20 I=1,NLAYER
        READ(4,*) VP(I),VS(I),Z(I)
20    CONTINUE
      READ(4,*) VP(NLAYER+1), VS(NLAYER+1)

* Read in the coordinates of the search volume and determine the center
* of the search volume.

      WRITE(6,*) 'Specify the unit of the file containing the search '
      WRITE(6,*) 'volume: 8=VOLUME1 9=VOLUME2 10=VOLUME3'
      READ(5,*) FILE
      DO 22 I=1,8
        READ(FILE,*) (CUBE(I,J),J=1,3)
22    CONTINUE

      CUBE(9,1)=(CUBE(1,1)+CUBE(4,1))/2
      CUBE(9,2)=(CUBE(1,2)+CUBE(2,2))/2
      CUBE(9,3)=(CUBE(1,3)+CUBE(5,3))/2

* Convert times into seconds after subtracting time to the nearest hour and
* minute-1.  Times are coded as HHMMSS.ss. Check that times are in the same
* 1 hour period.


      DO 24 I=1,7
      IF(WP(I) .GT. 0.01)THEN
        HOUR=INT(0.0001*TP(I))
        GO TO 25
      ENDIF
24    CONTINUE

25    CONTINUE
      DO 26 I=1,7
        VAR=WP(I)+WS(I)
        IF(INT(0.0001*TP(I)) .NE. HOUR .AND.  VAR .GT. 0.02)THEN
          WRITE(6,*) 'WARNING - ARRIVAL TIMES IN DIFFERENT 1 HOUR '
     +          PERIOD'
         GO TO 1000
        ENDIF
        VAR=0.0
26    CONTINUE
      HOUR=HOUR*10000

      DO 30 I=1,7
        TP(I)=TP(I)-HOUR
        TS(I)=TS(I)-HOUR
        IF(WP(I) .LT. 0.1)THEN
          TP(I)=0.0
        ENDIF
        IF(WS(I) .LT. 0.1)THEN
          TS(I)=0.0
        ENDIF
        TP(I)=TCONV(TP(I))
        TS(I)=TCONV(TS(I))
```

```
 30     CONTINUE
        HOUR=HOUR*0.0001

* Calculate the difference in arrival times between all stations.

        DO 40 I=1,7
          DO 35 J=1,7
            PT(I,J)=TP(I)-TP(J)
            ST(I,J)=TS(I)-TS(J)
 35       CONTINUE
          SP(I)=TS(I)-TP(I)
 40     CONTINUE

* Initialize ERRLOC and the boundaries of the search volume.

        XMAX=CUBE(1,1)
        YMAX=CUBE(1,2)
        XMIN=CUBE(4,1)
        YMIN=CUBE(2,2)
        ERRLOC=0.050
        INITZ=CUBE(5,3)-CUBE(1,3)
        INCR=CUBE(1,1)-CUBE(4,1)
        BOTTOM=CUBE(5,3)
        TOP=CUBE(1,3)


* The operator is prompted to specify the number of times the
* geometric search is to be repeated.

        WRITE(6,*) 'Specify the number of SIMPLEX searches:'
        READ(5,*) NSTEP
        DO 600 STEP=1,NSTEP

* The following major loop calculates the residuals at the 8 corners
* of the enclosing volume, selects or prompts for the next corner and
* recalculates the residuals until the enclosing volume in less than that
* required by the error in location.


          DO 500 ITER=1,100

          IF(INCR .LE. 2*ERRLOC) THEN
            GO TO 550
          ENDIF

          DO 149 I=1,9
             RR(I)=0.0
149       CONTINUE

          DO 150 CORNER=1,9
            CALL EVENT(CUBE(CORNER,1),CUBE(CORNER,2),CUBE(CORNER,3))
            CALL RCALC(RR(CORNER))
150       CONTINUE
```

```
* Echo the residuals to the screen. If in the manual mode, prompt for the
* corner about which the reduced search volume is to be constructed.
* If in the automatic mode, search the residuals to find the minimum
* and construct the reduced search volume around it.

            IF(ECHO .EQ. 'Y')THEN
              WRITE(6,*) 'SUMMARY OF RESIDUALS FOR ITERATION:',ITER
              WRITE(6,*) 'RECTANGULAR VOLUME DIMENSIONS IN X,Y:',INCR,
     +          ' KM'
              DO 160 I=1,9
                WRITE(6,*) 'AT CORNER',I,' RESIDUAL IS',RR(I)
160           CONTINUE
            ENDIF

            IF(MODE .EQ. 'M') THEN
              WRITE(6,*) 'SPECIFY CORNER FOR NEXT ITERATION:'
              READ(5,*) NEXT
            ELSE

              NEXT=1
              MIN=RR(1)
              DO 170 I=2,9
                IF(RR(I) .LT. MIN) THEN
                  MIN=RR(I)
                  NEXT=I
                ENDIF
170           CONTINUE
              ENDIF
* Set up the coordinates of the next search volume. The volume is
* shrunk by different factors depending upon the whether the initial
* or final search is being conducted.

            IF(STEP .EQ. 1)THEN
                INCR=INCR/1.5
            ELSE
              INCR=INCR/1.5
            ENDIF
            X=CUBE(NEXT,1)
            Y=CUBE(NEXT,2)
            ZZ=CUBE(NEXT,3)

* The depth of the search volume is not changed until the search volume becomes a cube.

            IF(NEXT .LT. 5)THEN

              DO 190 I=1,4
                CUBE(I,3)=ZZ
190           CONTINUE

                DO 200 I=5,8
                  IF(INCR .LT. INITZ)THEN
                    CUBE(I,3)=ZZ+INCR
                  ELSE
```

```
                                CUBE(I,3)=ZZ+INITZ
              ENDIF
200           CONTINUE

              IF(INCR .LT. INITZ)THEN
                CUBE(9,3)=ZZ+0.5*INCR
              ELSE
                 CUBE(9,3)=ZZ+0.5*INITZ
              ENDIF

            ELSE IF(NEXT .GE. 5 .AND. NEXT .LT. 9)THEN

              DO 210 I=1,4
                IF(INCR .LT. INITZ)THEN
                                CUBE(I,3)=ZZ-INCR
                ELSE
                  CUBE(I,3)=ZZ-INITZ
                ENDIF
210           CONTINUE

              DO 220 I=5,8
                CUBE(I,3)=ZZ
220           CONTINUE

              IF(INCR .LT. INITZ)THEN
                CUBE(9,3)=ZZ-0.5*INCR
              ELSE
                CUBE(9,3)=ZZ-0.5*INITZ
              ENDIF

            ELSE

              DO 230 I=1,4
                IF(INCR .LT. INITZ)THEN
                                CUBE(I,3)=ZZ-0.5*INCR
                ELSE
                                CUBE(I,3)=ZZ-0.5*INITZ
                ENDIF
230           CONTINUE

              DO 235 I=5,8
                IF(INCR .LT. INITZ)THEN
                                CUBE(I,3)=ZZ+0.5*INCR
                ELSE
                                CUBE(I,3)=ZZ+0.5*INITZ
                ENDIF
235           CONTINUE

              CUBE(9,3)=ZZ

            ENDIF
```

```
IF(NEXT .EQ. 1 .OR. NEXT .EQ. 5) THEN
  CUBE(1,1)=X
  CUBE(1,2)=Y
  CUBE(2,1)=X
   CUBE(2,2)=Y-INCR
  CUBE(3,1)=X-INCR
  CUBE(3,2)=Y-INCR
  CUBE(4,1)=X-INCR
  CUBE(4,2)=Y
  CUBE(9,1)=X-0.5*INCR
  CUBE(9,2)=Y-0.5*INCR
ELSE IF(NEXT .EQ. 2 .OR. NEXT .EQ. 6) THEN
  CUBE(1,1)=X
  CUBE(1,2)=Y+INCR
  CUBE(2,1)=X
  CUBE(2,2)=Y
  CUBE(3,1)=X-INCR
  CUBE(3,2)=Y
  CUBE(4,1)=X-INCR
  CUBE(4,2)=Y+INCR
  CUBE(9,1)=X-0.5*INCR
  CUBE(9,2)=Y+0.5*INCR
ELSE IF(NEXT .EQ. 3 .OR. NEXT .EQ. 7) THEN
  CUBE(1,1)=X+INCR
  CUBE(1,2)=Y+INCR
  CUBE(2,1)=X+INCR
  CUBE(2,2)=Y
  CUBE(3,1)=X
  CUBE(3,2)=Y
   CUBE(4,1)=X
   CUBE(4,2)=Y+INCR
   CUBE(9,1)=X+0.5*INCR
   CUBE(9,2)=Y+0.5*INCR
ELSE IF(NEXT .EQ. 4 .OR. NEXT .EQ. 8)THEN
  CUBE(1,1)=X+INCR
  CUBE(1,2)=Y
  CUBE(2,1)=X+INCR
  CUBE(2,2)=Y-INCR
   CUBE(3,1)=X
   CUBE(3,2)=Y-INCR
  CUBE(4,1)=X
  CUBE(4,2)=Y
  CUBE(9,1)=X+0.5*INCR
  CUBE(9,2)=Y-0.5*INCR
ELSE IF(NEXT .EQ. 9)THEN
  CUBE(1,1)=X+0.5*INCR
  CUBE(1,2)=Y+0.5*INCR
   CUBE(2,2)=Y-0.5*INCR
  CUBE(3,1)=X-0.5*INCR
   CUBE(3,2)=Y-0.5*INCR
   CUBE(4,1)=X-0.5*INCR
  CUBE(4,2)=Y+0.5*INCR
  CUBE(9,1)=X
  CUBE(9,2)=Y
```

```
                ELSE
                  WRITE(6,*)'WHAT THE HECK? NEXT IS OUT OF RANGE!'
                  GO TO 1000
                ENDIF

                DO 240 I=1,4
                  CUBE(I+4,1)=CUBE(I,1)
                  CUBE(I+4,2)=CUBE(I,2)
240             CONTINUE

                RSUM=0.0
                DO 250 I=1,9
                   RSUM=RSUM+RR(I)
250             CONTINUE

                IF(RSUM .LT. RLEAST)THEN
                  RLEAST=RSUM
                  XLEAST=(CUBE(1,1)+CUBE(4,1))/2.0
                  YLEAST=(CUBE(1,2)+CUBE(2,2))/2.0
                  ZLEAST=(CUBE(1,3)+CUBE(5,3))/2.0
                ENDIF

* Set the residuals equal to zero prior to the next calculation of the
* corner residuals.

                DO 300 I=1,9
                  RR(I)=0.0
300             CONTINUE



500       CONTINUE
550     CONTINUE


* Once a final search volume is reached, take the center of this cube to be
* the focus and calculate the residuals associated with it.


              X=CUBE(9,1)
              Y=CUBE(9,2)
              ZZ=CUBE(9,3)


              IF(X .GT. XMAX) X=XMAX
              IF(Y .GT. YMAX) Y=YMAX
              IF(Y .LT. YMIN) Y=YMIN
              IF(X .LT. XMIN) X=XMIN



* An initial search is made to determine a provisional solution.  The cube is
* then re-expanded about this point and the search restarted.
```

```
      IF(STEP .EQ. 2)THEN
        NSD=20.0
      ELSE
        NSD=10.0
      ENDIF

      INITZ=NSD
      NSD=NSD/2.0
      DIFB=ZZ+NSD-BOTTOM
      DIFT=TOP-ZZ+NSD
      IF(ZZ-NSD .LT. TOP .OR. ZZ+NSD .GT. BOTTOM)THEN
       IF(DIFT .GT. DIFB)THEN
        INITZ=2*(ZZ-TOP)
       ELSE
        INITZ=2*(BOTTOM-ZZ)
       ENDIF
      ELSE
       CONTINUE
      ENDIF

      DO 560 I=1,4
       IF(INITZ .LT. 2*NSD)THEN
        CUBE(I,3)=ZZ-(0.5*INITZ)
        CUBE(I+4,3)=ZZ+(0.5*INITZ)
       ELSE
        CUBE(I,3)=ZZ-NSD
        CUBE(I+4,3)=ZZ+NSD
       ENDIF

560    CONTINUE
      CUBE(1,1)=X+NSD
      CUBE(1,2)=Y+NSD
      CUBE(2,1)=X+NSD
      CUBE(2,2)=Y-NSD
      CUBE(3,1)=X-NSD
      CUBE(3,2)=Y-NSD
      CUBE(4,1)=X-NSD
      CUBE(4,2)=Y+NSD

      DO 561 I=5,8
        CUBE(I,1)=CUBE(I-4,1)
        CUBE(I,2)=CUBE(I-4,2)
561    CONTINUE

      CUBE(9,1)=(CUBE(1,1)+CUBE(4,1))/2
      CUBE(9,2)=(CUBE(1,2)+CUBE(2,2))/2
      CUBE(9,3)=(CUBE(1,3)+CUBE(5,3))/2

      NSD=2.0*NSD
      INCR=CUBE(1,1)-CUBE(4,1)

600    CONTINUE

      X=XLEAST
```

```
      Y=YLEAST
      ZZ=ZLEAST
      WRITE(6,*)' AFTER SIMPLEX SEARCH:',X,Y,ZZ
      WRITE(6,*) 'RESIDUAL HERE=',RLEAST/9.0
      RMIN=RLEAST
      CALL GRAD(X,Y,ZZ,CUTOFF,RMIN)

      WRITE(6,*) 'LEAST RESIDUAL=',RMIN
      WRITE(6,*) 'AT (',X,Y,ZZ,')'

* Determine the origin time by subtracting the travel time for each
* station from the arrival time and taking the weighted average for all sites.

      WTOT=0.0


      DO 610 I=1,7
        IF(WP(I) .GT. 0.01) TQP(I)=TP(I)-TTP(I)
610   CONTINUE

      T=0.0

      DO 620 I=1,7
        IF(WP(I) .GT. 0.0001)THEN
          NUM=NUM+1
          T=T+TQP(I)
        ENDIF
620   CONTINUE

      T=T/NUM

* Determine the travel time from the focus to the stations. Use the
* calculated origin time, travel times and observed arrival times to
* calculate the weighted RMS sum of the P and S residuals.

      CHI=0.0
      CALL EVENT(X,Y,ZZ)

      DO 650 I=1,7
        SDS=0.0
        SDP=0.0
        IF(WP(I) .GT. 0.0 .OR. WS(I) .GT. 0.0 )THEN
          DO 640 J=1,5
          IF( ABS(WP(I)-SIGMA(1,J)) .LT. 0.01)THEN
          SDP=SIGMA(2,J)
          NDA=NDA+1
        ENDIF
        IF(ABS(WS(I)-SIGMA(1,J)) .LT. 0.01)THEN
          NDA=NDA+1
          SDS=SIGMA(2,J)
        ENDIF
640   CONTINUE
      IF(WP(I) .GT. 0.0)THEN
       CHI=CHI+(1000000.0*((ABS(TP(I)-(T+TTP(I)))**2))/SDP)
```

```
      ENDIF
      IF(WS(I) .GT. 0.0)THEN
       CHI=CHI+(1000000.0*((ABS(TS(I)-(T+TTS(I)))**2))/SDS)
      ENDIF
        ENDIF
650   CONTINUE

      CHI=CHI**0.5


* Calculate the azimuthal angle THETA from focus to station.

      DO 700 I=1,7

        R=( (SITE(I,1)-X)**2 + (SITE(I,2)-Y)**2 )**0.5
        THETA(I)=ACOS( (SITE(I,2)-Y)/R )
        IF( SITE(I,1)-X .LT. 0.0)THEN
          THETA(I)=2*PI-THETA(I)
        ENDIF
        THETA(I)=(THETA(I)/(2*PI))*360.0
        PHI(I,1)=(PHI(I,1)/(2*PI))*360.0

* Fill in returns from non-detecting stations with zeroes

        DO 690 J=1,7
          IF( WP(I) .LT. 0.001)THEN
            PHI(I,1)=0.0
            THETA(I)=0.0
          ENDIF
690     CONTINUE

700   CONTINUE

* Invert the origin time back to hours, minutes and seconds for printout.

      T=TINV(T)
      MINIT=INT(T/100)
      SEC=T-(MINIT*100.0)
      HR=INT(HOUR)

      WRITE(7,1) 'RESULTS FOR EVENT ',QUAKE
      WRITE(7,2) 'FOCUS AT X=',X,' KM'
      WRITE(7,3) 'Y=',Y,' KM'
      WRITE(7,3) 'Z=',ZZ,' KM'
      WRITE(7,4) 'ORIGIN TIME',INT(DAY),':',HR,':',MINIT,':',SEC
      WRITE(7,5) 'Minimum time difference residual:',RMIN
      WRITE(7,5) 'CHI SQUARED residual:',CHI
      WRITE(7,12) 'Number of detected arrivals was:',NDA
      WRITE(7,6) 'TAKE OFF ANGLES'
      WRITE(7,7) 'Station','Azimuth','Dip','P first motion'

      DO 750 I=1,7
        WRITE(7,8)I+7,THETA(I),PHI(I,1),FMP(I)
        WRITE(11,8) I+7,THETA(I),PHI(I,1),FMP(I)
```

```
750   CONTINUE
      WRITE(7,2) 'The dimensions of the smallest cube:',INCR,' Km'
      WRITE(7,11) 'The search volume was specified by FILE ',FILE

 1    FORMAT(T20,A,F6.2)
 2    FORMAT(/,T5,A,F7.2,A)
 3    FORMAT(T14,A,F7.2,A)
 4    FORMAT(/,T5,A,I4,A,I3,A,I3,A,F4.1,/)A
 5    FORMAT(/,T5,A,F12.4,/)
 6    FORMAT(T20,A,/)
 7    FORMAT(T5,A,T20,A,T35,A,T50,A,/)
 8    FORMAT(T5,I3,T20,F6.2,T35,F6.2,T56,A)
 11   FORMAT(/,T5,A,I3)
 12   FORMAT(/,T5,A,I3,/)


1000  STOP
      END



*************************************************************************
*                  TCONV
*
*   This function converts formatted arrival times into seconds. Arrival time
* in the format MMSS.ss is passed in.
*
*************************************************************************
      FUNCTION TCONV(T)
      REAL T
      INTEGER MIN
      T=T*0.01
      MIN=INT(T)
      T=T-MIN
      T=T*100
      TCONV=MIN*60+T
      RETURN
      END


*************************************************************************
*                  TINV
*
*   This function takes origin times (in seconds) and converts them into
* the formatted time MMSS.s
*************************************************************************
      FUNCTION TINV(T)
      REAL T,SEC
      INTEGER MIN
      MIN=INT(T/60.0)
      SEC=T-(MIN*60)
      TINV=MIN*100+SEC
       RETURN
```

```
      END

*****************************************************************************
*
*                EVENT
*
* This subroutine calculates the travel times, SP separations and difference
* in arrival times for rays originating at a given focus.  Arrival times for
* direct ray and refracted rays are computed and the minimum is chosen as the
* arrival time.  Calls are made to RPATH and DPATH to effect this.  Variables
* used include:
*          XEQ,YEQ,ZEQ - The coordinates of the earthquake
*          SITE(I,J)  - The coordinates (J=1,2,3=x,y,z) of the I=1,7
*                stations in the array.
*          TTP(L),TTS(L) - The theoretical travel times for P and S waves
*               from focus to receiver for L stations.
*          PTT(K,L)  -The theoretical difference in arrival times for
*          STT(K,L)  P and S waves: ?TT=TT?(K)-TT?(L) where ? is P or S
*          SPT(L)    - The theoretical SP separation for station L.
*          VP(I),Z(I) - The velocities and depths to lower boundary of I
*          VS(I)      layers.
*          NLAYER    - The number of layers in the velocity model (max=4)
*          H,DX,DZ   - The thickness of a layer in the velocity model, the
*               epicentral distance and depth from nearest upper
*               boundary to focus.
*          SK,D   - Dummy variables for (1)The difference of the square
*               of the refracting layer and an upper layer (used in
*               place of trig functions) and (2) the running sum of
*               critical distance components.
*          DEL    - the critical distance for a refracted ray: working
*               from top to bottom, it is calculated to determine
*               how many possible refracted rays could travel from
*               focus to receiver (NRL-number of refracting layers)
*          WAVE   - Type of seismic wave (P=1 or S=2)
*          LOC    - Location number of receiver (max=7)
*          PHI(L,W) - The take off angles for site L and wave type W=1,2
*          TPHI(W,K) - The take off angle for wave type W and layer K=0,N
*               where 0 denotes direct wave. This variable is used
*               internally and the least value for a given location
*               is assigned to PHI.
*          TT(wave,layer)- An internal variable denoting the theoretical
*               travel time.  Least of these for a given wave
*               type is assigned to either TTP or TTS.
*
* The coordinates of the focus are the input parameters and TTP,TTS,SPT,PTT
* and STT are passed back to MAIN via a common block.
*
*****************************************************************************
      SUBROUTINE EVENT(XEQ,YEQ,ZEQ)
      INTEGER NLAYER,NRL,WAVE,LOC,I,J,K,L,LAYER
      REAL SITE(7,3),V(5),TTP(7),TTS(7),DEL
      REAL D,XEQ,YEQ,ZEQ,PTT(7,7),STT(7,7),SPT(7),TT(2,0:4),TPHI(2,0:4)
```

```
      REAL DX,DZ,SK,H,PHI(7,2),RR(9)
      REAL VP(5),VS(5),Z(5),WP(7),WS(7),PT(7,7),ST(7,7)

      COMMON/BLOCK1/V,Z
      COMMON/BLOCK2/NLAYER,VP,VS
      COMMON/BLOCK3/TTP,TTS,SPT,PTT,STT,PHI
      COMMON/BLOCK4/SITE
      COMMON/BLOCK5/WP,WS,RR,PT,ST
      COMMON/BLOCK6/TT

* Initialize the theoretical travel time arrays since these are always
* recalculated for each new focus.

      DO 2 I=1,7
        TTP(I)=0.0
        TTS(I)=0.0
        DO 1 J=1,7
            PTT(I,J)=0.0
            STT(I,J)=0.0
1       CONTINUE
2     CONTINUE

      DO 3 I=1,5
        TT(1,I)=0.0
        TT(2,I)=0.0
3     CONTINUE

* Determine the layer in which the focus is located. If an event
* occurs on a layer boundary, drop it down 10 meters.

      DO 5 I=1,NLAYER
        IF((ABS(Z(I)-ZEQ)) .LT. 0.001)THEN
          ZEQ=ZEQ+0.010
        ENDIF
5     CONTINUE

      J=0
      IF(ZEQ .LT. Z(1) .OR. NLAYER .EQ. 0)THEN
        J=1
      ELSE IF(ZEQ .LT. Z(NLAYER))THEN
        DO 10 I=2,NLAYER
          IF(ZEQ .GT. Z(I-1) .AND. ZEQ .LT. Z(I)) THEN
            J=I
          ENDIF
10      CONTINUE
      ELSE
        J=NLAYER+1
      ENDIF

* This loop calculates P and S arrival times for the 7 stations.

      DO 500 LOC=1,7
        DO 400 WAVE=1,2
```

```
      DO 20 I=1,NLAYER+1
        IF(WAVE .EQ. 1)THEN
          V(I)=VP(I)
        ELSE
          V(I)=VS(I)
        ENDIF
20      CONTINUE

* Calculate the direct ray travel time.

      IF(WP(LOC) .LT. 0.001 .AND. WAVE .EQ. 1) THEN
        GO TO 21
      ELSE IF(WS(LOC) .LT. 0.001 .AND. WAVE .EQ. 2)THEN
        GO TO 21
      ELSE
        CALL DPATH(XEQ,YEQ,ZEQ,SITE(LOC,1),SITE(LOC,2),SITE(LOC,3),
     +    TT(WAVE,0), TPHI(WAVE,0),J)
      ENDIF
* Compute the critical distance for refracted rays working top down.
* Keep a running subtotal of NRL and exit from the loop before all the
* layers are done if a DEL > DX is calculated. First initialize variables
* and calculate DX and DZ for this receiver and wave type.

21    DX=( (XEQ-SITE(LOC,1))**2 + (YEQ-SITE(LOC,2))**2 )**0.5
      NRL=0
      IF(J .EQ. 1) THEN
        DZ=ZEQ-SITE(LOC,3)
      ELSE
        DZ=ZEQ-Z(J-1)
      ENDIF

* Calculate the critical distance for the various layers and
* compare with the station-focus separation. Count the number
* of refracting layers.

      IF(J .EQ. NLAYER+1)THEN
        CONTINUE
      ELSE
        DO 120 LAYER=J,NLAYER
          D=0.0
          DEL=0.0
          D=-1*(DZ/(V(LAYER+1)**2-V(J)**2)**0.5)
          DO 100 I=1,LAYER

*If the focus is layer 1 then the depth is taken from surface; take
* it from the layer above otherwise.

            IF(I .EQ. 1)THEN
            H=Z(I)-SITE(LOC,3)
            ELSE
            H=Z(I)-Z(I-1)
            ENDIF

            SK=(V(LAYER+1)**2 - V(I)**2)**0.5
```

```
                IF(I .LT. J) THEN
                D=(H*V(I))/SK
                ELSE
                D=2*(H*V(I)/SK)
                ENDIF

                DEL=DEL+D

100           CONTINUE

              IF(DEL .LT. DX) THEN
                NRL=NRL+1
              ELSE
                 GOTO 120
              ENDIF

120           CONTINUE

* Compute the travel times of all possible refracted rays.

*             IF(NRL .GT. 0) THEN

                DO 160 I=J,NRL+J-1
                  IF(WP(LOC) .LT. 0.001 .AND. WAVE .EQ. 1)THEN
                   GO TO 159
                  ELSE IF(WS(LOC) .LT. 0.001 .AND. WAVE .EQ. 2) THEN
                   GO TO 159
                  ELSE
                   CALL RPATH(J,I,XEQ,YEQ,ZEQ,SITE(J,OC,1),SITE(LOC,2),
     +             SITE(LOC,3),TT(WAVE,J),TPHI(WAVE,J))
                  ENDIF
159               CONTINUE
160             CONTINUE
              ENDIF
            ENDIF

* Select the minimum travel time and the corresponding take off angle
* for each of the wave types.

            IF(WAVE .EQ. 1) THEN
              TTP(LOC)=TT(1,0)
              PHI(LOC,1)=TPHI(1,0)
            ELSE
              TTS(LOC)=TT(2,0)
              PHI(LOC,2)=TPHI(2,0)
            ENDIF

* Having set the direct ray as the starting minimum, compare it with all
* refracted ray travel times and replace if one of these is less.

            DO 170 I=1,NLAYER

              IF(WAVE .EQ. 1) THEN
```

```
            IF((TT(1,I) .LT. TTP(LOC)).AND.(TT(1,I) .GT. 0.001))THEN
               TTP(LOC)=TT(1,I)
               PHI(LOC,1)=TPHI(1,I)
            ENDIF
          ELSE IF((TT(2,I) .LT. TTS(LOC)).AND.(TT(2,I) .GT. 0.001))THEN
            TTS(LOC)=TT(2,I)
            PHI(LOC,2)=TPHI(2,I)
          ENDIF

170       CONTINUE

400     CONTINUE

500   CONTINUE

      DO 550 K=1,7
        DO 525 L=1,7
          PTT(K,L)=TTP(K)-TTP(L)
          STT(K,L)=TTS(K)-TTS(L)
525     CONTINUE
        SPT(K)=TTS(K)-TTP(K)
550   CONTINUE

      RETURN
      END


*************************************************************************
                SUBROUTINE DPATH
*
*  This subroutine calculates the direct ray travel time from focus to
* station.  Parameters are:
*
*             T,PHI - The travel time and take off angle from focus to
*                station.
*
*             J  - The layer in which the focus is located.
*              The layer boundary below is numbered J
*              from the top down.
*
*
*           XSTN,YSTN,ZSTN - The coordinates of the receiving station.
*
*           XEQ,YEQ,ZEQ  - The coordinates of the earthquake focus.
*
*  Common block parameters include VP(I), VS(I), Z(I) (P and S velocities and
*  depths to refractors for I layers)
*
*  Variables used:   XH1,XH2,TRYXH - Minimum, maximum and best estimate
*                    of the intercept of the ray on the first
*                    refractor.
*
*               PHI1,PHI2,TRYPHI - Minimum, maximum and best estimate of
```

```
*                take off angle.
*
*              DEL1, DEL2,TRYDEL - Minimum, maximum and best estimate
*                epicentre to station distance.
*
*              P, THETA  - Ray parameter and angle of ray in
*                subsequent overlying layers.
*************************************************************************
      SUBROUTINE DPATH (XEQ,YEQ,ZEQ,XSTN,YSTN,ZSTN,T,PHI,J)
      INTEGER J,I
      REAL XEQ,YEQ,ZEQ,XSTN,YSTN,ZSTN,TEMP,PHI,PHI1,PHI2,DX,X1,X2,
     +   XH1,XH2,TRYXH,TRYDEL,P,T,THETA,Z(5),
     +   P1,P2,TRYP,TRYPHI,V(5),H,PI


      COMMON/BLOCK1/V,Z
      PI=4.0*ATAN(1.0)

* For the first layer, compute travel time and take off angle using straight
* line distance and quit.

      IF(J .EQ. 1) THEN
        T=((XSTN-XEQ)**2 + (YSTN-YEQ)**2 + (ZSTN-ZEQ)**2)**0.5
        T=T/V(1)
        TEMP=( (XSTN-XEQ)**2 + (YST-YEQ)**2 )**0.5
        PHI=-1.0*ATAN( (ZEQ-ZSTN)/TEMP )
        GO TO 1000
      ENDIF

* Set initial values of the take off angle prior to commencing the first
* iteration for focii located in layer 2 or below.

      DZ=ZEQ-Z(J-1)
      DX=( (XEQ-XSTN)**2 + (YEQ-YSTN)**2 )**0.5
      PHI1=ATAN(DX/(ZEQ-ZSTN))
      PHI2=ATAN(DX/DZ)
      P1=SIN(PHI1)/V(J)
      P2=SIN(PHI2)/V(J)
      XH1=DZ*TAN(PHI1)
      XH2=DZ*TAN(PHI2)
      X1=RAY (J,PHI1,XH1, P1, ZSTN)
      X2=RAY (J,PHI2,XH2, P2, ZSTN)
      TRYXH=FUNC1 ( XH1, XH2 )
      TRYPHI=ATAN(TRYXH/DZ)
      TRYP=SIN(TRYPHI)/V(J)
      TRYDEL=RAY (J,TRYPHI,TRYXH,TRYP,ZSTN)

* The following loop performs the iterative correction to TRYPHI unti* TRYDEL converges to * within
50 meters of the recording site. If the
* trial angle causes the ray to fall short of the station, it replaces —
* PHI1, if it overshoots, TRYPHI replaces PHI2. A new best estimate is
* calculated and the process repeated.        If the process fails to converge after
* 5000 iterations, a warning is printed on the screen.
```

```
      DO 90 I=1,5000
        IF( ABS(DX-TRYDEL) .LT. 0.050 ) THEN
          GO TO 100
        ENDIF

          IF (TRYDEL .LT. DX) THEN
            X1=TRYDEL
            XH1=TRYXH
          ELSE
            X2=TRYDEL
            XH2=TRYXH
          ENDIF

          TRYXH=FUNC1 ( XH1, XH2 )
          TRYPHI=ATAN(TRYXH/DZ)
          TRYP=SIN(TRYPHI)/V(J)
          TRYDEL=RAY (J,TRYPHI,TRYXH,TRYP,ZSTN)


   90     CONTINUE
          WRITE(6,*) 'WARNING - DIRECT RAY DID NOT CONVERGE!'
  100   CONTINUE

* Compute the direct ray travel time in the case that the ray has
* been refracted on its upwards path.

      P=SIN(TRYPHI)/V(J)
      T=DZ/(COS(TRYPHI)*V(J))


      DO 150 I=J-1,1,-1
        THETA=ASIN(P*V(I))
        IF(I .EQ. 1) THEN
          H=Z(I)-ZSTN
        ELSE
          H=Z(I)-Z(I-1)
        ENDIF
        TEMP= H / (V(I)*COS(THETA))
        T=T+TEMP
  150   CONTINUE

* The take off angle points upwards. Convert this angle, measured from the
* vertical, to one which is measured from the horizontal with upwards being
* negative. This convention is used to facilitate subsequent plotting on an equal area net.

      PHI=TRYPHI
       PHI=PHI-(PI/2.0)

 1000   CONTINUE
        RETURN
        END
```

```
*******************************************************************************
                FUNC1
*
*  This function calculates values of TRYXH using the ratio outlined by Lee and Stewart (1981) *  as
modified by moi.
*
*          Variables:
*               X1, X2  - Minimum and maximum epicentral distances
*               calculated using minimum and maximum  PHI's.
*
*******************************************************************************
          FUNCTION FUNC1 ( XH1,XH2 )
          REAL XH1,XH2,T
           T=0.0
          T=XH1 + 0.5*(XH2-XH1)
          FUNC1=T
          RETURN
          END


*******************************************************************************
                RAY
*
*  This function calculates the epicentral distance (DEL) from focus to station* using basic trigonometry.
The incident angles are determined from the ray
* parameter and Snell's Law.
*  Input parameters passed are:
*                J - the layer in which the focus occurs
*
*                PHI - the take-off angle
*
*                XH  - the horizontal distance traveled
*                 in the bottom layer
*
*                P - the ray parameter.
*  Layer boundary depths (Z(I)) and velocities (VP(I) & VS(I)) are included
*in the COMMON block.  The working velocity array from PATH (V) is also
* COMMON.
*******************************************************************************
          FUNCTION RAY (J,PHI,XH,P,ZSTN)
           INTEGER I,J
          REAL PHI,XH,P,Z(5),H,THETA,DEL,V(5)

          COMMON/BLOCK1/V,Z

          DEL=0.0
          THETA=0.0
          H=0.0
          D=0.0
*  Calculate horizontal distance for layers above that containing the focus.

          DO 100 I=J-1,1
```

```
      IF( I .EQ. 1 ) THEN
        H=Z(I)-ZSTN
      ELSE
        H=Z(I)-Z(I-1)
      ENDIF

      THETA=ASIN(V(I)*P)
      D=H*TAN(THETA)
      DEL=DEL+D

100   CONTINUE

*Add the horizontal distance travelled in the bottom layer.

      DEL=DEL+XH
      RAY=DEL
      RETURN
      END

*****************************************************************************
*
*              RPATH
*
* This subroutine calculates the travel time and take-off angle for refracted
* rays.
*       Input parameters:
*            J,K - Layer in which focus is located; refracting
*              layer.  Note that the index K applies to the
*              base of the layer with velocity V(K) - this
*              differs from the notation of Lee and Stewart.
*
*           XEQ,YEQ,ZEQ - Coordinates (UTM) of the focus.
*
*           XSTN,YSTN,ZSTN - Coordinates of the receiving station.
*
*       COMMON variables:
*
*           V(I),Z(I)  - Ray velocity and depth of layers in velocity
*             model.
*
* Other variables used include:
*
*             H - Thickness of a given layer.
*
*             TEMP  - A dummy variable containing interval travel
*               times.
*
*             DX,DZ  - Epicentral distance; vertical distance from
*               focus to first overlying layer.
*
* Output:
*             T,PHI  - Travel time and take-off angle.
*
*****************************************************************************
```

```
      SUBROUTINE RPATH( J,K,XEQ,YEQ,ZEQ,XSTN,YSTN,ZSTN,T,PHI )
      REAL V(5),Z(5),XEQ,YEQ,ZEQ,XSTN,YSTN,ZSTN,TEMP,H,DX,DZ,T,PHI
      INTEGER I,J

      COMMON/BLOCK1/V,Z

* Initialize variables

      DZ=0.0
      DX=0.0
      TEMP=0.0
      H=0.0
      T=0.0
      PHI=0.0

* Calculate the first two terms of the travel time sum.

      IF(J .EQ. 1)THEN
        DZ=ZEQ-ZSTN
      ELSE
        DZ=ZEQ-Z(J-1)
      ENDIF

      DX=((XEQ-XSTN)**2 + (YEQ-YSTN)**2 )**0.5
      T=(DX/V(K+1)) -(DZ*((V(K+1)**2-V(J)**2)**0.5)/(V(J)*V(K+1)))

* Calculate the terms contained in the two summations.

      DO 10 I=1,J-1

        IF (I .EQ. 1) THEN
          H=Z(I)-ZSTN
        ELSE
          H=Z(I)-Z(I-1)
        ENDIF

        TEMP=(H*((V(K+1)**2-V(I)**2)**0.5)) / (V(I)*V(K+1))
        T=T+TEMP

10    CONTINUE

      DO 20 I=J,K

        IF( J .EQ. 1) THEN
          H=Z(1)-ZSTN
        ELSE
          H=Z(I)-Z(I-1)
        ENDIF

        TEMP=2*(H*((V(K+1)**2-V(I)**2)**0.5)) / (V(I)*V(K+1))
        T=T+TEMP

20    CONTINUE
```

```
      PHI=(3.1415926/2) - ASIN(V(J)/V(K+1))
      RETURN
      END

*****************************************************************************
*
*              RCALC
*
*  This subroutine calculates the space residuals for a given focus.
* The measured time differences are stored in TP/TS and the calculated time
* differences are stored in TTP/TTS.
*
*****************************************************************************

      SUBROUTINE RCALC(RPASS)
      INTEGER J
      REAL PTT(7,7),STT(7,7),SPT(7),PHI(7,2),TTP(7),TTS(7)
      REAL TEMP1,WS(7),WP(7),RPASS
      REAL RR(9),PT(7,7),ST(7,7),SP(7)

      COMMON/BLOCK3/TTP,TTS,SPT,PTT,STT,PHI
      COMMON/BLOCK5/WP,WS,RR,PT,ST
      COMMON/BLOCK8/SP

      RPASS=0.0
      TEMP1=0.0

        DO 50 I=1,7
          DO 40 J=1,7
            IF(I .NE. J)THEN
              IF(WP(I) .GT. 0.0 .AND. WP(J) .GT. 0.0)THEN
                TEMP1=WP(I)*WP(J)*(ABS(PT(I,J)-PTT(I,J)))**2+TEMP1
              ENDIF
              IF(WS(I) .GT. 0.0 .AND. WS(J) .GT. 0.0)THEN
                TEMP1=TEMP1+WS(I)*WS(J)*(ABS(ST(I,J)-STT(I,J)))**2
              ENDIF
            ENDIF

 40         CONTINUE
 50       CONTINUE

* F is a factor weighting the SP separation.
        F=2.0
        RPASS=0.5*TEMP1
        TEMP1=0.0
        DO 70 I=1,7
          TEMP1=TEMP1+(F*WP(I)*WS(I)*(ABS(SP(I)-SPT(I))**2))
 70     CONTINUE

        RPASS=(RPASS+TEMP1)**0.5

      RETURN
      END
```

```
*****************************************************************************
*
*                GRAD
*
* This subroutine conducts a PARTAN search for a solution using the gradient
* at a single point over 4 legs. The search is restarted at the fifth
* point to ensure that convergence is similar to that of the Conjugate
* Gradient Method. If the search diverges or if convergence to a global
* minimum does not occur after 15 legs, the search is stopped and the
* operator prompted for a new search point.
*
* Variables used include:
*              P(Num=1-4,coordinates=1,3) - The coordinates
*                 of the 4 search points.
*              ORIGIN - The point around which the gradient
*                 is calculated.
*              DCOSX,DCOSY,DCOSZ - The direction cosines of
*                 the gradient vector
*              FX,FY,FZ - Partial derivatives with respect to
*                 X,Y,Z in the normal sense (X + delta X, etc)
*              FXM,FYM,FZM - Partial derivatives with respect
*                 X,Y,Z calculated in the negative sense
*                 (X-deltaX).
*              RGLOBE - The least residual found during an
*                 entire PARTAN  search.
*              RLEAST - A global minimum residual found on a
*                 particular leg of the PARTAN search.
*              RMIN - has two values: as passed=minimum residual
*                found during search, in subroutine= the
*                starting value of the least residual.
*              NSTEP _ The number of STEPs, 125m long, along
*                 each segment of the 4 point partan search.
*              RLAST - The residual of the point immediately
*                 before the one under consideration:
*                 Used to find a local minimum during a
*                 search down a particular leg.
*              RNEW - The residual at a given point in the search.
*              XL,YL,ZL - The coordinates of the point where
*                 RLEAST occurs.
*
*****************************************************************************

      SUBROUTINE GRAD(X,Y,Z,CUTOFF,RMIN)
      INTEGER LEG,POINT,STEP,DIV,NSTEP
      REAL X,Y,Z,RMIN,XL,YL,ZL,CUTOFF,RNEW,HYPOT,RLAST,D
      REAL INC,DCOSX,DCOSY,DCOSZ,ORIGIN,XPDX,YPDY,ZPDZ,XN,YN,ZN
      REAL PTT(7,7),STT(7,7),SPT(7),PHI(7,2),TTP(7),TTS(7)
      REAL WP(7),WS(7),RR(9),PT(7,7),ST(7,7),P(4,3),RGLOBE,XG,YG,ZG
      REAL FX,FY,FZ,FXM,FYM,FZM,XMDX,YMDY,ZMDZ,RLEAST,DC
      CHARACTER*1 NOMIN,ANS,RESET,CONSTR,ANS2

      COMMON/BLOCK3/TTP,TTS,SPT,PTT,STT,PHI
       COMMON/BLOCK5/WP,WS,RR,PT,ST
```

```
      RGLOBE=RMIN
      RMIN=99999.9
      RNEW=999999.9
      INC=0.125
       DIV=0
      WRITE(6,*) 'SPECIFY SEARCH RADIUS IN KM:'
      READ(5,*)D
      WRITE(6,*) 'DO YOU WANT TO SET A NEW START POINT?'
      READ(5,'(A)')ANS2
      IF(ANS2 .EQ. 'Y')THEN
        WRITE(6,*) 'INPUT NEW COORDINATES'
        READ(5,*) X,Y,Z
      ENDIF

      NSTEP=INT(8.0*D)


* Initialize the coordinates of the least residual along a search using
* the coordinates of the origin.

  5   CONTINUE
       XL=X
      YL=Y
      ZL=Z
 10   CONTINUE
      WRITE(6,*) 'DO YOU WANT TO CONSTRAIN DEPTH?'
      READ(5,'(A)') CONSTR
       IF( CONSTR .EQ. 'Y')THEN
        WRITE(6,*) 'SPECIFY CONSTRAINED DEPTH:'
        READ(5,*) DC
         Z=DC
       ENDIF

* Perform the search on up to 10 legs with 4 points to each PARTAN search.

      DO 100 LEG=1,15

* If the search fails to find a smaller minimum after 5 legs ( of 4 point
* PARTAN searches each ) then the search is deemed to be diverging and
* the operator is prompted for a new search point.  The search distance may
* be reset from the default of 2.0 km at this point.

        IF(DIV .LT. 5)THEN
          P(1,1)=X
          P(1,2)=Y
          P(1,3)=Z
          IF(CONSTR .EQ. 'Y') Z=DC
        ELSE
          DIV=0
          WRITE(6,*) 'Gradient search is diverging: '
          WRITE(6,*) 'Specify new search point:'
          READ(5,*) X,Y,Z
          WRITE(6,*) 'DO YOU WANT TO RESET THE SEARCH DISTANCE?'
```

```
      READ(5,'(A)') RESET
      IF(RESET .EQ. 'Y')THEN
        WRITE(6,*) 'INPUT NEW SEARCH DISTANCE:'
        READ(5,*)D
        NSTEP=INT(8*D)
      ENDIF
      RGLOBE=9999.9
      GO TO 10
    ENDIF

* Conduct a PARTAN search along 3 line segments using the gradient along
* the first two and the vector between points 1 and 3 for the last leg.

      DO 90 POINT=1,3

        IF(POINT .LT. 3)THEN

* The gradient is calculated in both the positive and negative X,Y and Z
* directions and the average taken as being the true gradient. The partial derivatives are calculated
*  numerically over a distance INC.

          CALL EVENT(P(POINT,1),P(POINT,2),P(POINT,3))
          CALL RCALC(ORIGIN)
          CALL EVENT(P(POINT,1)+INC,P(POINT,2),P(POINT,3))
          CALL RCALC(XPDX)
          CALL EVENT(P(POINT,1),P(POINT,2)+INC,P(POINT,3))
          CALL RCALC(YPDY)
          IF(CONSTR .NE. 'Y')THEN
            CALL EVENT(P(POINT,1),P(POINT,2),P(POINT,3)+INC)
            CALL RCALC(ZPDZ)
          ENDIF
          FX=(XPDX-ORIGIN)/INC
          FY=(YPDY-ORIGIN)/INC
          IF(CONSTR .NE. 'Y')THEN
            FZ=(ZPDZ-ORIGIN)/INC
          ENDIF

          CALL EVENT(P(POINT,1)-INC,P(POINT,2),P(POINT,3))
          CALL RCALC(XMDX)
          CALL EVENT(P(POINT,1),P(POINT,2)-INC,P(POINT,3))
          CALL RCALC(YMDY)
          IF(CONSTR .NE. 'Y')THEN
            CALL EVENT(P(POINT,1),P(POINT,2),P(POINT,3)-INC)
            CALL RCALC(ZMDZ)
          ENDIF

          FXM=(ORIGIN-XMDX)/INC
          FYM=(ORIGIN-YMDY)/INC
          IF(CONSTR .NE. 'Y')THEN
            FZM=(ORIGIN-ZMDZ)/INC
          ENDIF
```

```
      HYPOT=(FX**2+FY**2+FZ**2)**0.5
      PDCOSX=-1*(FX/HYPOT)
      PDCOSY=-1*(FY/HYPOT)
      PDCOSZ=-1*(FZ/HYPOT)
      MDCOSX=-1*(FX/HYPOT)
      MDCOSY=-1*(FY/HYPOT)
      IF(CONSTR .NE. 'Y')THEN
        MDCOSZ=-1*(FZ/HYPOT)
      ENDIF
      DCOSX=(PDCOSX+MDCOSX)/2
      DCOSY=(PDCOSY+MDCOSY)/2
      IF(CONSTR .NE. 'Y')THEN
        DCOSZ=(PDCOSZ+MDCOSZ)/2
      ELSE
        DCOSZ=0.0
      ENDIF
    ELSE
      HYPOT=((P(1,1)-P(3,1))**2+(P(1,2)-P(3,2))**2+ (P(1,3)-P(3,3))**2)**0.5
      DCOSX=(P(3,1)-P(1,1))/HYPOT
      DCOSY=(P(3,2)-P(1,2))/HYPOT
      IF(CONSTR .NE. 'Y')THEN
        DCOSZ=(P(3,3)-P(1,3))/HYPOT
      ELSE
        DCOSZ=0.0
      ENDIF
      CALL EVENT(P(3,1),P(3,2),P(3,3))
      CALL RCALC(ORIGIN)
    ENDIF

* Initialize variables prior to searching along each vector.

      RNEW=0.0
      RLEAST=99999.9
      RMIN=ORIGIN
      NOMIN='Y'
      RLAST=9999.9

      DO 60 STEP=1,NSTEP

* Search for NSTEPxINC kilometers along each vector in steps INC long.
* If the residual is less than that at the start, the search is progressing
* towards a local (NOMIN=L) or global (NOMIN=G) minimum.  Reset RLEAST (for a
* local minimum) and RMIN ( for a global minimum ) as required.
* If no minimum is found, take the endpoint as the minimum.

      XN=P(POINT,1)+STEP*INC*DCOSX
      YN=P(POINT,2)+STEP*INC*DCOSY
      ZN=P(POINT,3)+STEP*INC*DCOSZ
      CALL EVENT(XN,YN,ZN)
      CALL RCALC(RNEW)

      IF(RNEW .LE. RMIN)THEN
        RMIN=RNEW
```

```
          XL=XN
          YL=YN
          ZL=ZN
          NOMIN='G'
        ELSE IF(RNEW .LT. RLAST .AND. RNEW .LT. RLEAST)THEN
          NOMIN='L'
          XL=XN
          YL=YN
          ZL=ZN
          RLEAST=RNEW
        ELSE IF(NOMIN .EQ. 'Y' .AND. STEP .EQ. 16)THEN
          XL=XN
          YL=YN
          ZL=ZN
          RMIN=RNEW
        ENDIF

* If the residual at any point falls below the cutoff value, exit the
* search.

        IF(RMIN .LT. CUTOFF)THEN
          X=XL
          Y=YL
          Z=ZL
            GO TO 1000
        ENDIF

        RLAST=RNEW


 60     CONTINUE

        IF(NOMIN .EQ. 'L')THEN
          RMIN=RLEAST
        ENDIF

          P(POINT+1,1)=XL
          P(POINT+1,2)=YL
          P(POINT+1,3)=ZL

 90     CONTINUE

        X=P(4,1)
        Y=P(4,2)
        Z=P(4,3)

        IF(RMIN .LT. RGLOBE)THEN
          XG=X
          YG=Y
          ZG=Z
          RGLOBE=RMIN
          DIV=0
        ELSE
          DIV=DIV+1
```

```
        ENDIF
        WRITE(6,*)' '
      WRITE(6,*)'Just finished leg',LEG,' at (',P(4,1),P(4,2),P(4,3),')'
      WRITE(6,*) 'Current residual=' ,RMIN,' Global residual=',RGLOBE

100   CONTINUE
      X=XG
      Y=YG
      Z=ZG
      RMIN=RGLOBE

      IF(RMIN .GT. CUTOFF)THEN
        WRITE(6,*) 'Do you wish to restart the search?'
        READ(5,*) ANS
        IF(ANS .EQ. 'Y')THEN
          WRITE(6,*) 'Specify the start of the new search:'
          READ(5,*) X,Y,Z
          RGLOBE=99999.9
          GO TO 5
        ENDIF
      ENDIF
1000  RETURN
      END
```

Appendix C. The Cement Creek Fault strain survey network.

Field work summarized in Chapter 2 indicates that the Cement Creek Fault between Bull and St. Clare Creeks may be currently active and thus is a favourable site at which to measure representative tectonic strain. To effect this, a network of 6 reinforced concrete survey monuments were constructed and surveyed-in; the survey procedure and data are compiled in this appendix for future reference.

The survey network is located at 61° 30' N 140° 16' W and is shown in relation to the Cement Creek Fault in figure 25. The survey monuments consist of square concrete pillars, 15 cm on a side and 1.0 m high. The pillars are reinforced by two pieces of rebar driven at least 18 inches into bedrock joint sets and by subsequent grouting. The tops are fitted with 3/8" coarse threaded nipples to accept the base plates owned by the Department of Physics . The monuments were allowed to settle for at least 10 days prior to surveying.

The distances between survey monuments was measured using the Sokkisha Red-1A owned by the Department of Physics (University of Alberta identification number 0118851). The instrument was calibrated prior to the field work at 4 PPM and prism constant (PC) of 3 and the measurement constant (k) was found to be -0.001. In the field, surveys were conducted in the early morning hours (between 0400 hrs and 0900 hrs) to ensure that the measurements were taken under optimal atmospheric conditions. Temperatures (wet and dry bulb) and barometric pressures were measured immediately prior to and after each survey session and at various times during the survey to ensure stability. Temperature variation between the instrument and reflector was monitored and never exceeded 3.0° C. Slight variations in the alignment of the prism and instrument introduced noticeable systematic variation into the measurements and to overcome this a sight was constructed for the reflecting prism and both the instrument and the reflector were alternatively adjusted until the optimum signal was indicated on the instrument meter. The process was repeated twice during each survey. All distances in the network were measured at least 100 times using these procedures and the measurements are tabulated in the following pages.

Figure 25. Cement Creek Fault strain array. Open circles designate concrete monuments . The fault trace is dashed where inferred.

Initial survey measurements

Leg AC	Initial wet bulb	4.8°C
EDM at C	Initial dry bulb	6.8°C
PPM=4	Final wet bulb	8.0°C
PC=3	Final dry bulb	10.0°C
	P=26.97" Hg	
	(Covers legs AC to AD)	

Measurements

747.093	747.098	747.093	747.089
747.097	747.093	747.092	747.092
747.093	747.09	747.094	747.092
747.094	747.09	747.092	747.093
747.094	747.091	747.092	747.09
747.095	747.096	747.096	747.093
747.093	747.095	747.094	747.09
747.095	747.094	747.093	747.093
747.093	747.092	747.093	747.092
747.093	747.095	747.093	747.094
747.096	747.092	747.092	747.088
747.093	747.092	747.092	747.092
747.092	747.093	747.095	747.092
747.094	747.096	747.095	747.09
747.095	747.091	747.095	747.089
747.098	747.09	747.09	747.092
747.098	747.094	747.095	747.093
747.093	747.093	747.096	747.087
747.093	747.091	747.091	747.087
747.093	747.091	747.092	747.091
747.096	747.093	747.092	747.089
747.093	747.092	747.095	747.092
747.094	747.092	747.09	747.094
747.094	747.095	747.09	747.096
747.097	747.096	747.09	747.094
747.09	747.091		

Leg BC
EDM at C
PPM=4
PC=3

Measurements

327.655	327.655	327.655	327.657
327.655	327.655	327.656	327.656
327.654	327.655	327.656	327.656
327.654	327.656	327.656	327.654
327.655	327.656	327.656	327.654
327.654	327.656	327.656	327.654
327.654	327.655	327.657	327.654
327.654	327.656	327.657	327.655
327.655	327.655	327.657	327.653
327.655	327.656	327.656	327.654
327.654	327.655	327.656	327.654
327.655	327.656	327.656	327.654
327.655	327.656	327.656	327.654
327.654	327.657	327.656	327.654
327.655	327.656	327.656	327.653
327.654	327.655	327.657	327.654
327.655	327.655	327.656	327.654
327.655	327.656	327.657	327.654
327.655	327.656	327.657	327.655
327.654	327.655	327.656	327.654
327.654	327.654	327.656	327.655
327.655	327.655	327.657	327.654
327.655	327.655	327.656	327.654
327.654	327.655	327.656	327.654
327.654	327.656	327.656	327.654
327.654	327.654	327.654	

Leg CD
EDM at D
PPM=4
PC=3

Measurements

664.95	664.949	664.948	664.948
664.949	664.946	664.949	664.948
664.948	664.948	664.949	664.949
664.945	664.948	664.952	664.95
664.948	664.946	664.949	664.95
664.946	664.945	664.951	664.948
664.948	664.952	664.951	664.948
664.949	664.947	664.949	664.945
664.946	664.948	664.947	664.948
664.951	664.947	664.949	664.948
664.947	664.944	664.951	664.947
664.949	664.946	664.951	664.946
664.95	664.943	664.949	664.948
664.949	664.945	664.953	664.947
664.945	664.947	664.948	664.948
664.95	664.946	664.952	664.948
664.949	664.947	664.953	664.948
664.946	664.947	664.948	664.947
664.95	664.945	664.951	664.948
664.946	664.949	664.949	664.948
664.948	664.943	664.952	664.95
664.951	664.947	664.952	664.95
664.947	664.949	664.951	664.949
664.948	664.947	664.948	664.945
664.952	664.947	664.949	664.949
664.948	664.947		

Leg BD
EDM at D
PPM=4
PC=3

Measurements

965.254	965.251	965.248	965.248
965.254	965.25	965.249	965.249
965.251	965.249	965.245	965.251
965.253	965.244	965.247	965.25
965.251	965.247	965.248	965.25
965.25	965.252	965.246	965.255
965.25	965.253	965.251	965.253
965.251	965.248	965.244	965.251
965.251	965.248	965.245	965.251
965.251	965.248	965.247	965.251
965.251	965.248	965.248	965.25
965.253	965.246	965.246	965.25
965.253	965.249	965.244	965.25
965.251	965.251	965.248	965.253
965.249	965.25	965.246	965.253
965.251	965.247	965.244	965.25
965.254	965.249	965.247	965.253
965.254	965.248	965.247	965.251
965.252	965.245	965.247	965.248
965.251	965.245	965.246	965.248
965.249	965.246	965.244	965.25
965.25	965.246	965.246	965.252
965.25	965.25	965.243	965.251
965.251	965.249	965.243	965.252
965.249	965.247	965.249	965.251
965.25			

Leg AD
EDM at D
PPM=4
PC=3

Measurements

1324.555	1324.556	1324.561	1324.554
1324.554	1324.55	1324.556	1324.557
1324.556	1324.553	1324.557	1324.557
1324.555	1324.554	1324.553	1324.556
1324.551	1324.553	1324.552	1324.553
1324.55	1324.552	1324.557	1324.554
1324.554	1324.555	1324.554	1324.557
1324.55	1324.557	1324.556	1324.552
1324.551	1324.554	1324.556	1324.553
1324.555	1324.552	1324.552	1324.556
1324.553	1324.555	1324.555	1324.553
1324.551	1324.554	1324.554	1324.556
1324.55	1324.554	1324.555	1324.554
1324.555	1324.557	1324.554	1324.554
1324.557	1324.555	1324.556	1324.556
1324.556	1324.555	1324.554	1324.556
1324.552	1324.556	1324.558	1324.554
1324.554	1324.555	1324.556	1324.555
1324.552	1324.555	1324.556	1324.554
1324.555	1324.557	1324.556	1324.553
1324.554	1324.554	1324.555	1324.553
1324.555	1324.56	1324.553	1324.554
1324.547	1324.55	1324.555	1324.555
1324.552	1324.553	1324.553	1324.554
1324.551	1324.554	1324.557	1324.555
1324.554			

Leg AE	Initial wet bulb	2.9°C
EDM at E	Initial dry bulb	5.9°C
PPM=4	Final wet bulb	4.0°C
PC=3	Final dry bulb	7.5°C
	P=26.85" Hg	
	(covers leg EA to FC)	

Measurements

1252.783	1252.784	1252.779	1252.785
1252.78	1252.783	1252.782	1252.778
1252.781	1252.782	1252.781	1252.778
1252.783	1252.781	1252.78	1252.78
1252.78	1252.782	1252.784	1252.78
1252.78	1252.783	1252.78	1252.78
1252.782	1252.782	1252.781	1252.781
1252.78	1252.782	1252.783	1252.78
1252.783	1252.78	1252.785	1252.779
1252.78	1252.781	1252.784	1252.778
1252.78	1252.784	1252.78	1252.783
1252.781	1252.78	1252.78	1252.779
1252.78	1252.783	1252.782	1252.779
1252.783	1252.78	1252.781	1252.778
1252.783	1252.782	1252.783	1252.779
1252.78	1252.781	1252.781	1252.777
1252.781	1252.78	1252.784	1252.777
1252.781	1252.781	1252.781	1252.78
1252.781	1252.784	1252.784	1252.779
1252.779	1252.783	1252.785	1252.781
1252.779	1252.783	1252.781	1252.78
1252.782	1252.783	1252.784	1252.781
1252.778	1252.781	1252.784	1252.778
1252.781	1252.78	1252.78	1252.777
1252.777	1252.779	1252.782	1252.776
1252.779	1252.783		

Leg EB
EDM at E
PPM=4
PC=3

Measurements

964.484	964.487	964.488	964.483
964.483	964.489	964.486	964.487
964.485	964.488	964.488	964.485
964.486	964.483	964.488	964.49
964.485	964.485	964.484	964.49
964.484	964.487	964.486	964.483
964.488	964.488	964.486	964.486
964.484	964.486	964.485	964.485
964.485	964.487	964.488	964.486
964.487	964.488	964.488	964.489
964.484	964.488	964.486	964.486
964.488	964.486	964.487	964.485
964.487	964.489	964.485	964.488
964.484	964.486	964.49	964.485
964.489	964.489	964.485	964.486
964.487	964.49	964.49	964.485
964.486	964.486	964.485	964.487
964.488	964.487	964.485	964.489
964.489	964.487	964.489	964.486
964.485	964.491	964.487	964.488
964.485	964.487	964.488	964.484
964.487	964.489	964.486	964.488
964.488	964.49	964.49	964.49
964.485	964.49	964.484	964.486
964.49	964.486	964.489	964.486
964.487	964.485	964.487	

Leg EC
EDM at E
PPM=4
PC=3

Measurements

725.715	725.713	725.711	725.712
725.715	725.713	725.711	725.711
725.713	725.709	725.714	725.711
725.715	725.711	725.714	725.711
725.715	725.71	725.712	725.706
725.713	725.711	725.713	725.711
725.715	725.712	725.714	725.712
725.717	725.711	725.711	725.711
725.718	725.709	725.713	725.711
725.716	725.71	725.713	725.713
725.716	725.713	725.712	725.712
725.713	725.712	725.712	725.713
725.714	725.712	725.718	725.712
725.719	725.711	725.715	725.707
725.715	725.711	725.712	725.711
725.716	725.713	725.714	725.712
725.715	725.71	725.714	725.707
725.72	725.712	725.713	725.707
725.714	725.712	725.714	725.709
725.714	725.709	725.716	725.712
725.717	725.708	725.714	725.71
725.716	725.714	725.715	725.709
725.716	725.713	725.712	725.711
725.716	725.712	725.714	725.71
725.714	725.712	725.716	725.711
725.71	725.71	725.713	725.71

Leg FC
EDM at F
PPM=4
PC=3

Measurements

862.756	862.757	862.754	862.759
862.757	862.756	862.754	862.76
862.756	862.756	862.76	862.759
862.755	862.758	862.758	862.76
862.757	862.756	862.756	862.759
862.756	862.756	862.756	862.759
862.753	862.754	862.759	862.76
862.754	862.752	862.758	862.759
862.757	862.755	862.757	862.757
862.758	862.759	862.758	862.757
862.753	862.757	862.759	862.757
862.759	862.761	862.761	862.761
862.754	862.755	862.761	862.76
862.759	862.759	862.757	862.758
862.756	862.76	862.756	862.76
862.76	862.758	862.761	862.758
862.76	862.756	862.756	862.755
862.759	862.751	862.76	862.756
862.757	862.757	862.758	862.757
862.756	862.759	862.756	862.759
862.759	862.757	862.756	862.76
862.754	862.757	862.757	862.758
862.754	862.756	862.757	862.76
862.76	862.754	862.756	862.757
862.758	862.756	862.756	862.758
862.757	862.755	862.759	862.756

Leg FB
EDM at F
PPM=4
PC=3

Measurements

1010.509	1010.509	1010.507	1010.509
1010.506	1010.507	1010.508	1010.508
1010.506	1010.509	1010.508	1010.512
1010.507	1010.509	1010.510	1010.512
1010.512	1010.508	1010.512	1010.513
1010.511	1010.508	1010.510	1010.513
1010.509	1010.508	1010.512	1010.511
1010.508	1010.507	1010.511	1010.511
1010.508	1010.510	1010.512	1010.508
1010.511	1010.505	1010.507	1010.512
1010.509	1010.511	1010.510	1010.513
1010.506	1010.509	1010.515	1010.515
1010.509	1010.508	1010.508	1010.510
1010.509	1010.507	1010.51	1010.513
1010.505	1010.509	1010.512	1010.513
1010.507	1010.509	1010.511	1010.511
1010.507	1010.51	1010.507	1010.511
1010.509	1010.51	1010.511	1010.509
1010.509	1010.507	1010.509	1010.511
1010.505	1010.508	1010.511	1010.515
1010.505	1010.508	1010.509	1010.51
1010.507	1010.511	1010.509	1010.51
1010.508	1010.509	1010.513	1010.515
1010.508	1010.511	1010.511	1010.511
1010.507	1010.508	1010.513	1010.514
1010.511	1010.512	1010.511	1010.514

Leg AF
EDM at F
PPM=4
PC=3

Measurements

1192.177	1192.175	1192.173	1192.171
1192.179	1192.178	1192.174	1192.174
1192.178	1192.176	1192.174	1192.176
1192.177	1192.176	1192.172	1192.169
1192.178	1192.171	1192.176	1192.172
1192.18	1192.175	1192.177	1192.167
1192.175	1192.171	1192.173	1192.173
1192.175	1192.173	1192.172	1192.174
1192.176	1192.176	1192.171	1192.174
1192.174	1192.176	1192.173	1192.176
1192.177	1192.174	1192.173	1192.173
1192.174	1192.171	1192.173	1192.174
1192.175	1192.172	1192.172	1192.175
1192.178	1192.173	1192.173	1192.174
1192.181	1192.172	1192.171	1192.175
1192.173	1192.172	1192.169	1192.174
1192.176	1192.172	1192.171	1192.175
1192.177	1192.173	1192.172	1192.172
1192.177	1192.172	1192.172	1192.175
1192.175	1192.173	1192.171	1192.171
1192.177	1192.175	1192.17	1192.173
1192.175	1192.176	1192.171	1192.175
1192.173	1192.169	1192.172	1192.177
1192.173	1192.175	1192.175	1192.176
1192.177	1192.175	1192.171	1192.174
1192.173	1192.175	1192.174	1192.175
1192.174	1192.175	1192.174	1192.176

Leg EF	Initial wet bulb	1.7°C
EDM at F	Initial dry bulb	3.0°C
PPM=4	Final wet bulb	?????
PC=3	Final dry bulb	4.0°C
	P=26.90"Hg	
	(convers legs EF to DE)	

Measurements

327.706	327.705	327.71	327.71
327.707	327.711	327.712	327.711
327.705	327.712	327.71	327.71
327.705	327.711	327.71	327.71
327.705	327.711	327.71	327.707
327.704	327.709	327.71	327.706
327.706	327.71	327.71	327.706
327.706	327.711	327.711	327.707
327.706	327.711	327.711	327.707
327.705	327.711	327.711	327.706
327.705	327.71	327.711	327.707
327.706	327.711	327.71	327.707
327.706	327.711	327.711	327.707
327.705	327.709	327.711	327.707
327.705	327.711	327.711	327.706
327.706	327.711	327.71	327.706
327.706	327.71	327.711	327.706
327.706	327.711	327.71	327.707
327.706	327.711	327.711	327.705
327.705	327.711	327.711	327.707
327.708	327.711	327.71	327.706
327.706	327.711	327.71	327.709
327.706	327.71	327.71	327.707
327.705	327.711	327.709	327.707
327.705	327.711	327.71	327.707
327.707	327.708	327.707	327.707

Leg DF
EDM at F
PPM=4
PC=3

Measurements

604.082	604.082	604.085	604.088
604.083	604.089	604.085	604.083
604.083	604.089	604.081	604.084
604.083	604.088	604.086	604.085
604.085	604.087	604.089	604.091
604.08	604.088	604.086	604.084
604.081	604.089	604.086	604.086
604.083	604.086	604.086	604.085
604.083	604.09	604.089	604.084
604.08	604.088	604.085	604.086
604.079	604.084	604.089	604.087
604.083	604.089	604.086	604.086
604.083	604.086	604.084	604.086
604.085	604.09	604.085	604.082
604.079	604.089	604.086	604.085
604.082	604.087	604.087	604.085
604.081	604.087	604.087	604.089
604.081	604.087	604.089	604.086
604.081	604.086	604.086	604.088
604.082	604.089	604.088	604.089
604.083	604.091	604.082	604.089
604.083	604.086	604.088	604.086
604.08	604.085	604.087	604.088
604.082	604.088	604.09	604.089
604.082	604.086	604.085	604.085
604.087	604.085	604.084	604.083

Leg AB
EDM at B
PPM=4
PC=3

Measurements

432.518	432.516	432.517	432.51
432.517	432.518	432.512	432.512
432.518	432.518	432.509	432.507
432.518	432.517	432.51	432.513
432.517	432.516	432.509	432.515
432.516	432.517	432.508	432.513
432.517	432.517	432.513	432.513
432.516	432.518	432.508	432.514
432.517	432.517	432.507	432.514
432.516	432.517	432.511	432.512
432.517	432.518	432.51	432.513
432.515	432.517	432.511	432.511
432.517	432.517	432.513	432.515
432.517	432.517	432.511	432.512
432.516	432.518	432.51	432.513
432.517	432.517	432.51	432.513
432.517	432.517	432.509	432.512
432.517	432.518	432.506	432.513
432.518	432.516	432.508	432.518
432.518	432.518	432.509	432.509
432.516	432.516	432.509	432.51
432.518	432.517	432.508	432.513
432.517	432.518	432.509	432.513
432.518	432.517	432.507	432.513
432.516	432.517	432.509	432.513
432.512			

Leg DE
EDM at E
PPM=4
PC=3

Measurements

281.631	281.63	281.632	281.632
281.63	281.633	281.632	281.631
281.629	281.633	281.633	281.631
281.63	281.632	281.632	281.632
281.63	281.632	281.632	281.63
281.63	281.631	281.632	281.631
281.63	281.631	281.633	281.632
281.63	281.632	281.631	281.632
281.631	281.632	281.632	281.632
281.631	281.632	281.633	281.631
281.629	281.633	281.633	281.632
281.63	281.632	281.632	281.632
281.63	281.632	281.632	281.631
281.631	281.632	281.632	281.631
281.629	281.632	281.632	281.631
281.63	281.631	281.632	281.632
281.63	281.633	281.631	281.631
281.63	281.632	281.632	281.632
281.63	281.632	281.631	281.631
281.63	281.632	281.632	281.631
281.629	281.632	281.632	281.631
281.63	281.633	281.632	281.631
281.63	281.633	281.631	281.632
281.628	281.632	281.631	281.632
281.629	281.632	281.632	281.632
281.63	281.631	281.632	281.632
281.631			